T-3292

USE OF POST-CRITICAL SEISMIC REFLECTION AMPLITUDES, FOR EXPLORATION PURPOSES, INCLUDING DEPTH ESTIMATION

by

Mohammed Al-Faraj

ProQuest LLC.
789 East Eisenhower Parkway
P.O. Box 1346
Ann Arbor, MI 48106 – 1346

T-3292

A thesis submitted to the Faculty and the Board of Trustees of the Colorado School of Mines in partial fulfillment of the requirements for the degree of Master of Science (Geophysics).

Golden, Colorado
Date 4/24/1987

Signed: Mohd Alfaraj
Mohammed N. Al-Faraj

Approved: R L Sengbush
R.L. Sengbush
Thesis Advisor

Golden, Colorado
Date 4/24/87

P R Romig
Phillip R. Romig
Head of Department
Geophysics Department

ABSTRACT

Investigations of raw seismic data reveal that amplitude brightening occurs at a post-shear-critical angle for a shallow reflector (about 300 ms of two-way travel time and 260 m deep). The reflector responsible for the amplitude brightening is identified by amplitude-vs-offset (AVO) multi-layer modeling based on Zoeppritz' equations.

The target formation consisting mostly of limestone exhibits a relatively high compressional velocity of about 5000 m/s. Stacking velocity along two lines of study (a dip line and a strike line, CDP and shot gathers for each) averages about 2100 m/s down to the target reflector.

Theoretical studies of AVO from Zoeppritz' equations show that the effect of density is negligible. On the other hand, the effect of the compressional velocity variations in the overlying media is important in determining the angle of amplitude brightening, which is found to be about 6^{0} greater than the shear-critical angle for the target reflector in this research.

Depth calculations to the target reflector in the two-layer case is given by Z = X/(2 TAN Q), where Z = depth, X = offset distance of peak amplitude, and Q = IS + 6^{0} ; IS is the shear-critical angle based on the compressional stack-

ing velocity for Layer 1 and estimated shear velocity in Layer 2. A comparison of a two-layer model to a multi-layer model, on the basis of the offset corresponding to a peak amplitude, shows that the difference between the two is very small (about 15 m). The error arising in the depth calculations by assuming a two-layer model is minimized by normalizing the results to known depths from well logs.

Matching of post-critical amplitude peaks from theoretical and real-data AVO plots in the vicinity of wells improves the estimate of the shear velocity in the target formation. The estimated shear velocity along the strike line did not vary much (average = 2960 m/s), whereas the velocity along the dip line decreased linearly downdip at the rate of about 10 m/s per km.

A comparison of the depths calculated from the AVO method to those calculated from a time-dependent method shows that the two methods are comparable (on the basis of errors) for the strike line. The time method is deemed better than the AVO method for the dip line.

It is concluded that the AVO method has merit and may be useful for independently estimating depths of shallow reflectors as well as estimating shear velocities in shallow formations. The relative depth errors of the AVO method,

based on well control along the two lines, are of the order of 3 m when the results are tied to more than one well.

TABLE OF CONTENTS

LIST OF FIGURES

LIST OF TABLES

LIST OF SYMBOLS

AVO	:	Amplitude vs Offset
Gamma	:	The Angle by Which the Peak Amplitude Lags the Shear-Critical Angle
IP		P-Critical Angle Due to P-Wave Source
IS		PS-Critical Angle, S-Critical Angle Due to P-Wave Source
P or P1	:	P-Wave Velocity in First Layer
RHO	:	Density in g/cc
S or S2	:	S-Wave Velocity in Second Layer
SIG (Sigma)	:	Poisson's Ratio
t	:	Two-Way Travel Time
Q		Angle in Degrees that Corresponds to a Peak Amplitude
Vav		Average P-Wave Velocity
VP	:	P-Wave Velocity
VS	:	S-Wave Velocity
Z	:	Depth

ACKNOWLEDGEMENTS

I would like, first, to thank the Arabian American Oil Company (ARAMCO) for sponsoring this research and providing the seismic data and computer resources. I would also like to express my deep gratitude to Dr. E.F. Chiburis from the Research and Development Division, Exploration, ARAMCO, for suggesting this research. He devoted much of his valuable time directing and monitoring the progress of this project. Not only has he developed computer software that were most helpful to the R&D Division as a whole and to this project in particular, Dr. Chiburis was also involved in the boring and time-consuming process of interactively picking and analyzing reflection amplitudes.

I would like to express my sincere thanks to Professor R.L. Sengbush, my advisor from the Colorado School of Mines, for monitoring and suggesting constructive comments related to this project. I also apologize to Mr. Sengbush for the late-at-night phone calls. Phone calls served as a means of communication between us as this study was conducted in Dhahran, Saudi Arabia. I would also like to express my thanks to the other two members of my committee, Dr. Frank Hadsell and Dr. Jack Cohen, for their support.

My special thanks go also to Dr. A. Fouda and Mr. F.P. Cortes from the Training Division, Exploration, ARAMCO. Dr. Fouda provided support, enthusiasm, and administrative help in order to bring this thesis to completion. Mr. Cortes has suffered through the typing and the never-ending retyping of this thesis. I thank Mrs. Rory Rogers for the final typing of this thesis.

Last, but not least, I express my deep thanks and appreciation to my wife, Masouma. Without her, this journey would have never started nor ended.

CHAPTER ONE

Introduction

Objectives

In seismic reflections, amplitude brightening at the P-wave critical angle has been reported in the past. Richards (1960) observed amplitude brightening coming after the P-wave critical angle which he referred to as wide angle reflections. Meissner (1960) stated that vertical amplitudes are larger in the P critical angle region than in the near vertical region. Schultz et al (1983) suggested that a larger range of offsets be implemented in the seismic recording in order to improve the estimation of interval velocities. Winterstein and Hanten (1985) reported observations of amplitude brightening beyond the P-wave critical angle in P- and S-wave data. Experiments indicate that offset-amplitude, if properly balanced, can greatly add to conventional direct hydrocarbon interpretation (Gary Yu, 1985).

It appears that this thesis is the first research in which observations of post-shear-critical amplitude brightening are reported. Also, this thesis is the first to utilize amplitude-vs-offset (AVO) information for estimating depth.

In a shot or a CDP gather, the reflection amplitude of a given reflector varies with offset. Such amplitude variations are, in general, more noticeable when the reflector is shallow and produces post-critical reflections.

By using Zoeppritz' equations along with known or estimated parameters down to a shallow target formation, modeling can be done to obtain theoretical plots of amplitude vs offset (Chiburis, 1987, personal communication). The main objective of this thesis is to develop a time-independent equation for depth estimation of shallow reflectors. The parameters required in the depth equation are extracted from post-critical AVO data. With the help of inversion techniques, i.e., by comparing theoretical AVO plots to real-data AVO plots, an estimate of essential parameters can be made. One such parameter is the shear wave velocity in a target formation; this will be investigated in this thesis as well.

Two lines are considered in this study. Line 1 is along strike and is about 80 km long; Line 2 is along regional dip and is about 60 km long. The regional dip is very small (depth change of about 50 m over an interval of 50 km).

An example of a shot gather in Figure 1 shows that the event of interest occurs at an arrival time of about 300 ms

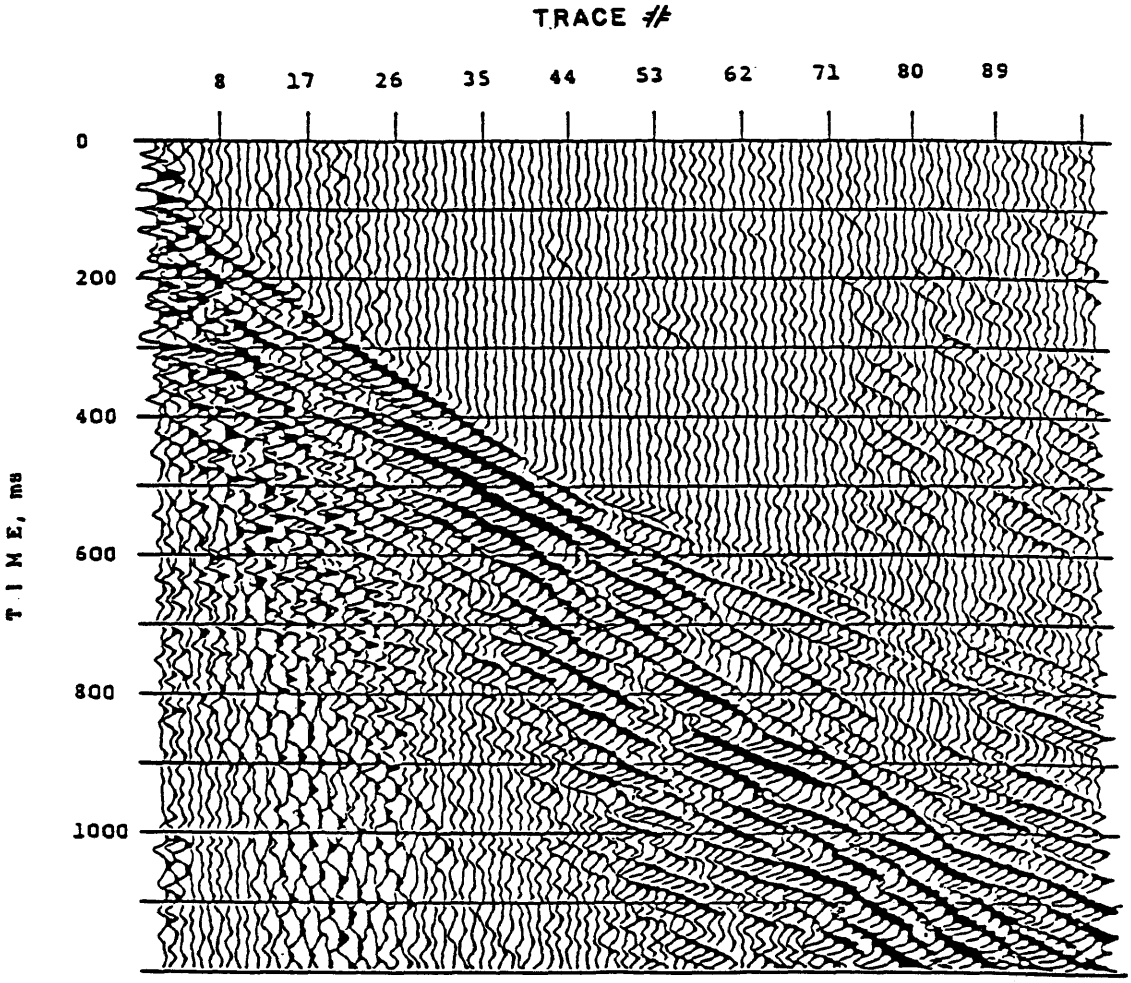

FIGURE 1 SHOT GATHER. LINE 1.

at Trace 1 and about 600 ms at Trace 50. The target formation shows a significant increase in amplitude on Traces 26-36, with travel times in the range of 400-500 ms. The trace spacing is about 24 m which yields an offset of about 700 m for the peak amplitude (Trace 30).

A typical shot gather flattened on the event of interest at about 300 ms in Figure 2 shows amplitude brightening between Traces 25 and 35. Refraction interference is noticeable on Trace 37. Theoretical studies of phase from Zoeppritz' equations show that the event of interest has a phase shift of 180 beyond the P-critical angle. This explains why the flattened event in Figure 2 at 300 ms has a trough on Traces 1-18 which changes to a peak thereafter. Typical plots of measured amplitude of the target reflector vs offset for nine shot gathers are shown in Figure 3. It is important to note that all gathers display amplitude enhancement in the vicinity of trace 30.

With the assumption that the layers are plane parallel and horizontal, the depth Z to a reflector for a two-layer case (Figure 4) can be calculated using the following equation,

$$Z = X/(2 \text{ TAN } Q), \qquad (1)$$

for a given offset X and corresponding angle of incidence Q.

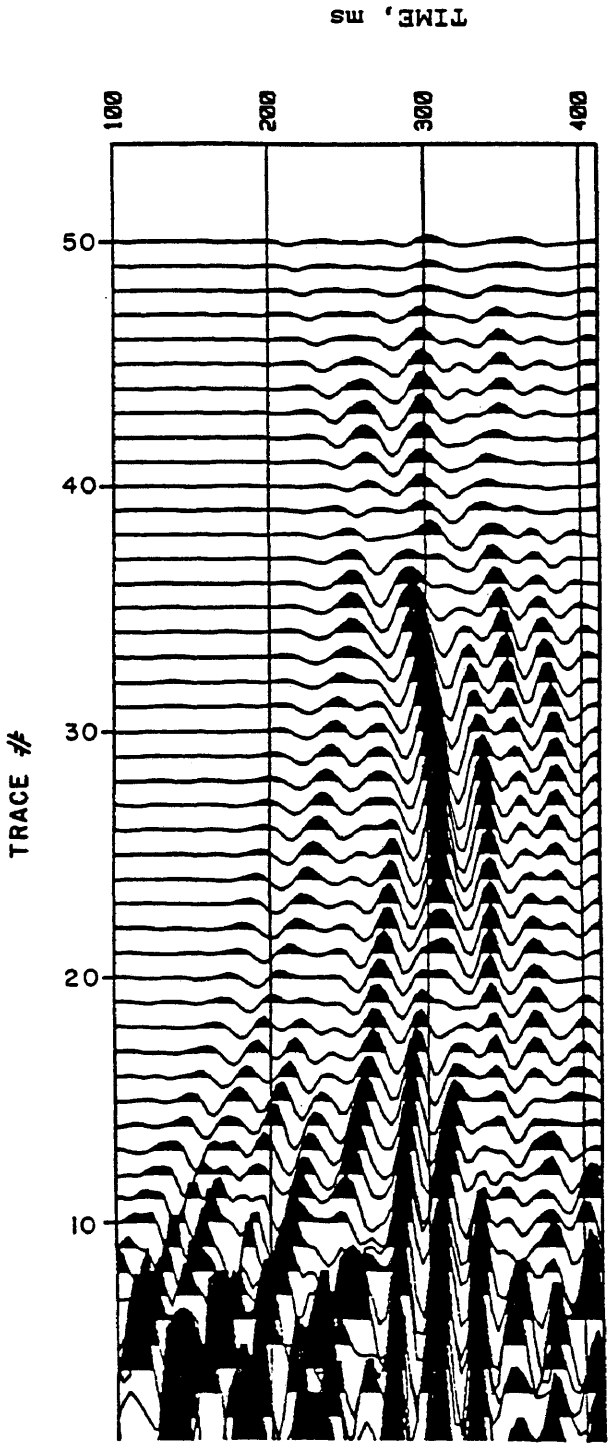

FIGURE 2. FLATTENED SHOT GATHER, LINE 1, SP 1400.

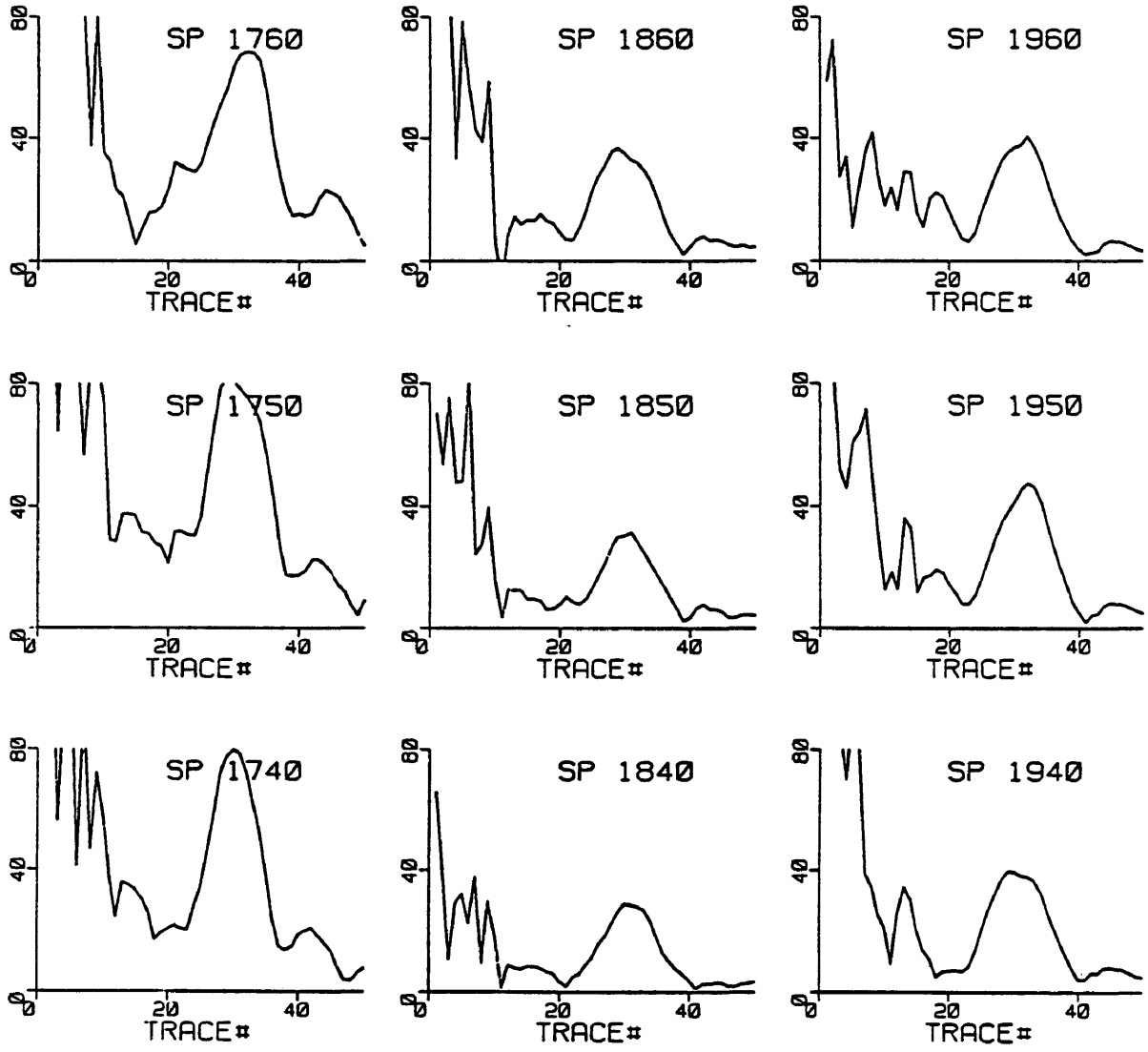

FIGURE 3. EXAMPLES OF AVO'S, LINE 1.

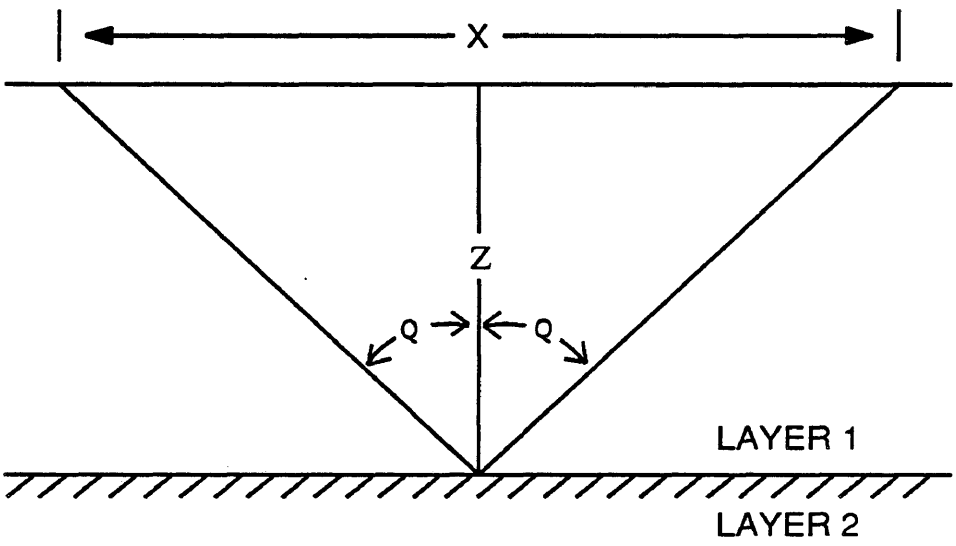

FIGURE 4. TWO-LAYER MODEL

Within each gather, as in Figure 3, an isolated peak occurs at about trace 30. Since the offset corresponding to each isolated peak is known, the depth to the target formation can be calculated directly from equation (1) once the corresponding angle of incidence Q is known. An effort will be devoted to investigating the parameters involved in determining the angle Q.

The overall discussion will be expanded in such a way that the model of equation (1) incorporates the multi-layer case as well as the two-layer case.

Geologic Background

The main objective of this research is to investigate the feasibility of estimating depths of a shallow reflector (about 300 ms of two-way travel time) by using post-critical AVO information. Two reflectors are of interest; they both seem to be capable of producing amplitude brightening due to their relatively high, and similar, P velocities.

One reflector of interest, referred to as Interface 1 in Figure 5, consists mostly of limestones and exhibits a relatively high P-velocity of about 5000 m/s. Interface 2 is the top of a ten-meter-thick shaly layer whose velocity is relatively low, resulting in a high impedance contrast.

The other reflector of interest, referred to as Interface 3 in Figure 5, is the top of a known formation

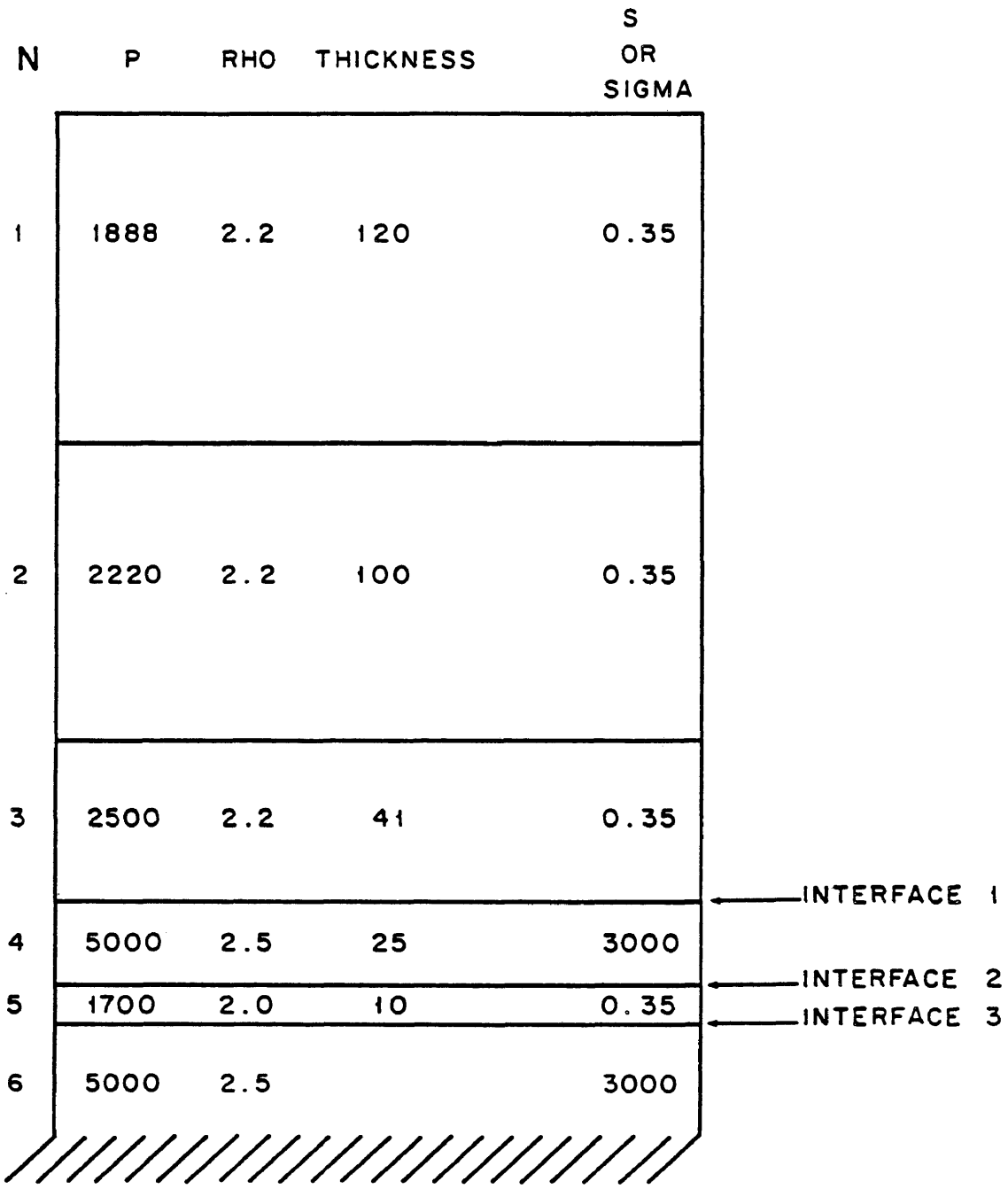

FIGURE 5. SIX-LAYER EARTH MODEL

which is of Eocene Age. The depth of this reflector is approximately 300 m throughout the area. The upper portion of this ofrmation consists of sparsely fossiliferous limestone underlaid by gypsum and anhydrite with thin limestones and shales. The formation is, in general, characterized by its high velocity limestone and anhydrite.

Therefore, the final picture gives a low velocity shaly layer sandwiched between two high velocity media. Hence, this suggests that the reflections seen on the gathers are due to either the upper high velocity formation whose top is Interface 1 or the lower formation whose top is Interface 3. This point will be further investigated in detail with the help of modeling.

CHAPTER TWO

Procedures

Velocity Information

Stacking velocities down to about 300 ms of two-way travel time are known every hundredth shot point for the two lines (Department of Geophysics, Aramco, 1986), as shown in Table 1.

In order to estimate a velocity for each gather, linear interpolation is carried out between the known stacking velocities (Figures 6 and 7). The stacking velocity varies by about 5%; this may be due to near surface effects.

Data Acquisition and Processing

This research deals with land data. The source is a compressional vibrator with an upsweep of 10-80 Hz. The receivers are standard eight-Hertz geophones (96 channels).

The two seismic lines considered in this study were each processed in two different ways, which yields a total of 4 line segments to be analyzed. The data was also vertically stacked (eleven-fold), but the stacked gathers were not favorable for AVO studies.

Processing A. The 96-channel data from Lines 1 and 2 were sorted into shot gathers. The target reflection for

Table 1. Stacking Velocities

Line 1		Line 2	
Shot point	Velocity, m/s	Shot point	Velocity, m/s
1150	2120	1150	2220
1250	2160	1250	2305
1350	2070	1350	2350
1450	2060	1450	2290
1550	2120	1550	2200
1650	2050	1650	2175
1750	2110	1750	2225
1850	2200	1850	2280
1950	2100	1950	2270
2050	2100	2050	2195
2150	2150	2150	2165
2250	2090	2250	2170
2350	2040	2350	2205
2450	2090	2450	2260
2550	2140	2550	2230
2650	2110	2650	2165
2750	2040	2750	2125
2850	2090	2850	2155
2950	2090	2950	2220
3050	2100	3050	2225
3150	2090	3150	2200
3250	2110	3250	2190
3350	2100	3350	2185
3450	2195	3450	2185
3550	2100	3550	2200
3450	2195	3650	2200
3550	2130	3750	2200
3650	2180		
3750	2100		
3850	2200		
3950	2160		
4050	2140		
4150	2300		
4250	2100		
4350	2150		
4450	2130		
4550	2020		

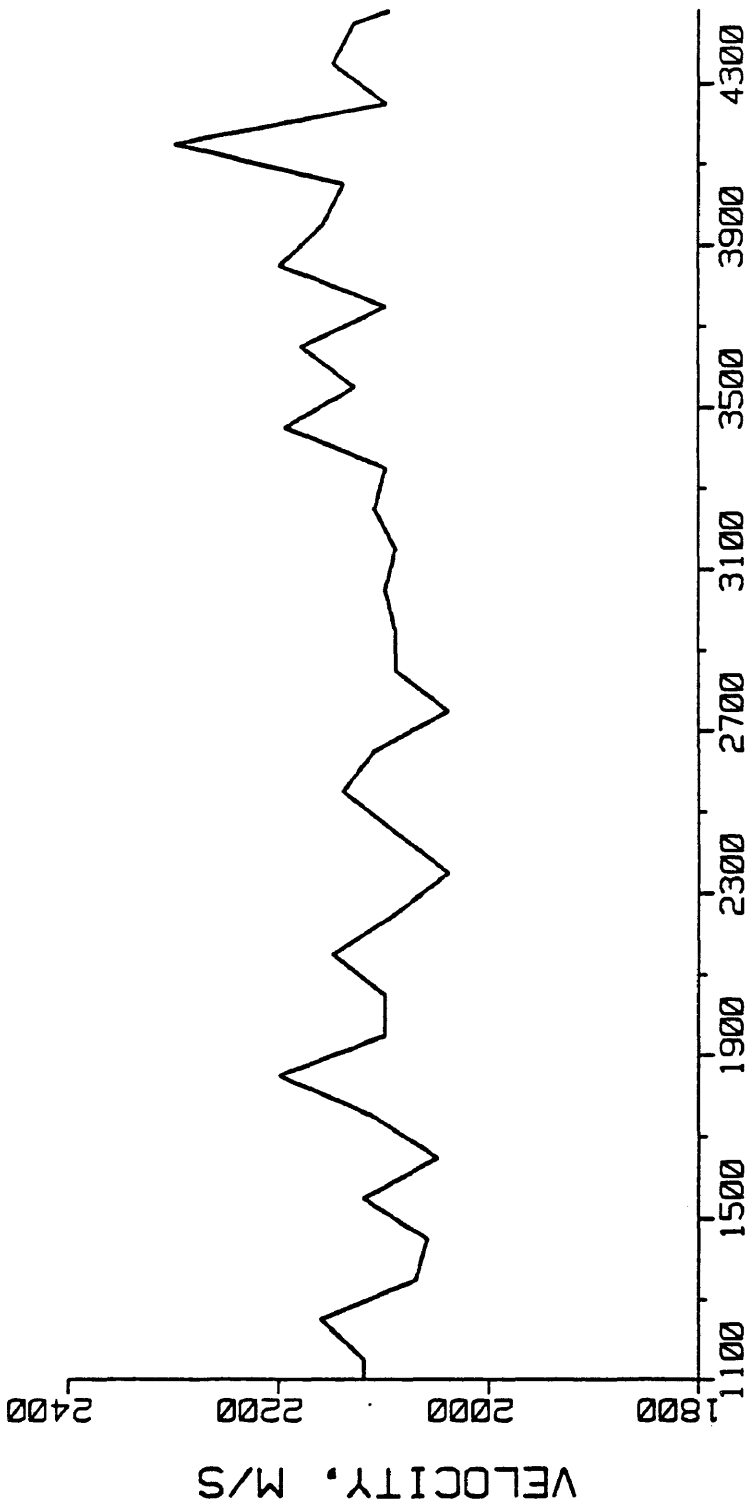

FIGURE 6. PROCESSED STACKING VELOCITY, LINE 1

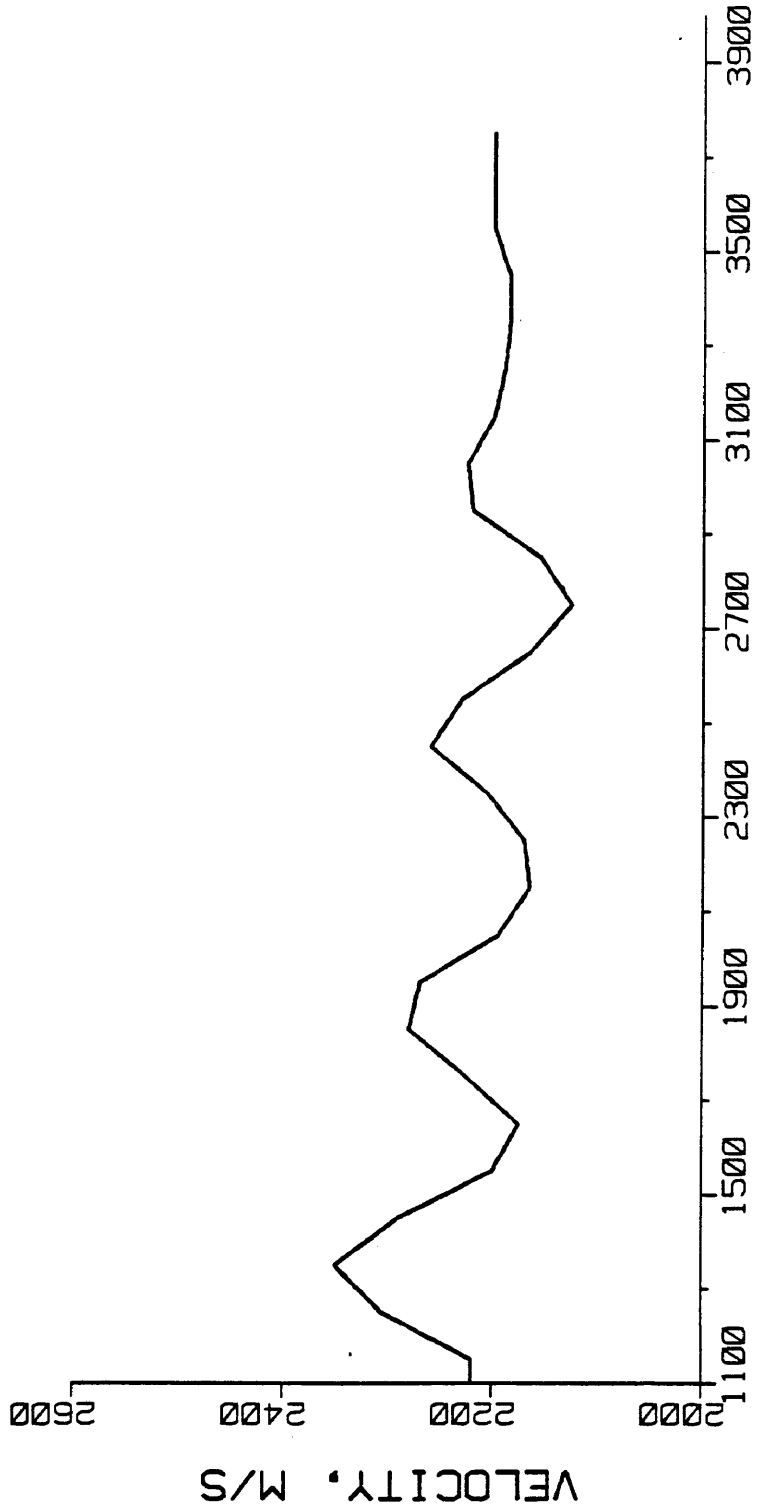

FIGURE 7 PROCESSED STACKING VELOCITY, LINE 2

each trace within a gather was flattened to about 300 ms by using the stacking velocities known along the two lines. Every tenth gather between shot points 1100 and 4480 was considered for Line 1; every tenth gather between shot points 1100 and 3700 was considered for Line 2. Line 1 yielded 339 50-trace gathers. Line 2 yielded 261 50-trace gathers.

Processing B. The 96-channel data from Lines 1 and 2 were sorted into CDP gathers. The reflection from the target formation for each trace was flattened to about 300 ms by using the stacking velocities. Every tenth gather between shot points 1120 and 4480 was considered for Line 1, and every tenth gather between shot points 1120 and 3700 was considered for Line 2. Line 1 yielded 337 40-trace CDP gathers. Line 2 yielded 259 40-trace CDP gathers.

Vertical Stacking. The shot gathers were vertically stacked (eleven-fold) in order to improve the signal-to-noise ratio. LIne 1 yielded 339 40-trace gathers; Line 2 yielded 261 40-trace gathers.

Since the proposed method of depth estimation depends on the peak of amplitude brightening, it is essential that the vertically-stacked data not in any way alter the overall picture of non-stacked data. Comparison of vertically-

stacked gathers to non-stacked ones showed significant differences on many gathers. As a result, the stacked gathers were ruled out from this analysis because the amplitude of the raw data is not preserved.

Concluding Remarks. The number of traces within each gather was truncated to either 40 or 50 traces. This was done to speed up the process of interactively picking amplitudes and has no effect on the analysis because the truncated traces are beyond the range of interest.

To summarize, the following four line segments were analyzed:

1- Line 1, 339 50-trace shot gathers;

2- Line 2, 261 50-trace shot gathers;

3- Line 1, 337 40-trace CDP gathers; and

4- Line 2, 259 40-trace CDP gathers.

Identification of Target Reflector

Based on density and sonic logs along the two lines, and also based on geological data in the area of study, a six-layer earth model is generated as shown in Figure 5.

The dominant thicknesses of Layers 1 through 5 are determined from well logs. The P velocities and densities of Layers 2 through 6 are determined from well logs as well. For the first layer, the P velocity is solved for in such a

way that the RMS velocity down to Layer 6 is equal to the observed average stacking velocity (2100 m/s).

The shear velocity in Layers 4 and 6 is assumed to be 3000 m/s (this corresponds to a Poisson's ratio of about 0.218). Theoretical AVO plots of normalized P-wave reflection amplitudes as a function of offset for Interfaces 1, 2, and 3 are shown in Figure 8. The normalization of these plots has no effect on the analysis as the shape of each plot (relative amplitudes) is the key factor in determining the target reflector.

In Figure 8, the reflections coming from Interfaces 2 and 3 terminate at an offset of about 750 m. This can be explained by the fact that no energy is transmitted beyond Interface 1 once the angle of incidence at Interface 1 reaches the shear critical angle. For the reflections coming from Interface 1, an isolated peak is developed at an offset of about 650 m. Interface 1 best resembles the observed AVO data in Figure 3. Hence, the target reflector for this research is Interface 1.

Depth Information

Seven wells on Line 1 and three wells on Line 2 provide known depths to the target reflector as listed in Table 2. The lines cross at SP 2990 (Line 1, Well 6) and SP 2560 (Line 2, Well 2).

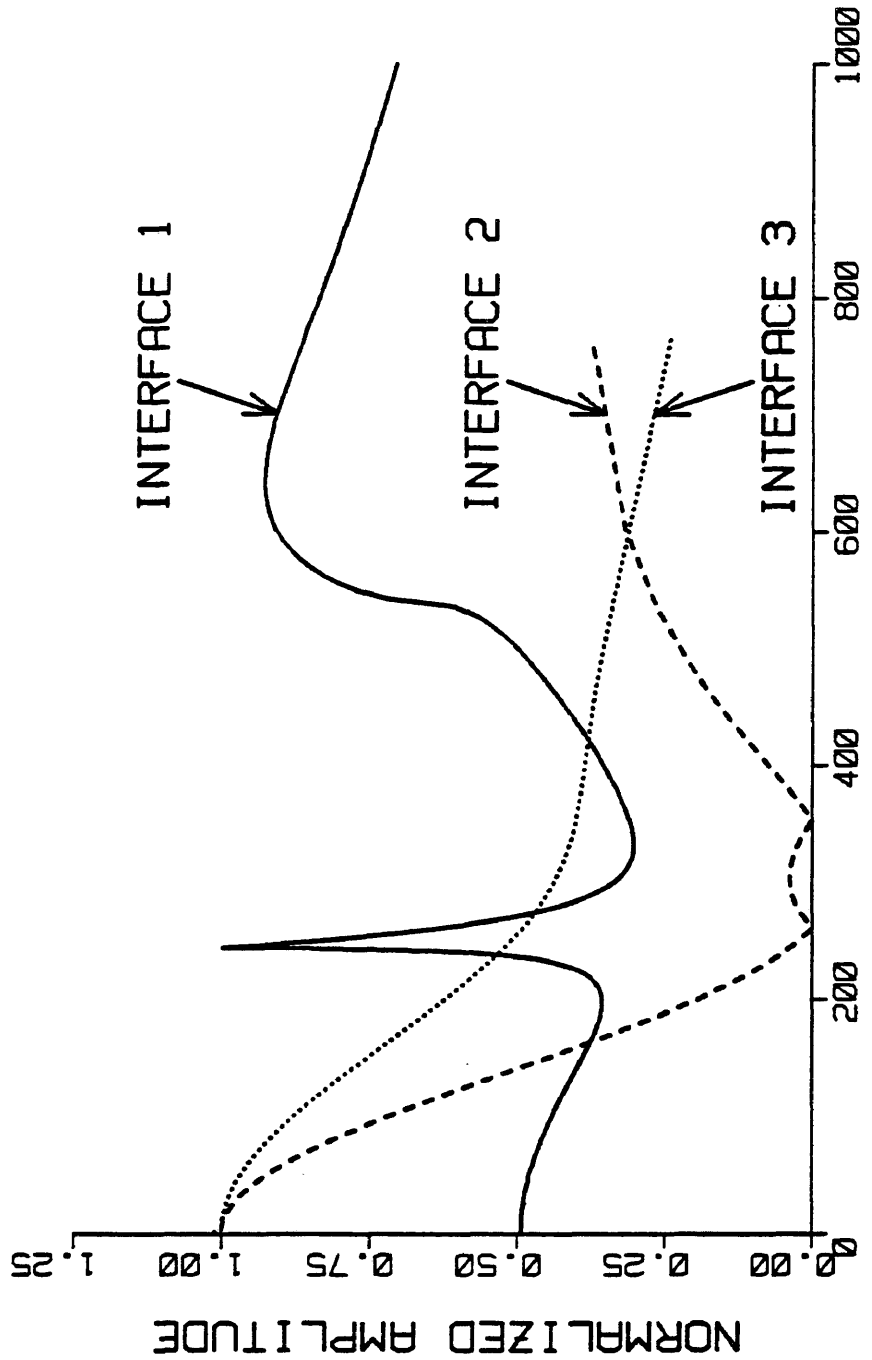

FIGURE 8. THEORETICAL AVO PLOTS OF P-REFLECTION AMPLITUDES FOR INTERFACES 1, 2, AND 3

TABLE 2. Depth Information

Line 1			Line 2		
Well	Shot point	Depth, m	Well	Shot point	Depth, m
1	1830	263.7	1	1260	255.4
2	2110	260.9	2	2560	256.0
3	2370	253.6	3	3340	246.3
4	2900	257.3			
5	3180	257.6			
6	2990	256.0			
7	4320	259.1			

Why Post-Critical

The offset that corresponds to the shear-critical angle at the target reflector (Interface 1, Figures 5 and 8) can be calculated quantitatively from Snell's Law. This offset can then be compared to the offset of the peak amplitude (650 m) as determined earlier (Figure 8).

The shear-critical angle, IS, at Interface 1 is calculated as follows:

$$IS = \text{ARCSIN}\ (2500/3000) = 56.4^{0}.$$

The corresponding angle of incidence at the interface between Layers 2 and 3 is given by:

$$\text{Angle 2-3} = \text{ARCSIN}\,[(2200/2500)\ \text{SIN}\ 56.4^{0}] = 47.1^{0}.$$

The angle at the interface between Layers 1 and 2 is given by:

$$\text{Angle 1-2} = \text{ARCSIN}\,[(1888/2220)\ \text{SIN}\ 47.1^{0}] = 38.5^{0}.$$

Since the thicknesses of the layers for this particular model (Figure 5) are known, the corresponding offset can be calculated as follows:

$$X = 2[120\ \text{TAN}\ 38.5^{0} + 100\ \text{TAN}\ 47.1^{0} + 41\ \text{TAN}\ 56.4^{0}] = 530\ \text{m}.$$

Since the offset of the peak amplitude (650 m) is greater than the offset that corresponds to the shear-critical angle (530 m), then the peak amplitude indeed occurs at a post-shear-critical angle. This peak amplitude will be referred to as post-critical amplitude brightening.

Amplitude And Offset Picking

For each gather, the peak reflection amplitudes and their corresponding trace numbers are read interactively with picking and editing algorithms due to Chiburis and Nietupski (1987). The corresponding offsets for all traces are provided in the headers. A plot of amplitude vs trace number was generated for all gathers from the two lines, as shown for example in Figure 3.

As a shot gather contains only discrete offsets, the specific offset corresponding to the peak amplitude in a given gather does not necessarily equal the offset of maximum amplitude had the data been continuous. Hence, we can observe the offset of maximum amplitude only to the nearest half trace (approximately 12 m).

To minimize the resolution error arising from the trace spacing, a least-squares quadratic curve-fitting technique was applied to the data in the vicinity of the trace of maximum amplitude. A three-point quadratic fitting was chosen (although 5, 7, 9, and 11 points were also tested) and the offset of maximum amplitude was analytically calculated for each gather.

CHAPTER THREE

Theoretical AVO

Effect of Depth Variation on AVO

The effect of depth variation on AVO is studied by assuming a two-layer earth model. The depth is varied from 200 m to 400 m and all other parameters are held constant. By studying the theoretical AVO plots for each depth it was found that the shear critical angle did not change and neither did the angle corresponding to maximum P-reflection amplitude. Hence, the difference between these angles, defined as the angle Gamma, is independent of depth.

In the first layer, a P velocity of 2100 m/s, a Poisson's ratio of 0.33,.and a density of 2.2 g/cc are assumed. For the second layer, the parameters are P velocity of 5000 m/s, shear velocity of 3000 m/s, and density of 2.5 g/cc. The value obtained for Gamma in all cases was about 6^{0}.

From the above result, it can be concluded that depth plays only one major role; namely, it controls the offset distance that corresponds to the peak amplitude of a given model. The deeper the depth, the greater the corresponding offset distance.

Multi-Layer vs Two-Layer Modeling

A four-layer earth model is studied here and compared to a two-layer earth model. The model is shown in Figure 5 with the target interface, as identified earlier, being Interface 1.

For the four-layer model, the RMS velocity to Interface 1 is held constant at 2100 m/s (average of observed stacking velocities). The thickness of Layer 1 is varied from 100 m to 140 m and the corresponding P velocity for that layer, called P1, is solved for in such a manner that the RMS velocity down to Interface 1 is constant. All other parameters, except for P1, are held constant as indicated in Figure 5. The P velocity in Layer 1, as a result, varied from 1850 m/s to 1918 m/s. The offset of peak reflection amplitude coming from Interface 1 was numerically determined for each thickness of overlying media by utilizing Zoeppritz' equations.

The same procedure was done for a two-layer case whose velocity down to the target interface was set equal to 2100 m/s. The depth to the target interface in the two-layer model was set equal to that of the four-layer model down to Interface 1.

The offset distance corresponding to the peak reflection amplitude was plotted against the thickness of

the overlying medium for the four-layer case as well as the two-layer case. The result in Figure 9 shows that the offset of the peak amplitude is linearly proportional to the thickness of the overlying medium for both cases. The main difference is that in the four-layer case, the corresponding offset is about 15 m greater on the average than that in the two-layer case.

If a two-layer model is assumed for depth calculations, instead of a four-layer model, the small difference between the two cases can be optimally overcome by normalizing the calculated depths to the known well depths.

Gamma Estimate and Effect of P-Velocity Variation

For the two-layer model previously mentioned, one can use Zoeppritz' equations to calculate the theoretical P and S reflected amplitudes as a function of incident angle (Chiburis, 1987, personal communication) for a plane P-wave source, as shown in Figure 10. The depth to the reflector was assumed to be 300 m. The P critical angle and the S critical angle are marked IP and IS respectively. It is clear from this plot that the second peak of the reflected P-wave lags the S-critical angle by about Gamma = 6^{0}. The densities in the first and second layer for this model are assumed to be 2.0 g/cc and 3.0 g/cc, respectively.

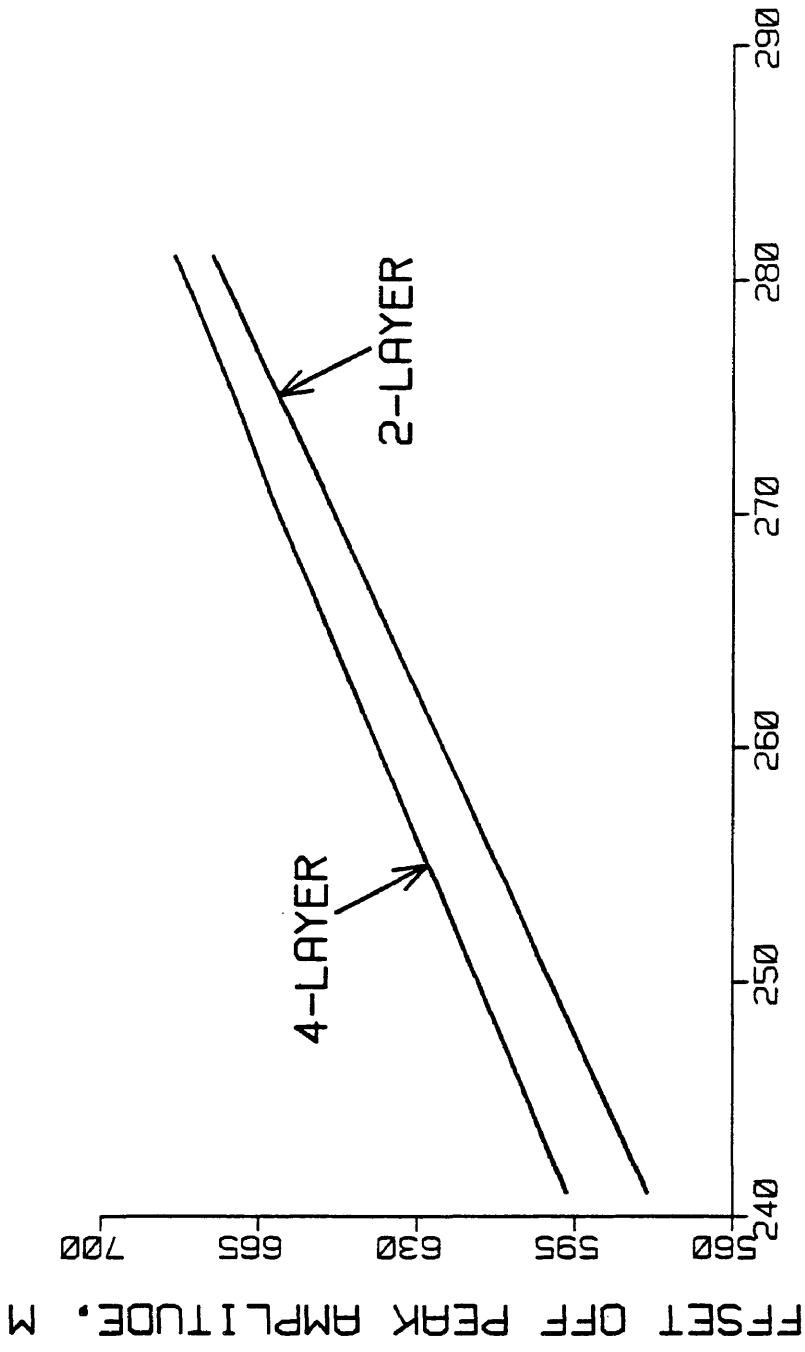

FIGURE 9. 2-LAYER AND 4-LAYER MODELING

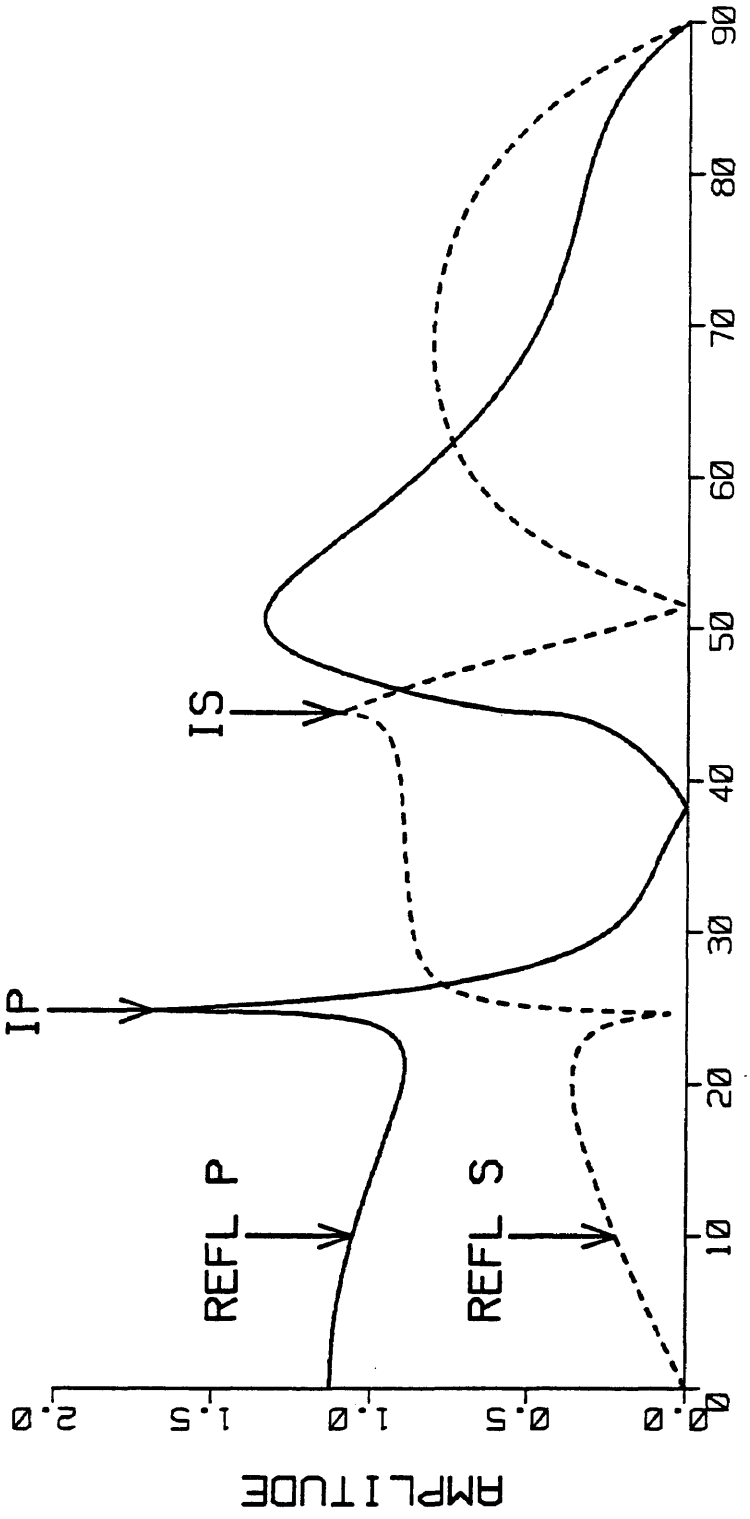

FIGURE 10 THEORETICAL REFLECTED AVO
P1=2100 SIG1=0.33 RHO1=2.0
P2=5000 S2=3000 RHO2=3.0

To investigate the sensitivity of Gamma to the various elastic constants, one has to decide which parameters should be held constant and which should be varied. Here, the depth is fixed at 300 m, the P-wave and the S-wave velocities in the second layer are held constant at 5000 m/s and 3000 m/s, respectively, and a Poisson's ratio of 0.33 is assumed for the first layer.

To study the effect of P-wave velocity in the first layer, P1 is varied from 1500 m/s to 3000 m/s. Note that P1 must be less than the S-wave velocity in the second layer, S2, in order for a shear-critical angle to exist. Theoretical plots of P-wave amplitude vs P-wave incident angle, with a variable P1 and all other elastic parameters held constant, are shown in Figure 11. Figure 12 shows a plot of Gamma vs velocity ratio P1/S2. It is clear from Figure 12 that Gamma is well behaved, and is nearly linear up to a velocity ratio of about 0.8.

The stacking velocities along the lines vary only by about 5%, with the minimum and maximum values being about 2000 m/s and 2350 m/s, respectively. If the stacking velocities are assumed proportional to P-wave velocities in the first layer, then the ratio of P1/S2 ranges from 0.67 to 0.78; a range in which Gamma is nearly constant with a value of about 6^{0} (see Figure 12).

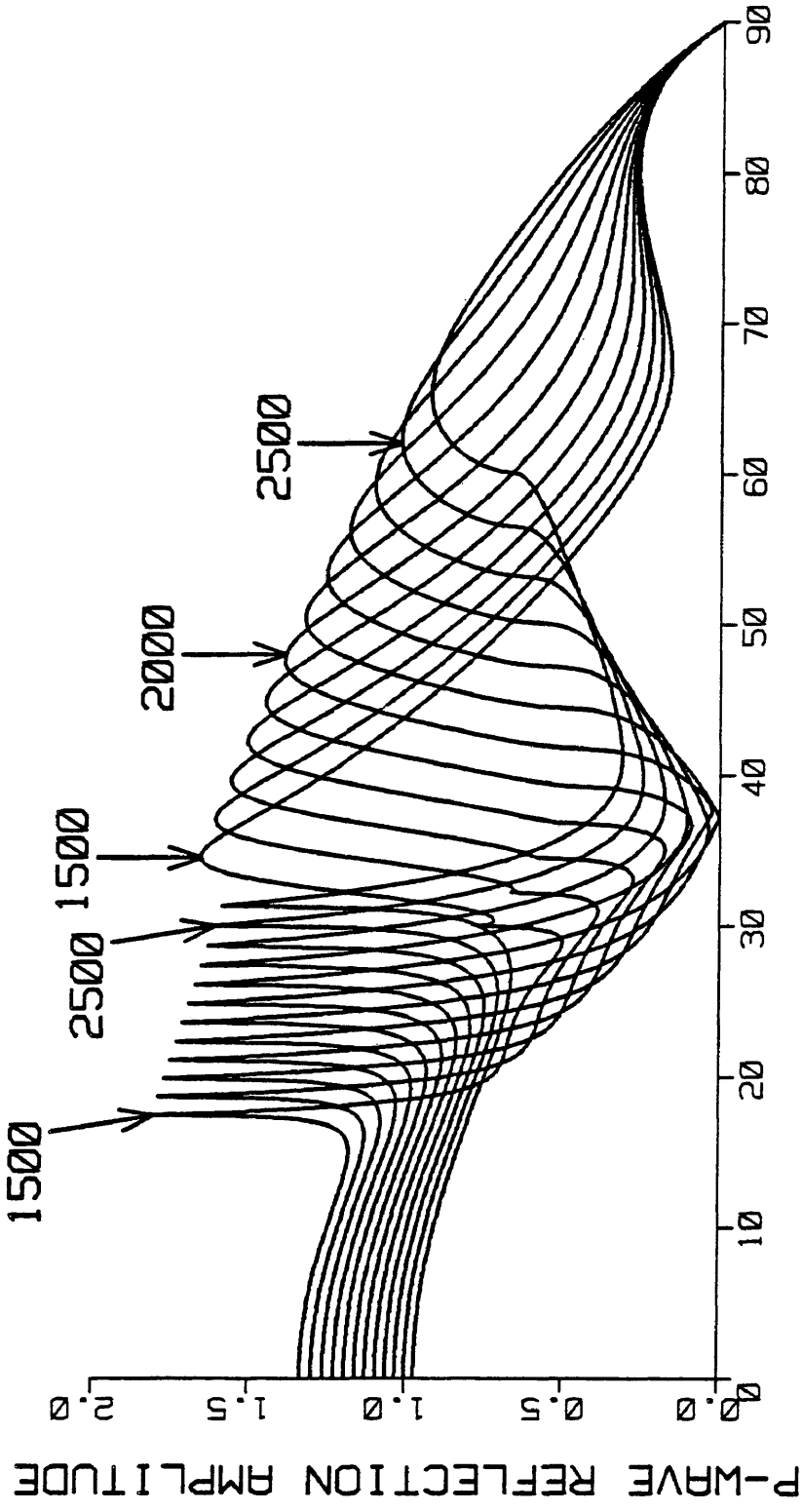

FIGURE 11. THEORETICAL AVO, P1 VARIABLE
SIG1=0.33 RHO1=2.0
P2=5000 S2=3000 RHO2=3.0 DEPTH=300

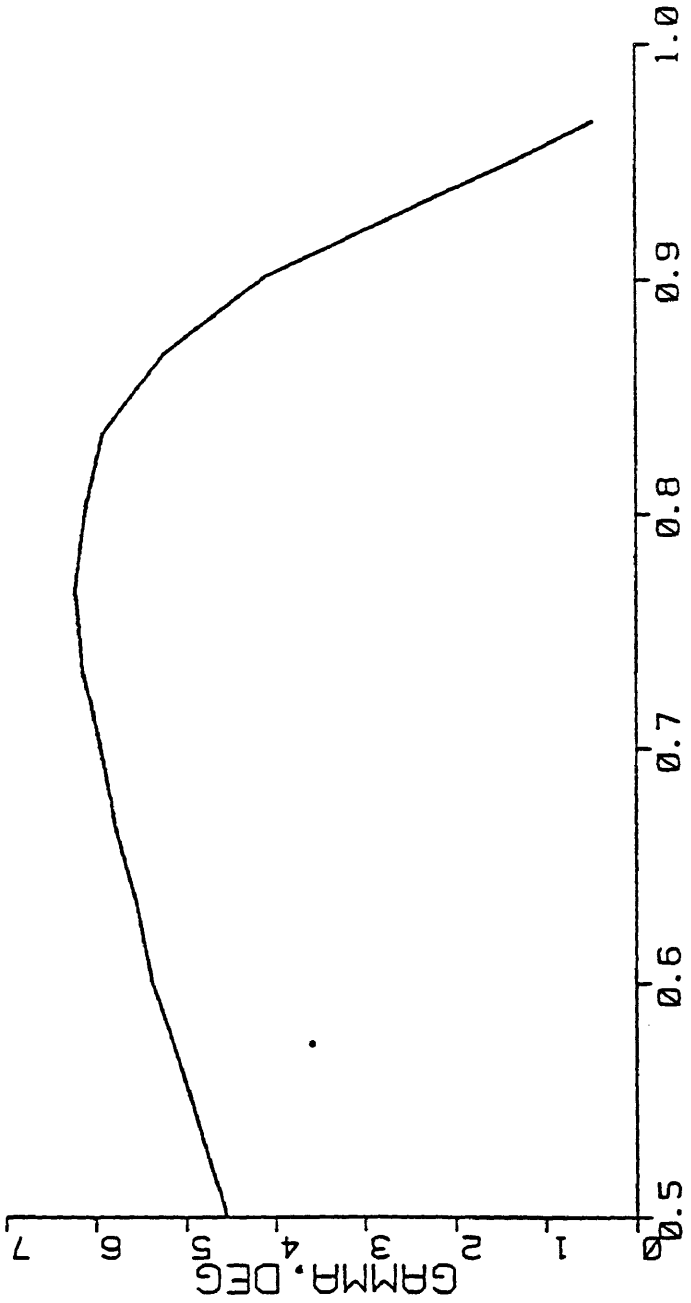

FIGURE 12. GAMMA STUDY, P1 VARIABLE.
SIG1=0.33 RHO1=2.0 DEPTH=300
P2=5000 S2=3000 RHO2=2.5

Therefore, for a two-layer earth model with the first layer having a P-wave velocity P1 and a Poisson's ratio of 0.33, and the second layer having a shear-wave velocity of 3000 m/s, the following points are concluded:

1. If P1 is constant and equal to the observed average stacking velocity along the lines (2100 m/s), then Gamma is about 6^{0}.
2. If P1 is changing drastically from the stated average stacking velocity, the angle Gamma is still fairly constant at about 6^{0}.

Effect of Density Variation on AVO

The AVO for the two-layer earth model is studied here with a variable density in either layer and all other elastic parameters held constant. To study variable density in the second layer, it was assumed that all parameters in the first layer are held constant, P1 = 2100 m/s, RHO1 = 2.0 g/cc, and Poisson's ratio, SIG1 = 0.33. In the second layer, P2 = 5000 m/s, S2 = 3000 m/s, and the depth to the second layer was assumed to be 300 meters.

Theoretical plots of amplitude vs P-wave incident angle are shown in Figure 13, with RHO2 varying from 1.0 g/cc to 4.0 g/cc with an increment of 0.5 g/cc. Even with such large and unrealistic variations in density, the post-critical amplitude peak shifted only about 5^{0} from the

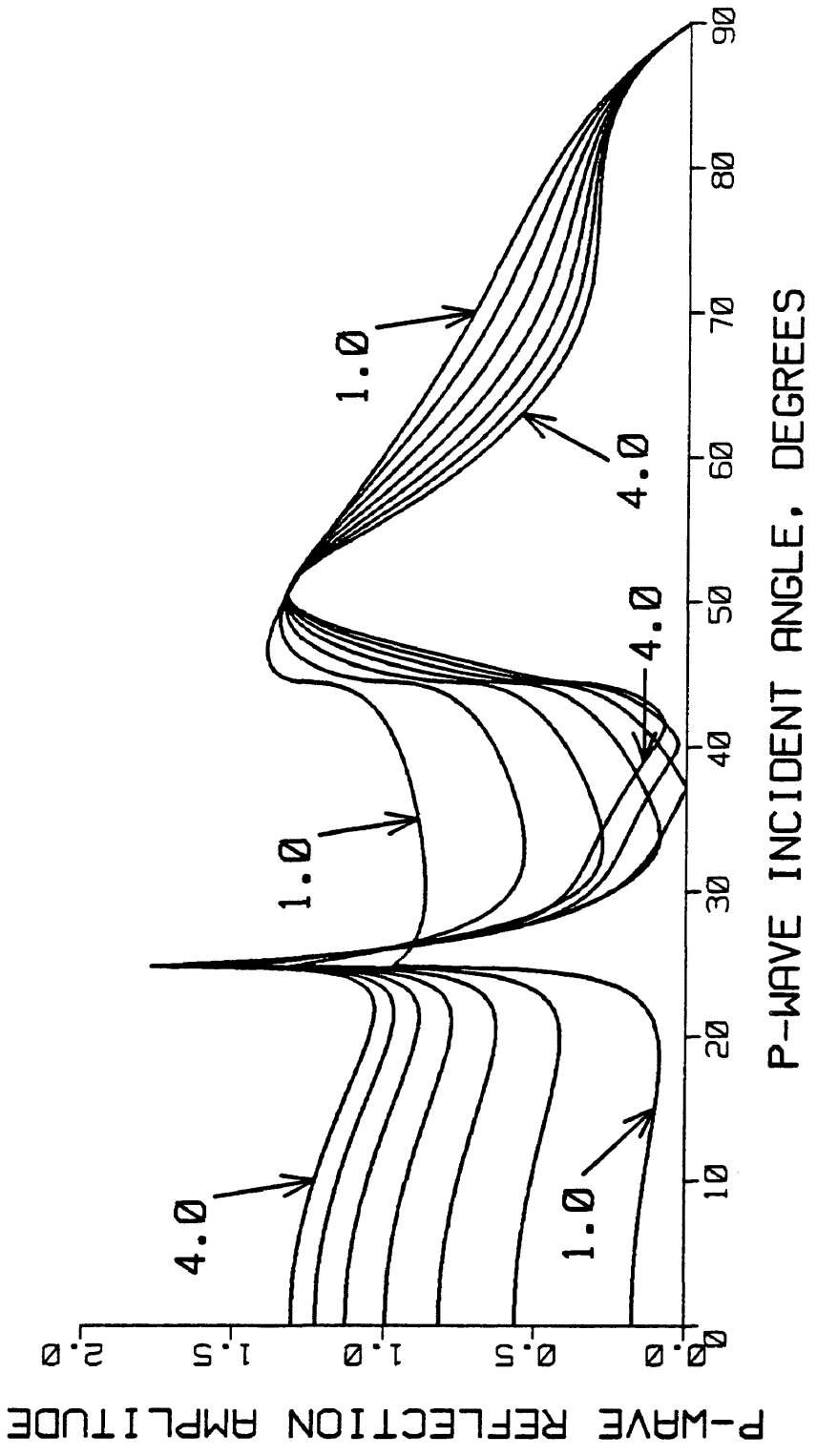

FIGURE 13. THEORETICAL AVO, RHO2 VARIABLE
P1=2100 SIG1=.33 RHO1=2
P2=5000 S2=3000 DEPTH=300

lowest density (1.0 g/cc) to the highest density (4.0 g/cc). It is obvious from these plots that the higher the density in the second layer, the larger the angle of secondary-peak response.

To see how Gamma changes with changing RHO1, Gamma was plotted against the ratio RHO2/RHO1 in Figure 14. Figure 15 is a plot of Gamma vs the ratio RHO2/RHO1 for the same model but with RHO2 variable and RHO1 constant at 2.0 g/cc. From Figures 14 and 15, it is clear that Gamma is in the range of 6^{0} for any reasonable ratio of RHO2/RHO1. The combination of a reasonable density ratio and a changing P velocity in the first layer (Figure 11) also results in about 6^{0} for Gamma. Hence, it can be concluded that Gamma is about 6^{0} for this particular two-layer model, for reasonable velocities and densities.

Final Depth Equation

The final depth equation, based on the results obtained, can be written as:

$$Z = X/(2 \text{ TAN } Q) \qquad (2)$$

where:

$Q = IS + Gamma$; and,

$IS = \text{ARCSIN } (P1/S2)$.

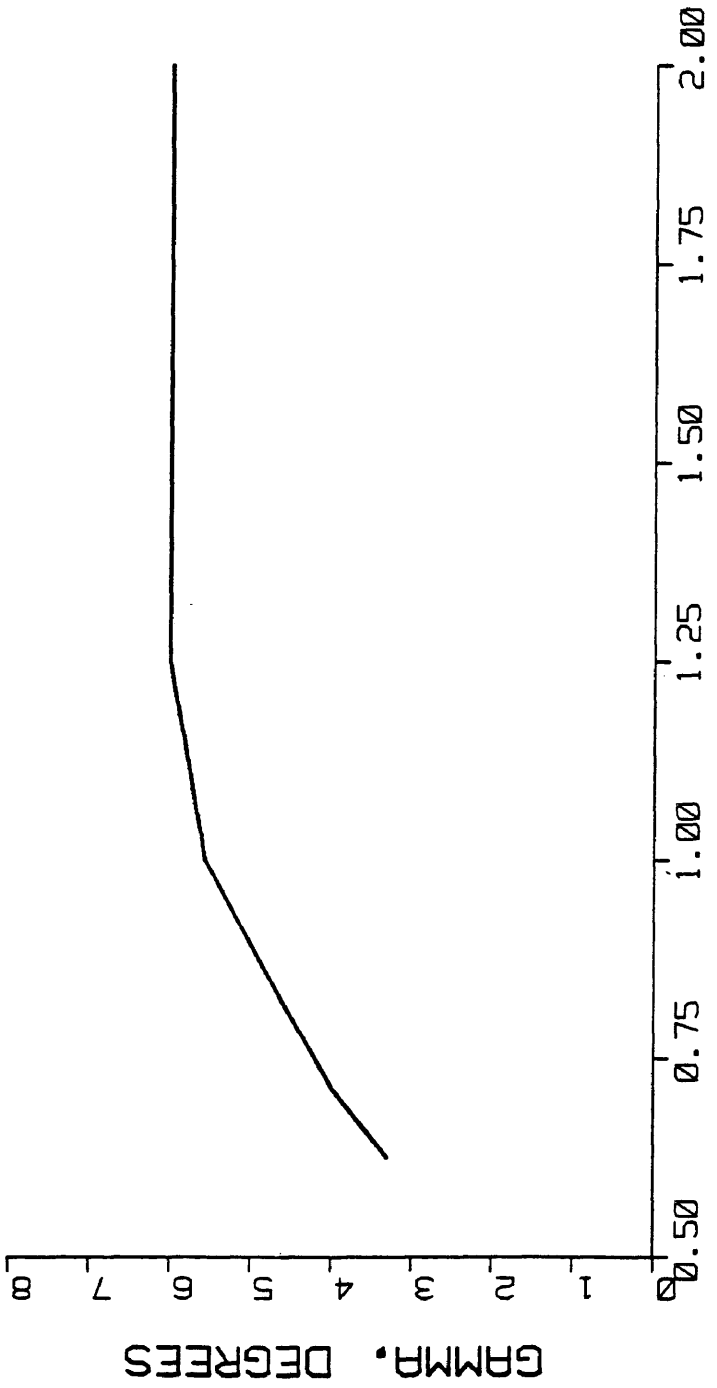

FIGURE 14. GAMMA STUDY, RHO1 VARIABLE
P1=2100 SIG1=0.33
P2=5000 S2=3000 RHO2=2.5

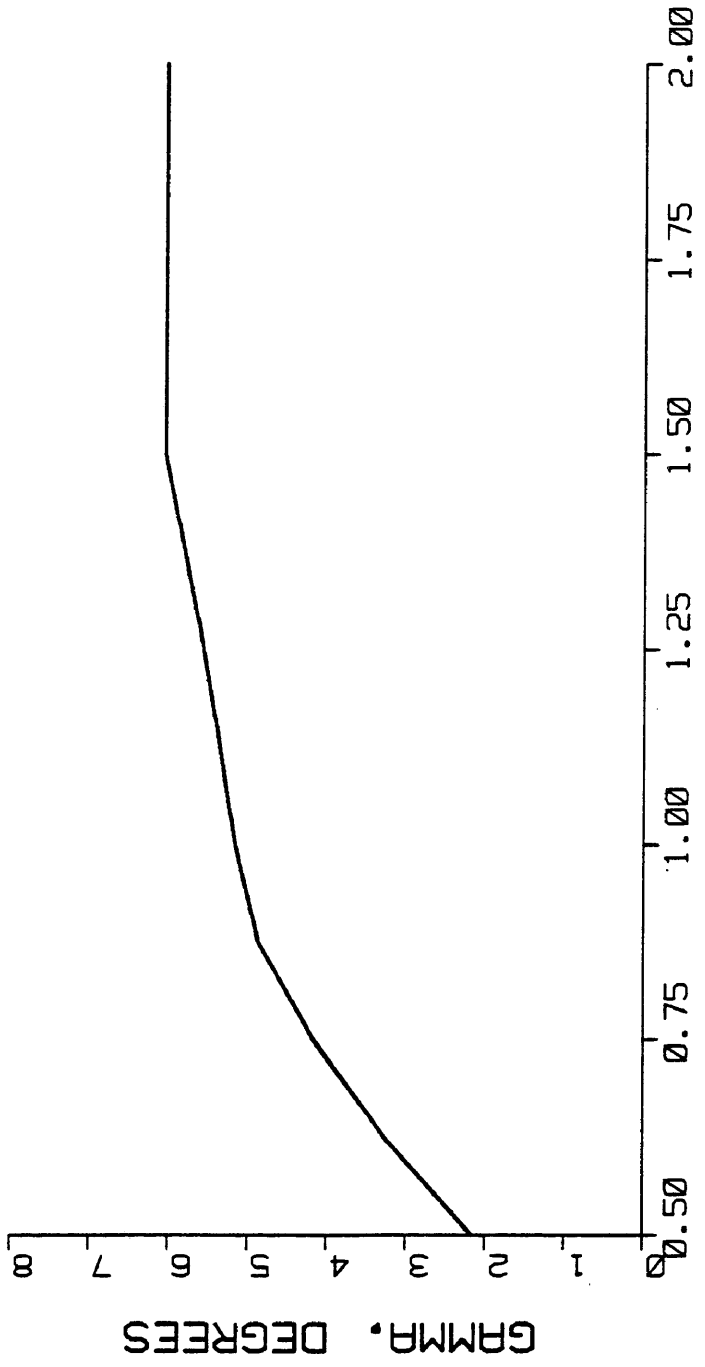

FIGURE 15. GAMMA STUDY, RHO2 VARIABLE
P1=2100 SIG1=0.33 RHO1=2.0
P2=5000 S2=3000

It is assumed that the layers are plane parallel with no appreciable dip; the earth model consists of two layers with the interface between the two layers being the target whose depth is to be calculated.

The symbols used in the above equations are defined as follows:

Z = depth;

Q = angle at which amplitude brightening occurs;

IS = shear-critical angle due to P-wave source;

Gamma = 6^{0};

P1 = P-wave velocity in the overlying medium; and

S2 = shear-wave velocity in the target medium.

CHAPTER FOUR

Results

Review

The final depth equation stated in the previous chapter, i.e. equation (2), was used for calculating depths from the AVO of the shot and CDP gathers. The depth was calculated along the two lines by assuming a constant shear velocity of 3000 m/s for the second layer (target formation). As a two-layer earth model was assumed, the P-wave velocity in the first layer, P1, was taken as the stacking velocity known for each gather.

The calculated depths were smoothed and/or tied to known well depths in many of the figures to come. Smoothing, when applied, was done in a three-point sense; the average of three consecutive depths was assigned to their corresponding middle point.

When calculated depths are tied to more than one well depth, the tie was done in such a way that the intervening calculated depths were scaled by linear interpolation.

Unless otherwise stated, the symbols (squares), in the figures, indicate actual depths to the target reflector determined from well logs. There are seven wells on Line 1 and three wells on Line 2.

Depths from Shot Gathers

Line 1. Figure 16 shows the calculated depths along Line 1 vs Shot Point. The mean error is 19.1 m whereas the RMS error is 9.7 m. The calculated depths are larger than the actual depths. The largest error, at Well 3, is 32.5 m; the smallest error, at Well 7, is 2.3 m. High spatial frequency content is noticeable on the plot.

Figure 17 shows the calculated depths tied to Well 1. The mean error is now 6.4 m, an improvement of 66.5%.

A smoothed version of the data shown in Figure 16 is shown in Figure 18 in which the average error is 19.8 m, and the high frequency content is reduced.

Figure 19 shows the smoothed version tied to Well 1. Figure 20 shows the smoothed version tied to Wells 1, 4, and 7. In Figure 20, the mean error is reduced to 3.1 m, as opposed to 19.1 m in Figure 16, an improvement of 83.8%. The largest error (9.5 m) occurred at Well 6; the smallest (2.8 m) at Well 5.

Line 2. Figure 21 shows the calculated depths for Line 2. The same data tied to Well 1 is shown in Figure 22, in which it can be seen that the calculated depths are again greater than those from well logs. The error at Well 2 is 45.5 m, and that at Well 3 is 100 m. A possible explanation

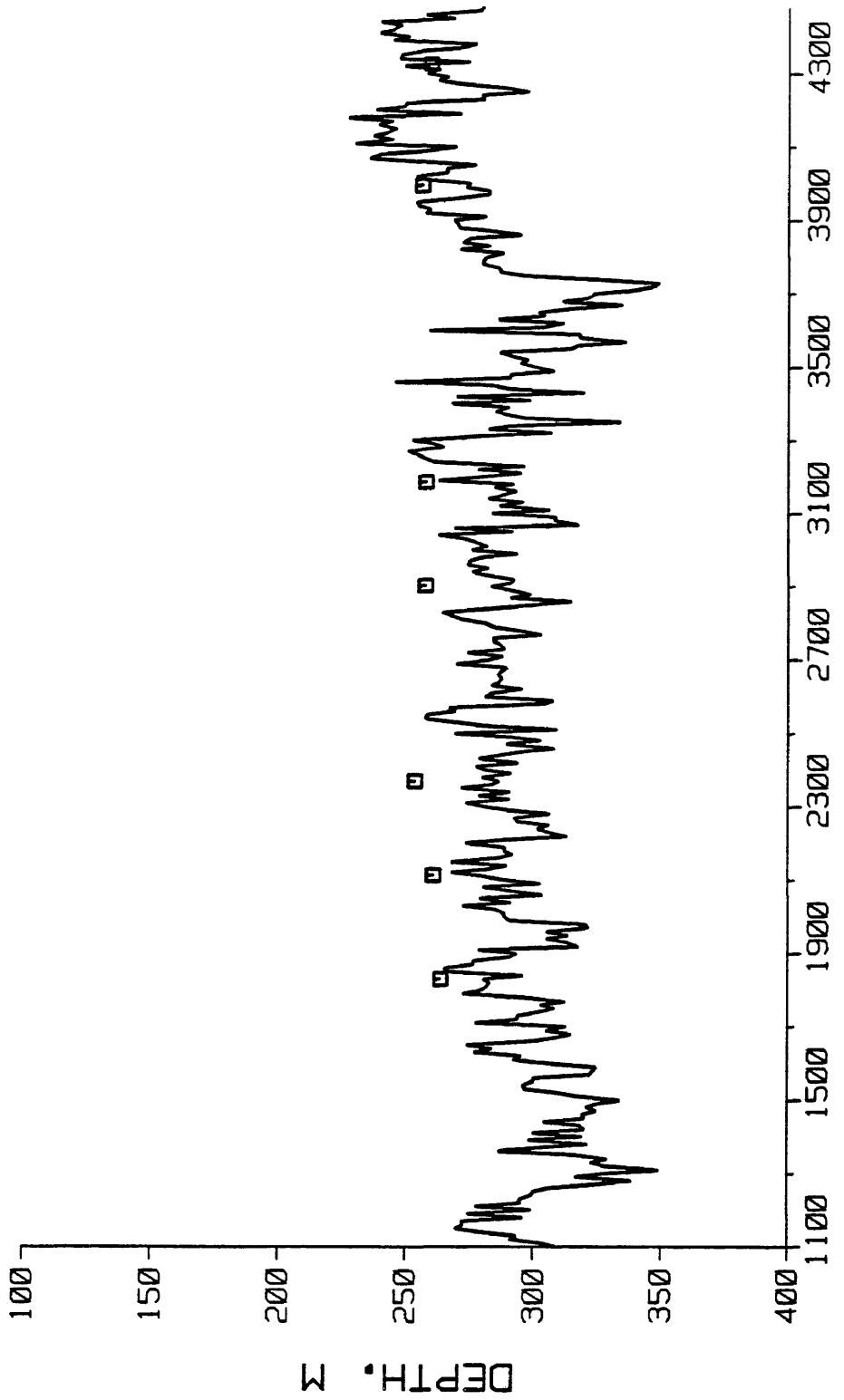

FIGURE 16. CALCULATED DEPTH, LINE 1, SHOT GATHERS.

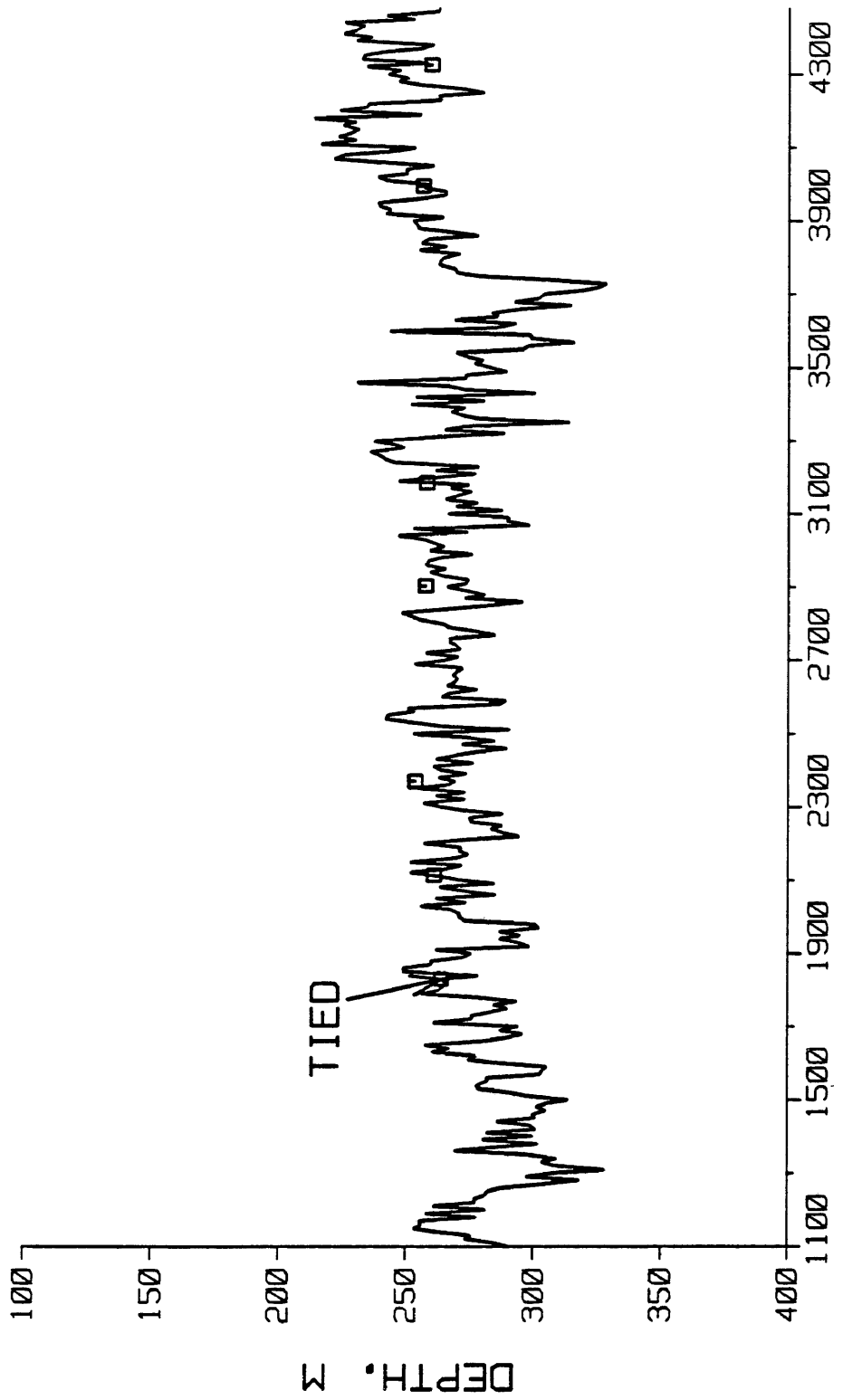

FIGURE 17. CALCULATED DEPTH, LINE 1, SHOT GATHERS. TIED TO WELL 1.

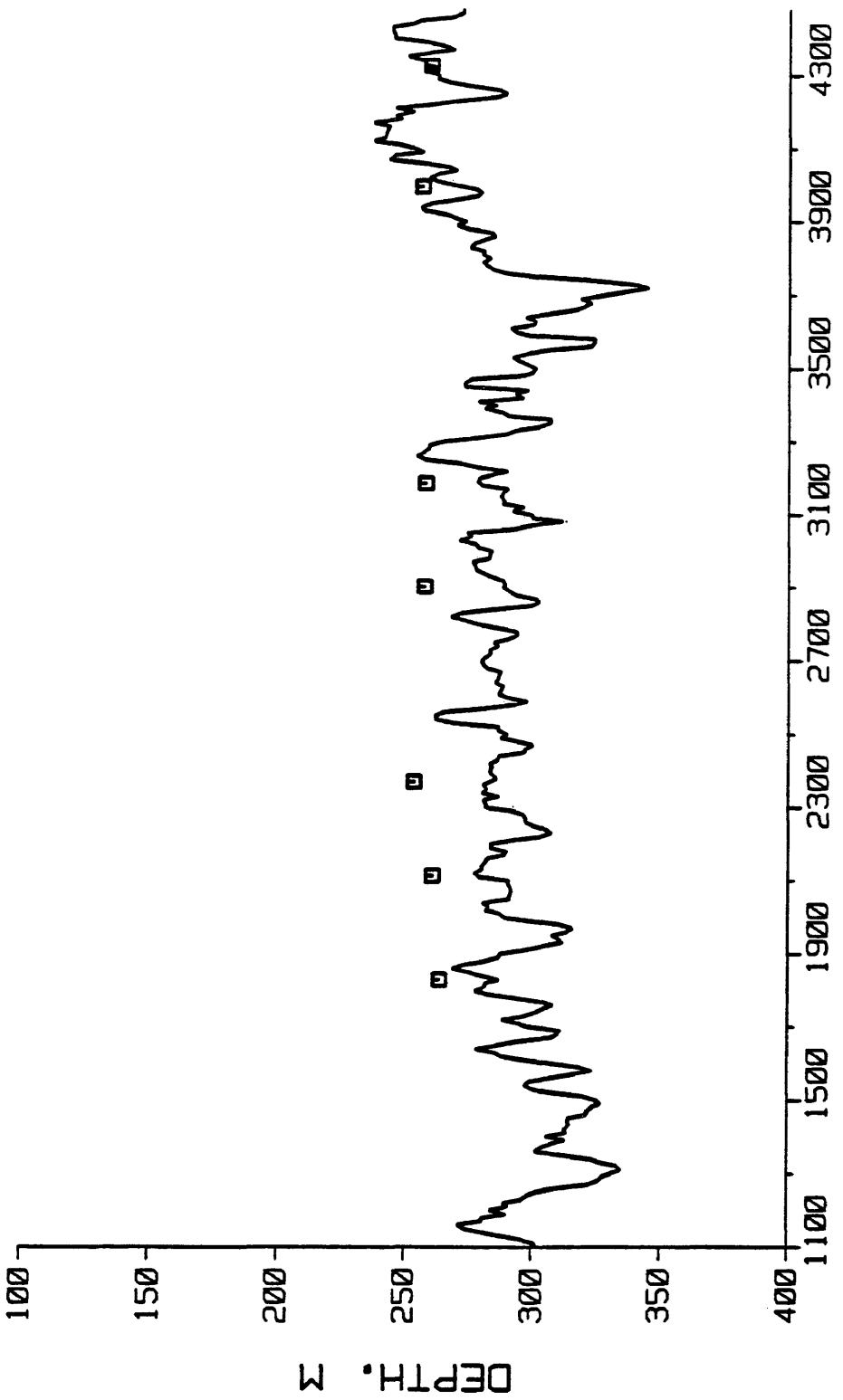

FIGURE 18. CALCULATED DEPTH, LINE 1, SHOT GATHERS. SMOOTHED.

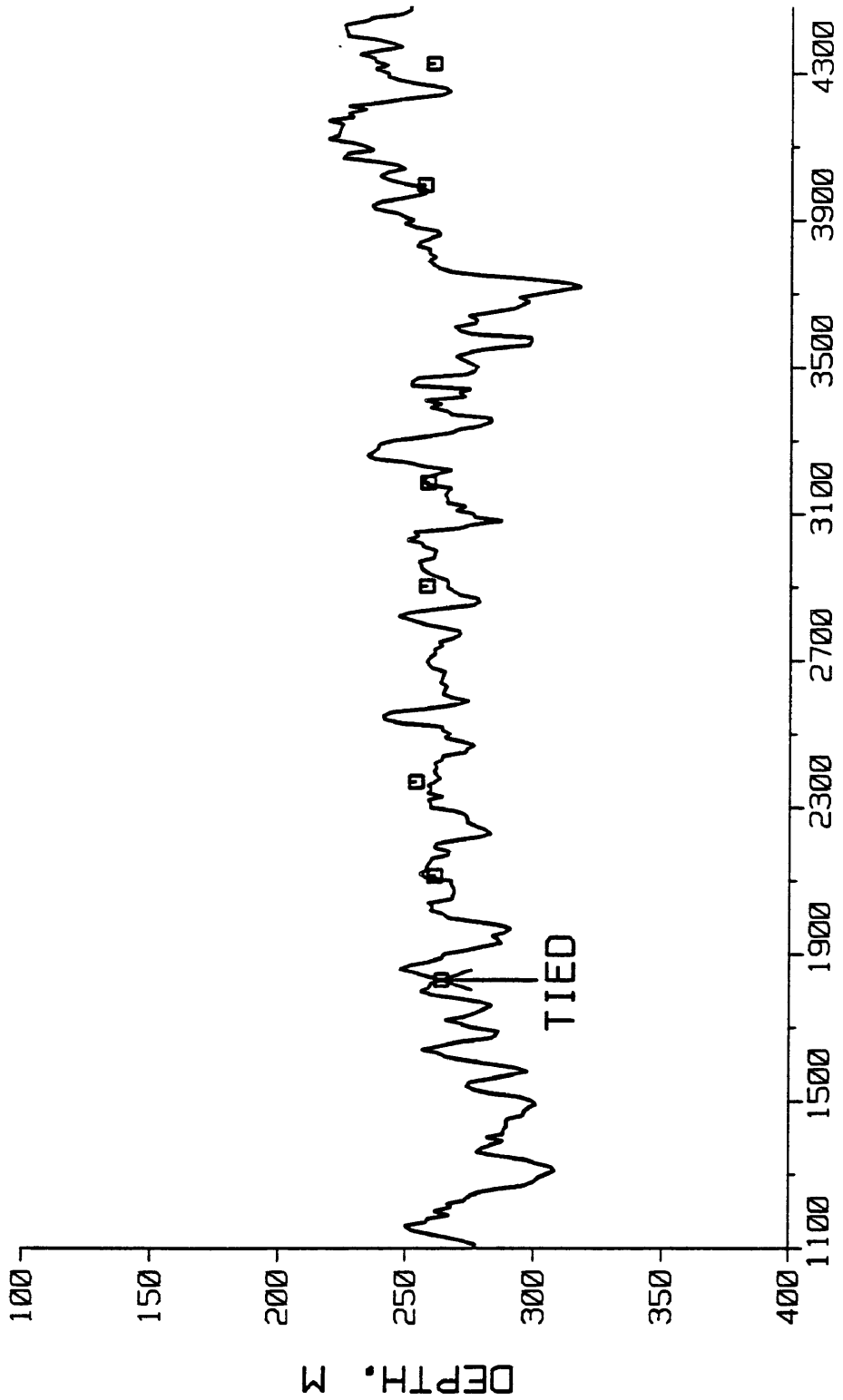

FIGURE 19. CALCULATED DEPTH, LINE 1, SHOT GATHERS. SMOOTHED; TIED TO WELL 1.

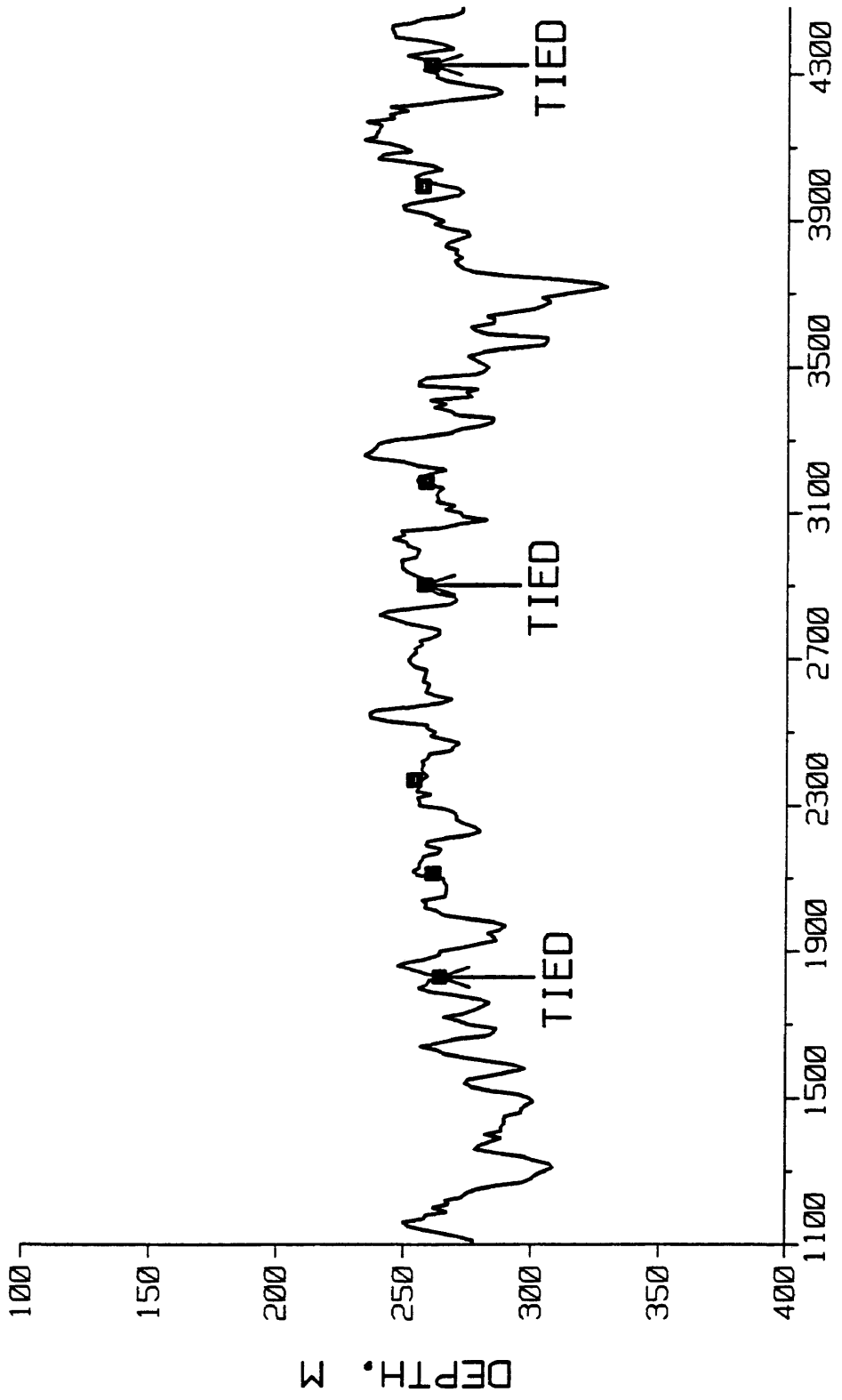

FIGURE 20. CALCULATED DEPTH, LINE 1, SHOT GATHERS. SMOOTHED; TIED TO WELLS 1, 4, AND 7.

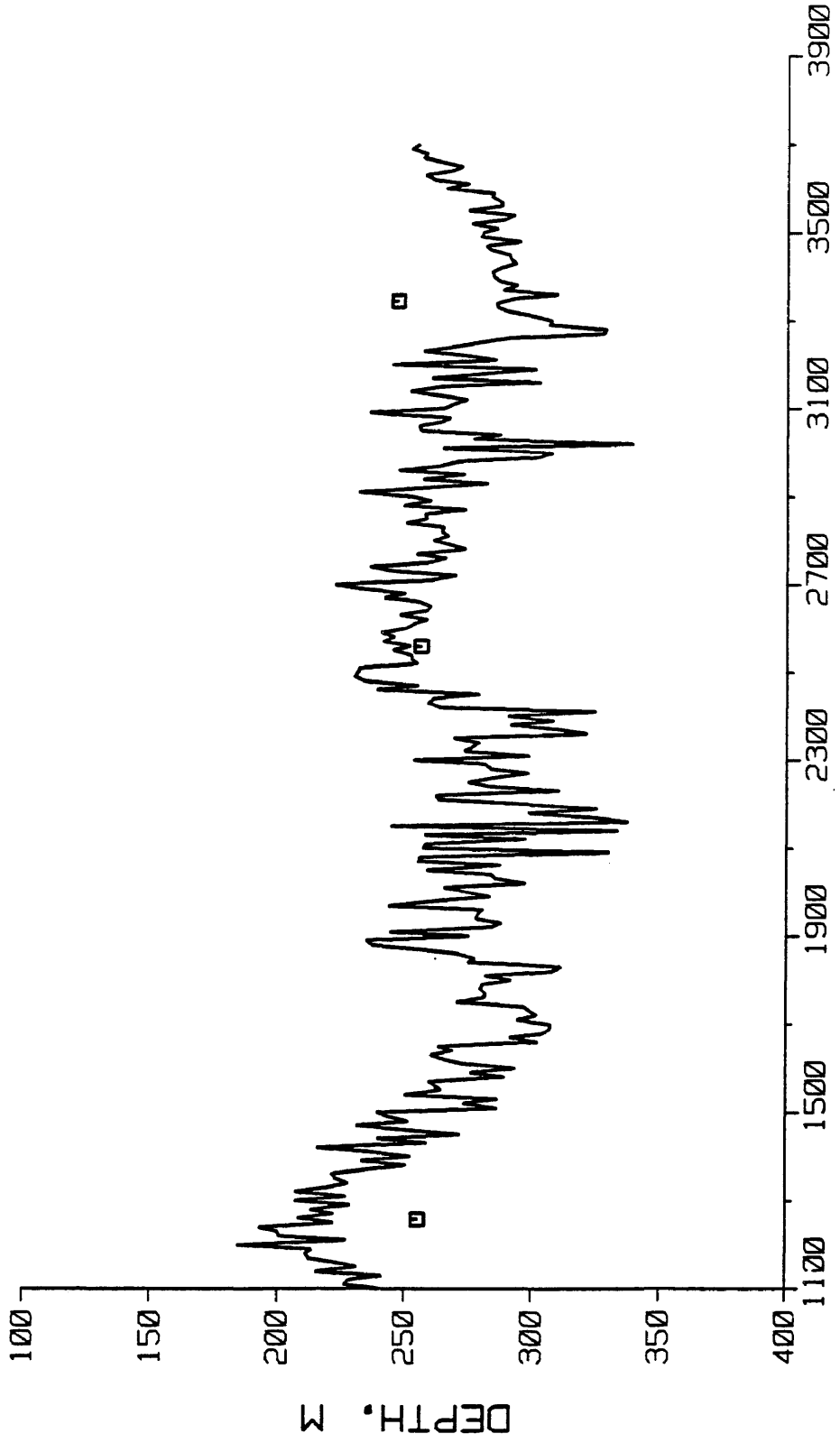

FIGURE 21. CALCULATED DEPTH, LINE 2, SHOT GATHERS.

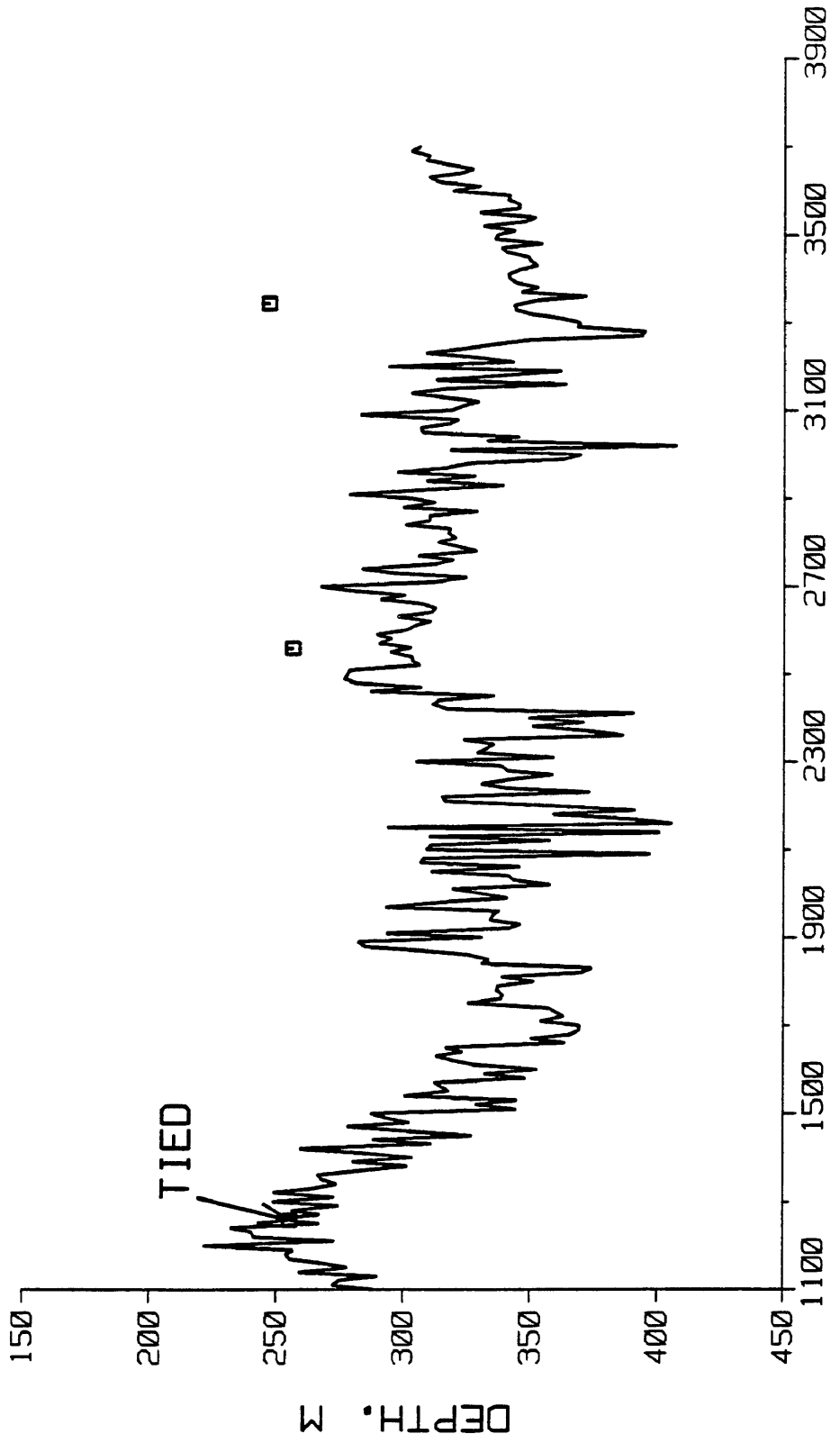

FIGURE 22. CALCULATED DEPTH, LINE 2, SHOT GATHERS. TIED TO WELL 1.

of this discrepancy, assuming that the model is approximately correct, is that the shear velocity of the target formation, S2, along Line 2 (dip line) is varying laterally.

Figure 23 is a smoothed version of the calculated, untied depths. The mean error from the smoothed version (tied to Well 1, Figure 24) is 45.6 m. When the smoothed depths are tied to Wells 1 and 3, the error at Well 2 is 15.7 m (Figure 25).

Shear Velocity, the Modeling Approach

The four-layer earth model shown in Figure 5 was considered for modeling in order to come up with an estimate to the shear velocity. It is assumed here that the discrepancies between the calculated and the actual depths were due to variations in shear velocities. The thickness and the P-velocity in the first layer were determined in such a way that the actual depth to the target reflector and the stacking velocity (taken as RMS velocity) were satisfied for each well.

Theoretical plots of amplitude vs offset were generated for each well by interactively assuming values of shear velocities for the target reflector. Once a theoretical offset of maximum amplitude matched that observed on the

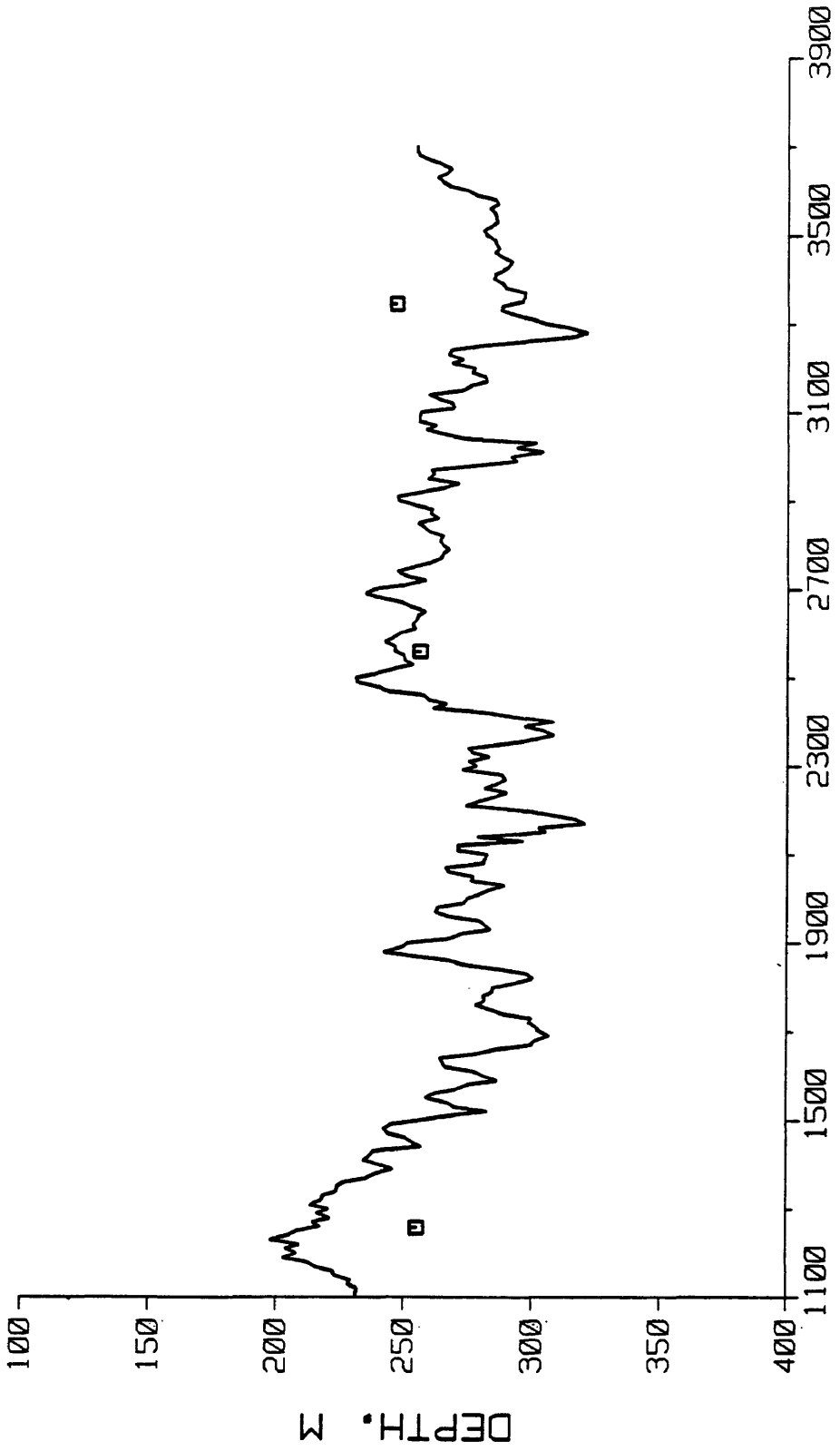

FIGURE 23. CALCULATED DEPTH. LINE 2. SHOT GATHERS. SMOOTHED.

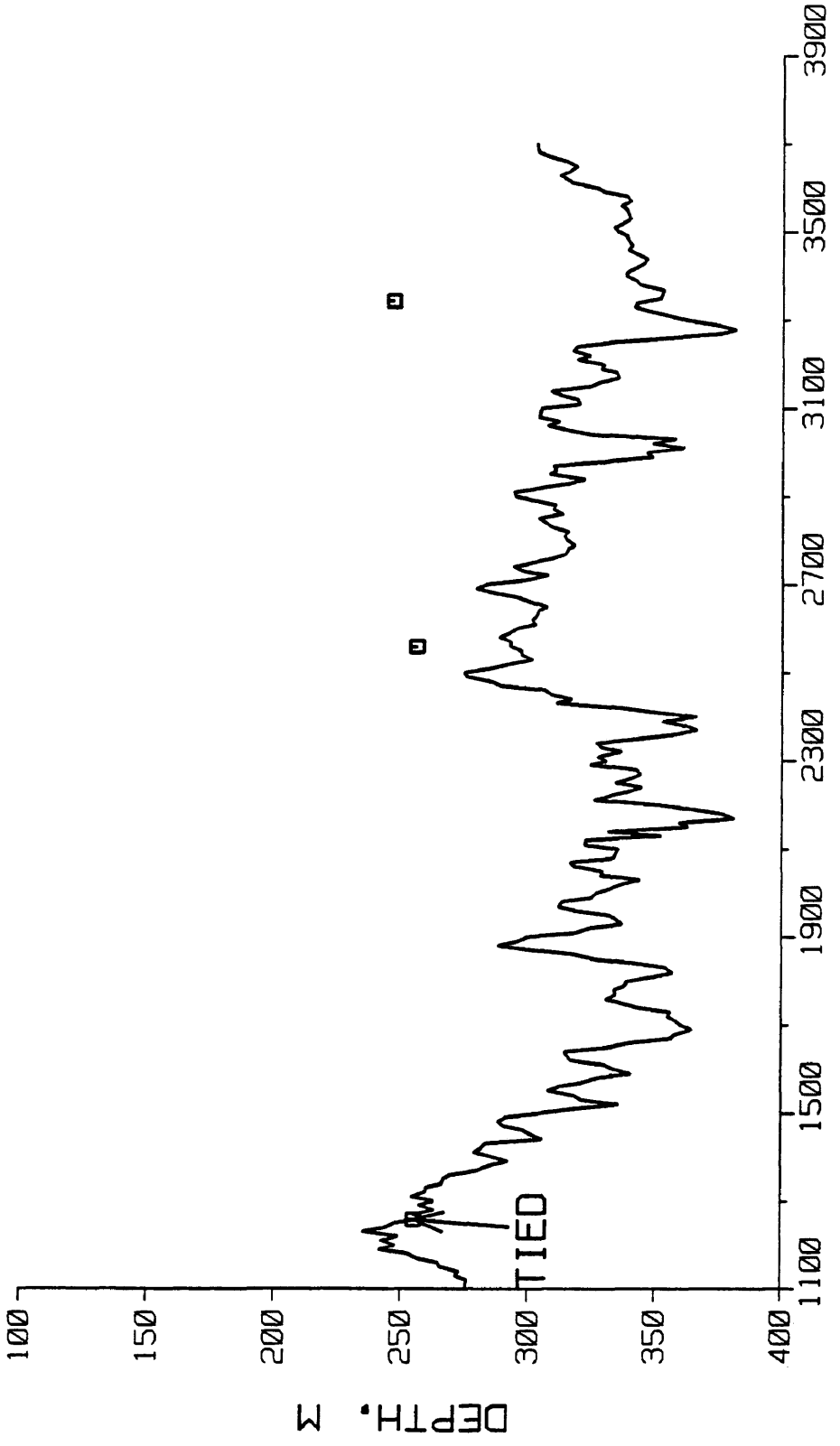

FIGURE 24. CALCULATED DEPTH, LINE 2, SHOT GATHERS. SMOOTHED, TIED TO WELL 1.

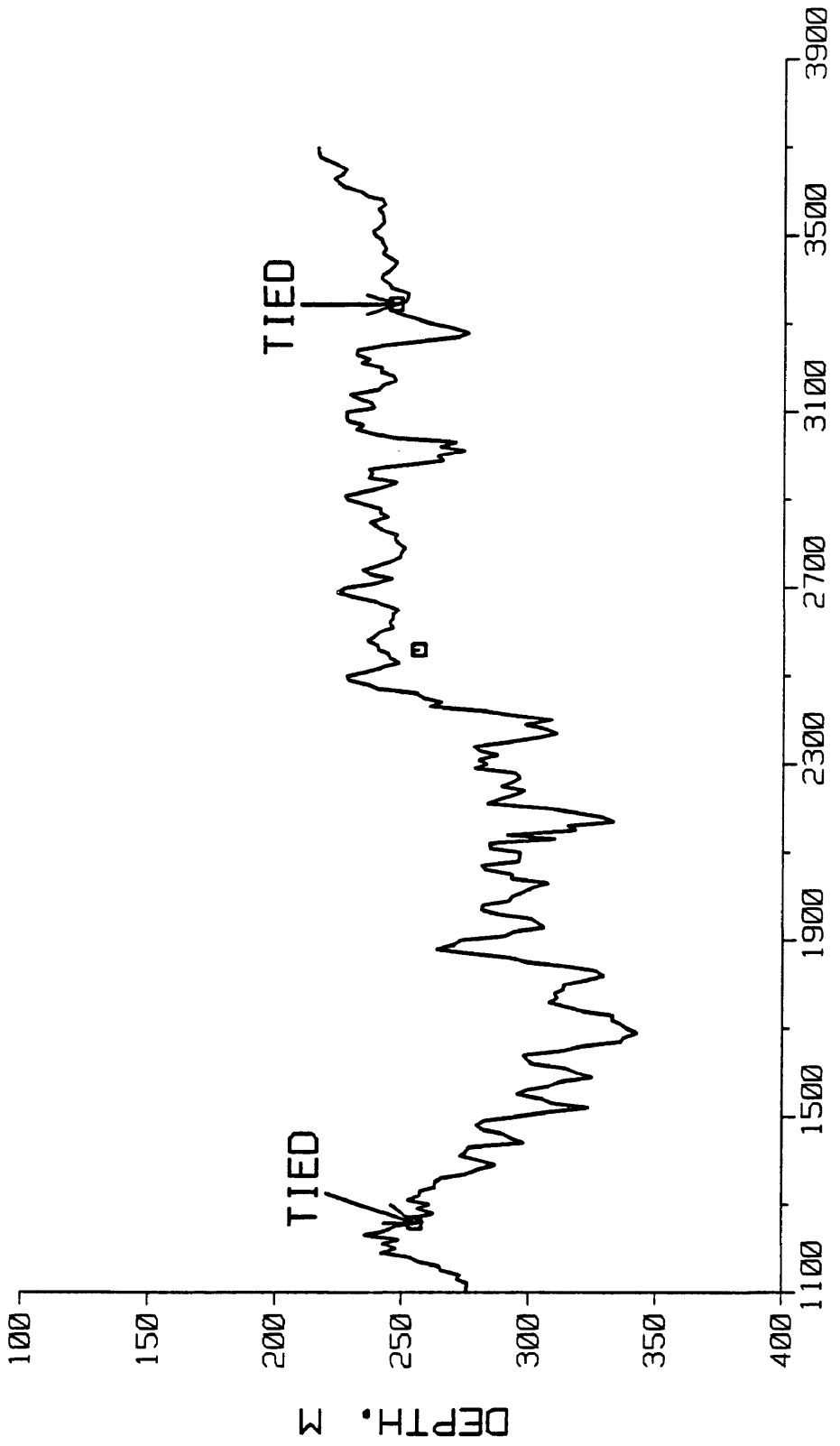

FIGURE 25. CALCULATED DEPTH, LINE 2, SHOT GATHERS. SMOOTHED, TIED TO WELLS 1 AND 3.

corresponding shot gather for each well, an estimate of the shear velocity was obtained.

Figures 26 through 32 compare the theoretical and the actual AVO plots for the seven wells along Line 1. Figures 33 through 35 show the same results for Line 2. Table 3 lists the results of the estimated shear velocities along the two lines.

Table 3. Estimated Shear Velocities.

Line 1			Line 2		
Well	Shot Point	Shear Vel., m/s	Well	Shot Point	Shear Vel., m/s
1	1830	2925	1	1260	3320
2	2110	2950	2	2560	3020
3	2370	2940	3	3340	2830
4	2900	2950			
5	3180	2900			
6	3990	2950			
7	4320	3110			

The offsets corresponding to maximum amplitudes seen on the data around each well, along with the parameters assumed for the first layer of the model, are listed against the offsets of maximum amplitude obtained by modeling in Tables 4 and 5. P1 and h1 are the P-velocity and the thickness in the first layer, respectively.

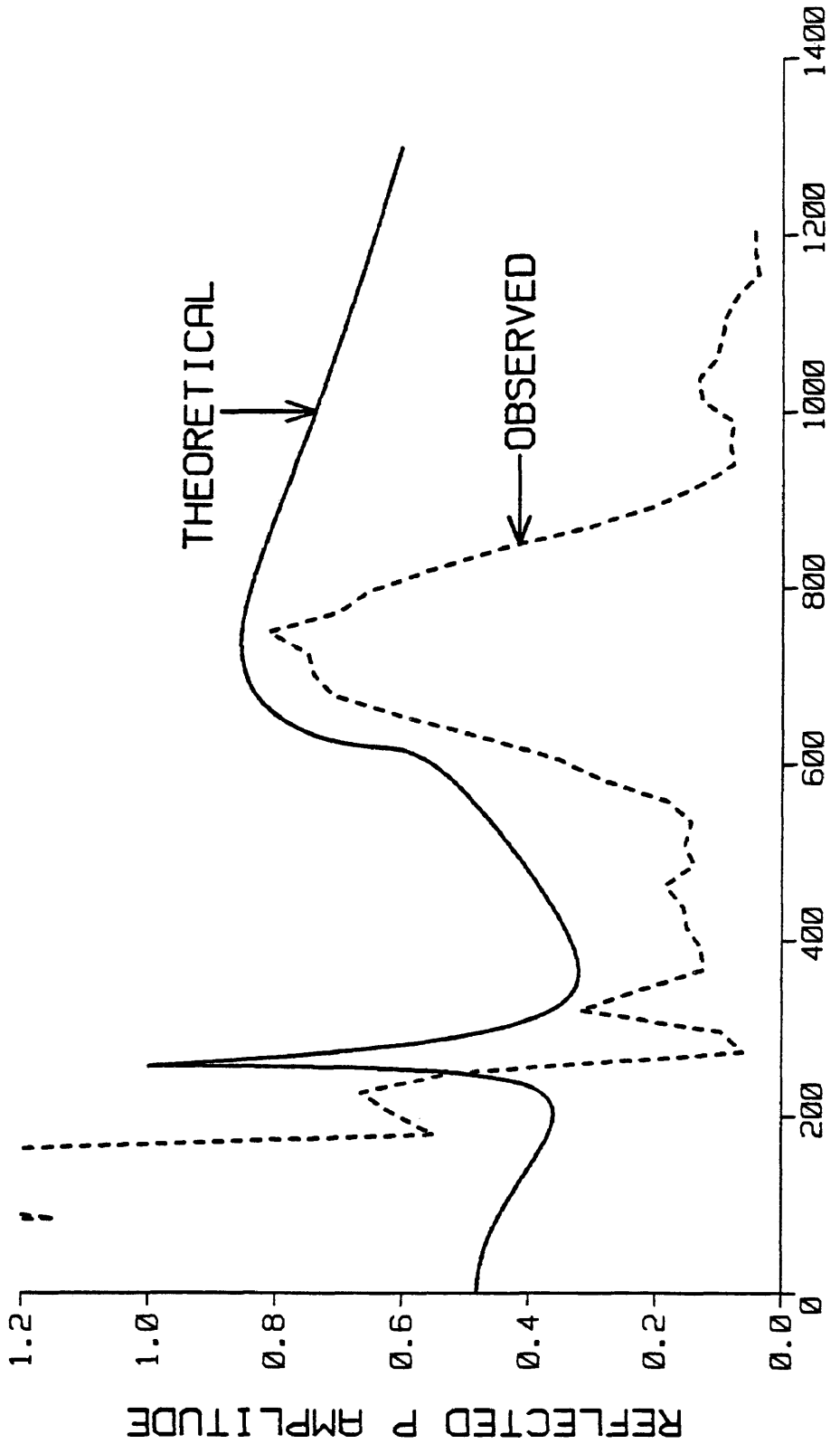

FIGURE 26. OBSERVED AND THEORETICAL AVO.
LINE 1 WELL 1 SHEAR VEL=2925

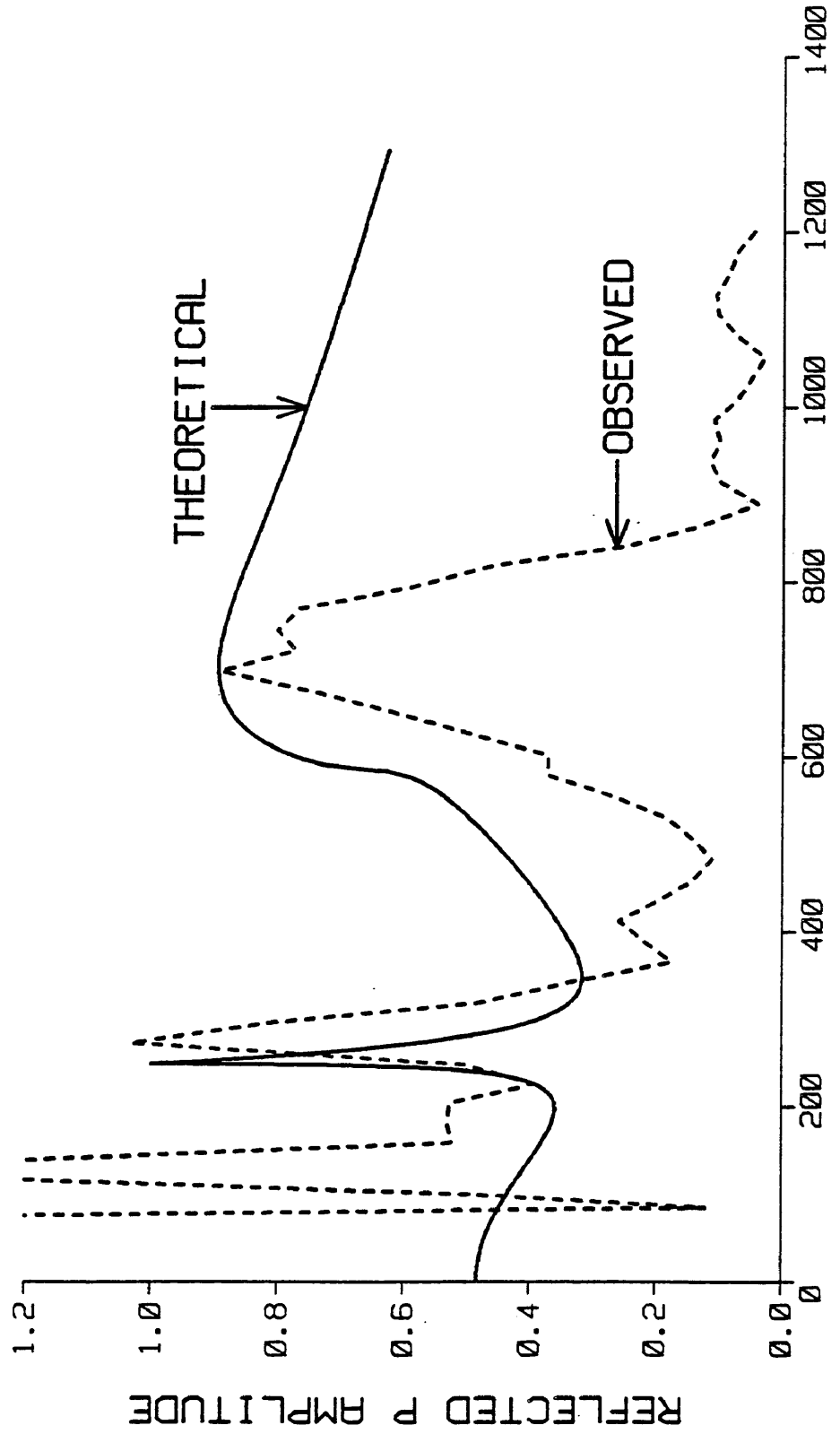

FIGURE 27. OBSERVED AND THEORETICAL AVO.
LINE 1 WELL 2 SHEAR VEL=2950

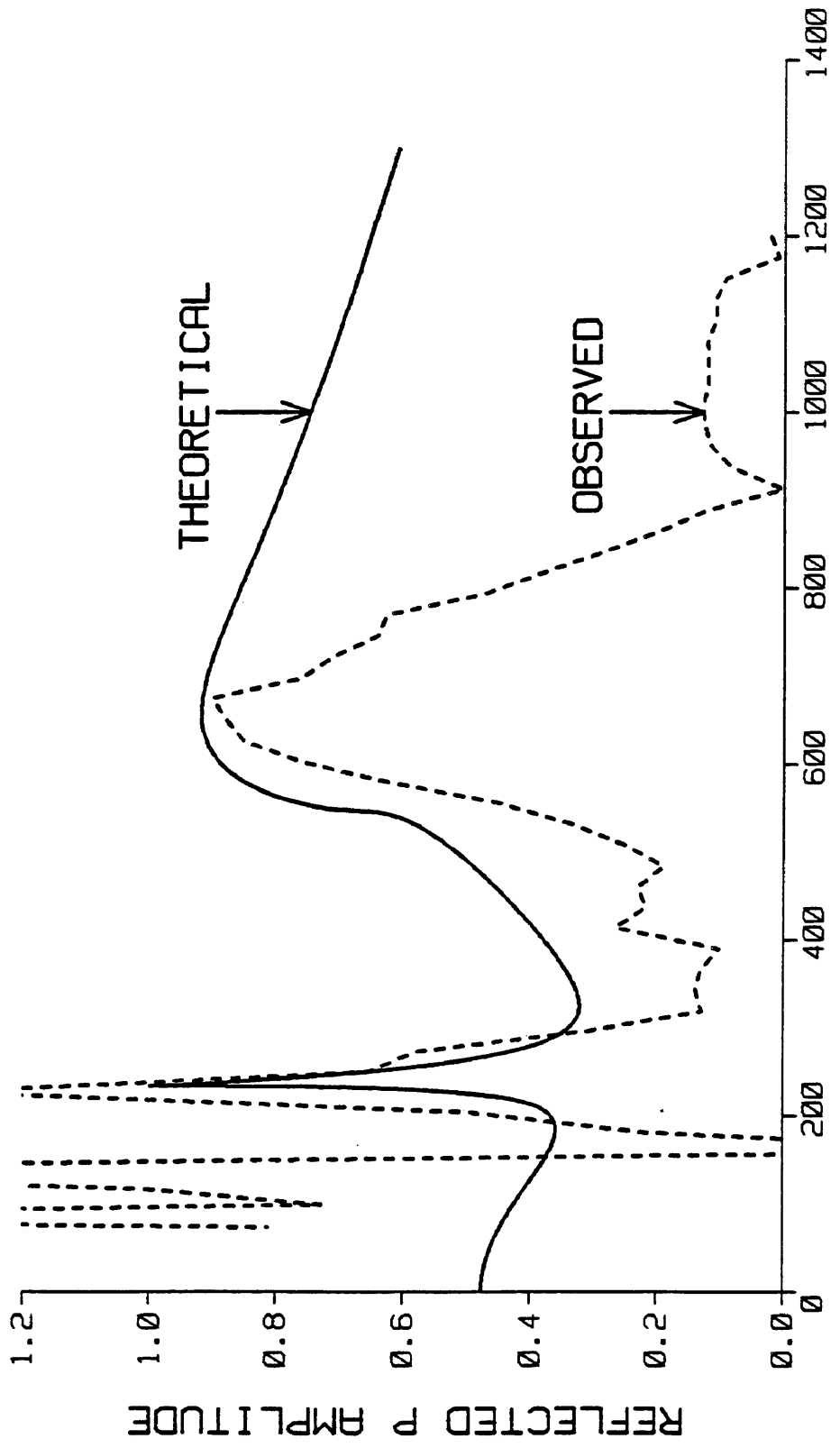

FIGURE 28. OBSERVED AND THEORETICAL AVO.
LINE 1 WELL 3 SHEAR VEL=2940

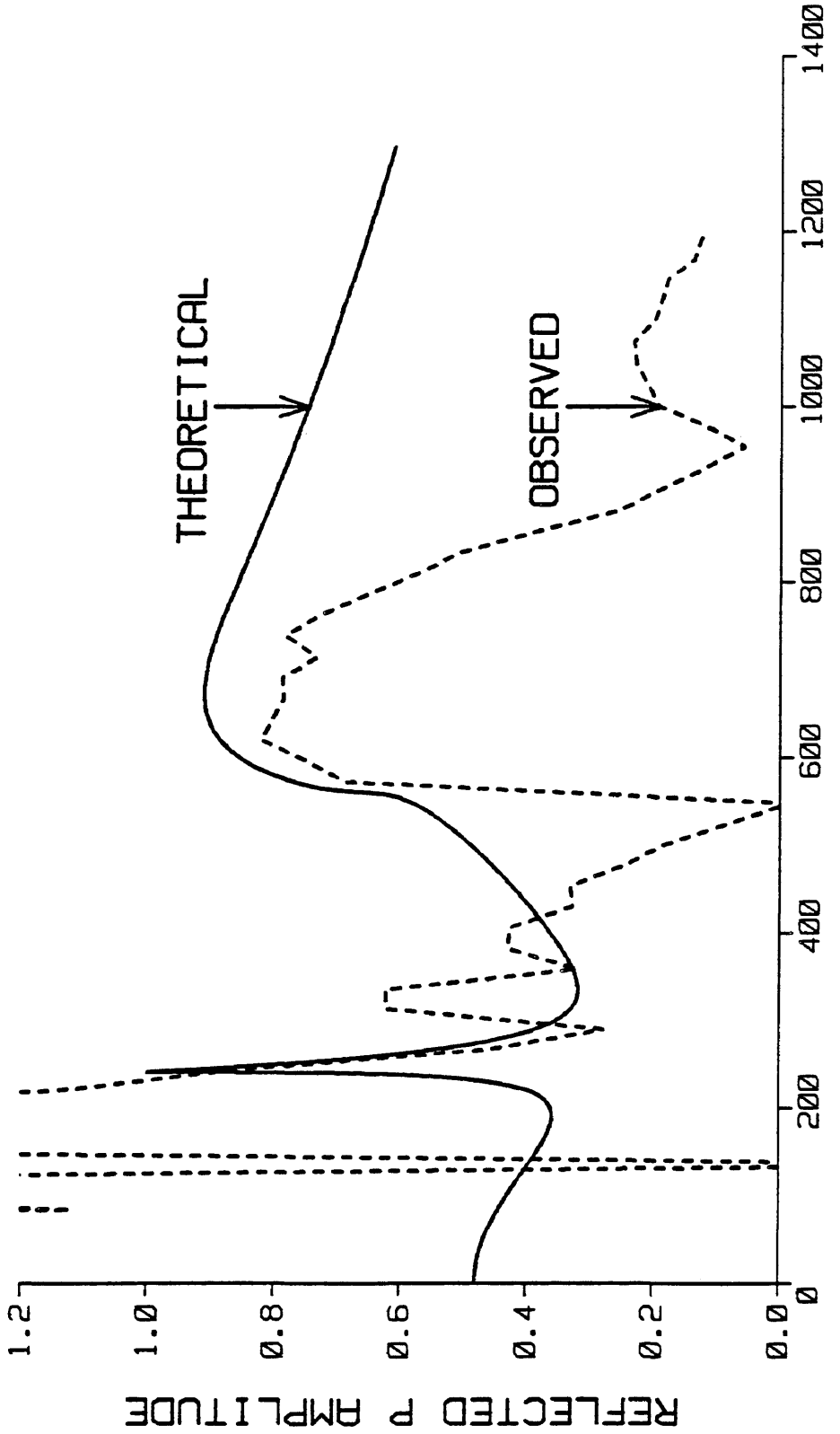

FIGURE 29. OBSERVED AND THEORETICAL AVO.
LINE 1 WELL 4 SHEAR VEL=2950

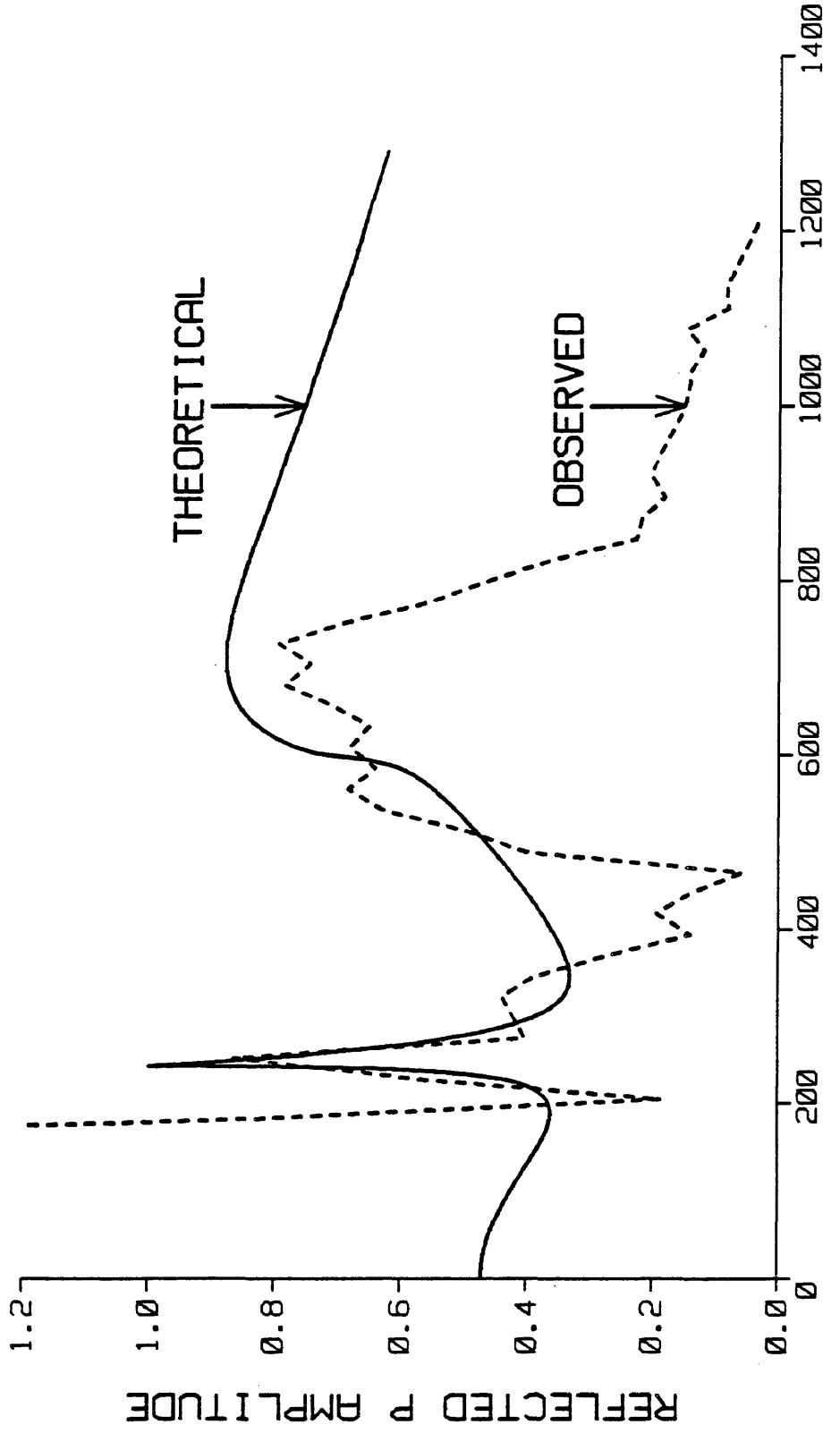

FIGURE 30. OBSERVED AND THEORETICAL AVO.
LINE 1 WELL 5 SHEAR VEL=2900

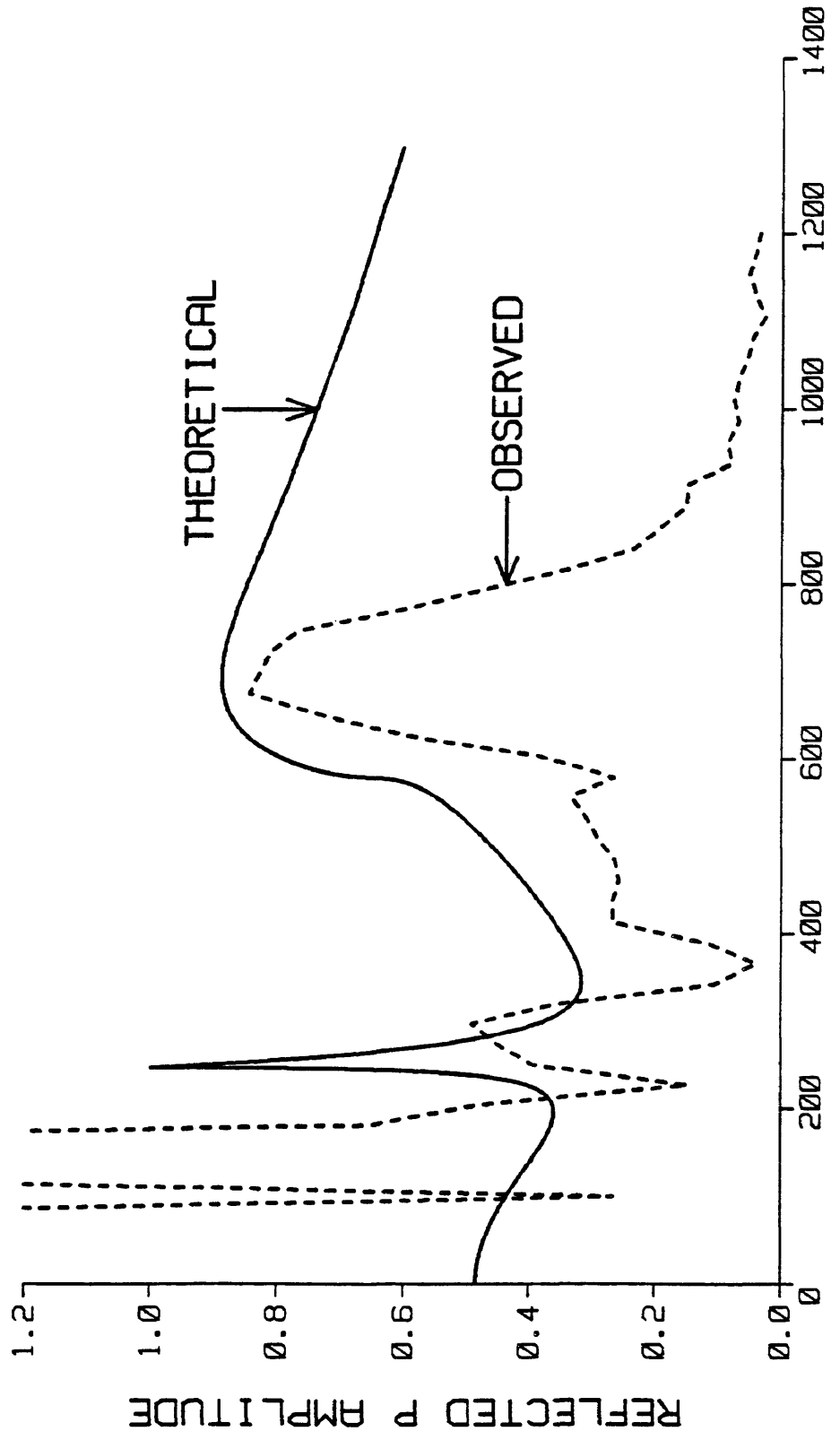

FIGURE 31. OBSERVED AND THEORETICAL AVO.
LINE 1 WELL 6 SHEAR VEL=2950

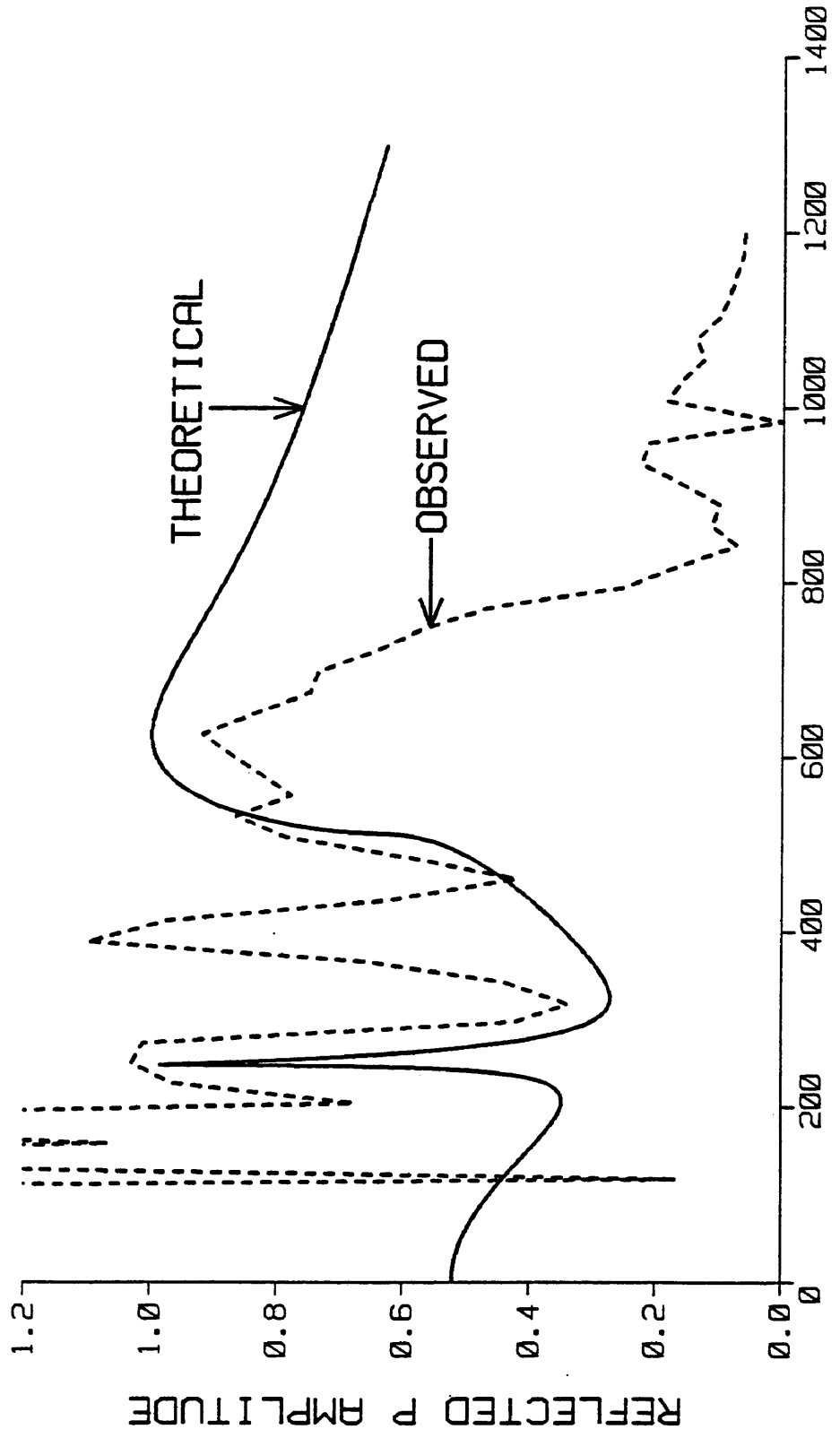

FIGURE 32. OBSERVED AND THEORETICAL AVO.
LINE 1 WELL 7 SHEAR VEL=3110

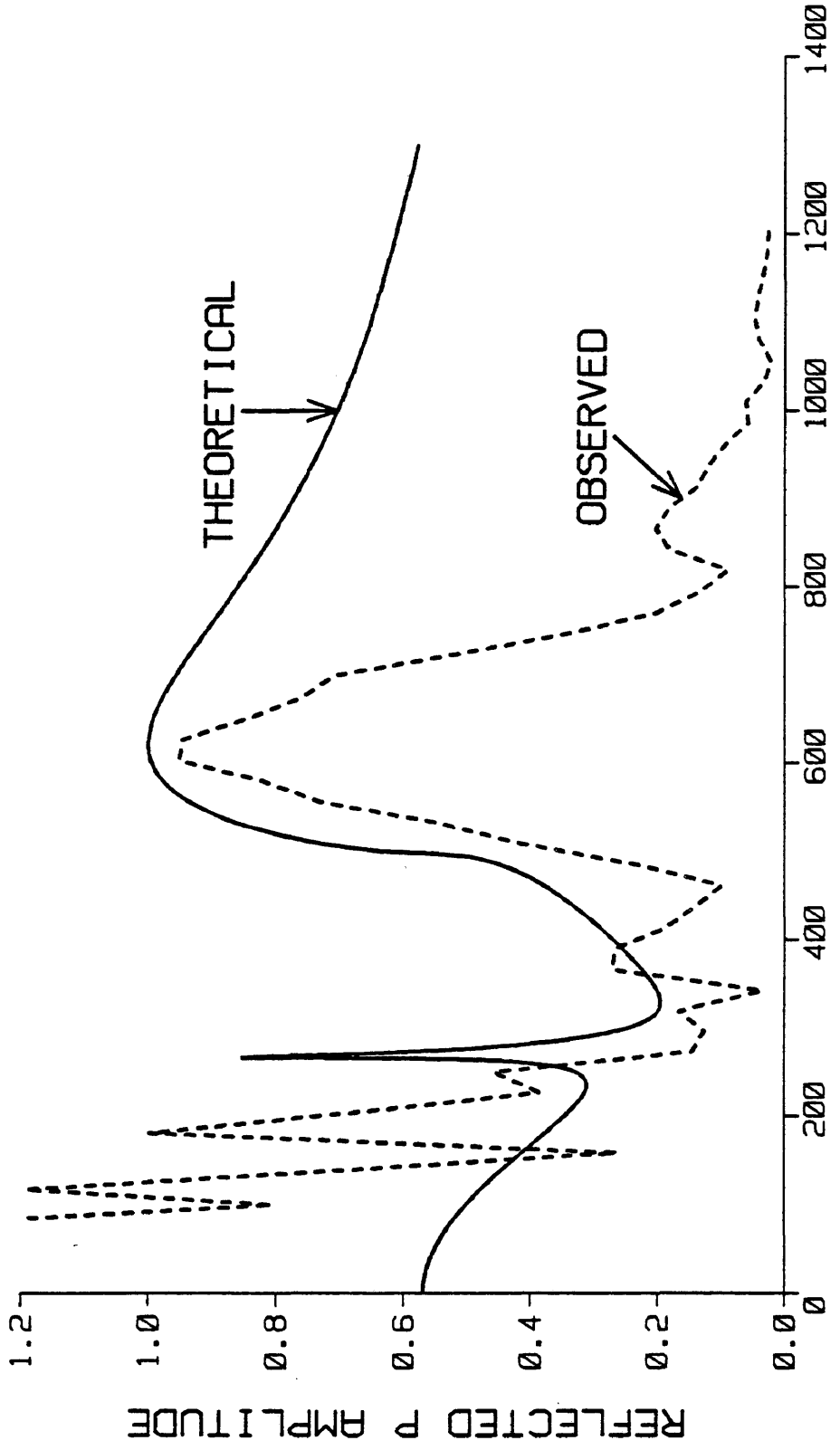

FIGURE 33. OBSERVED AND THEORETICAL AVO.
LINE 2 WELL 1 SHEAR VEL=3320

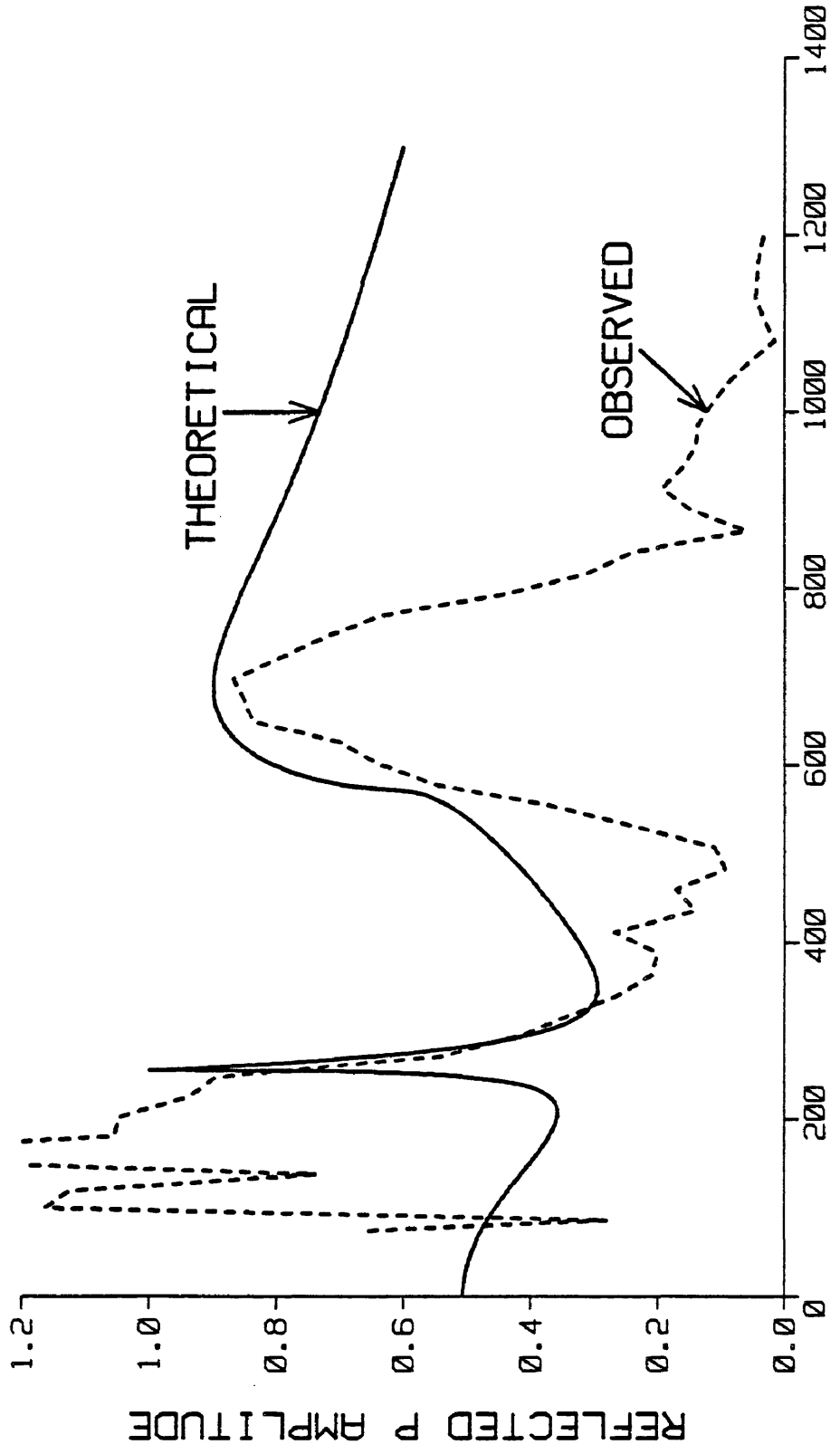

FIGURE 34. OBSERVED AND THEORETICAL AVO.
LINE 2 WELL 2 SHEAR VEL=3020

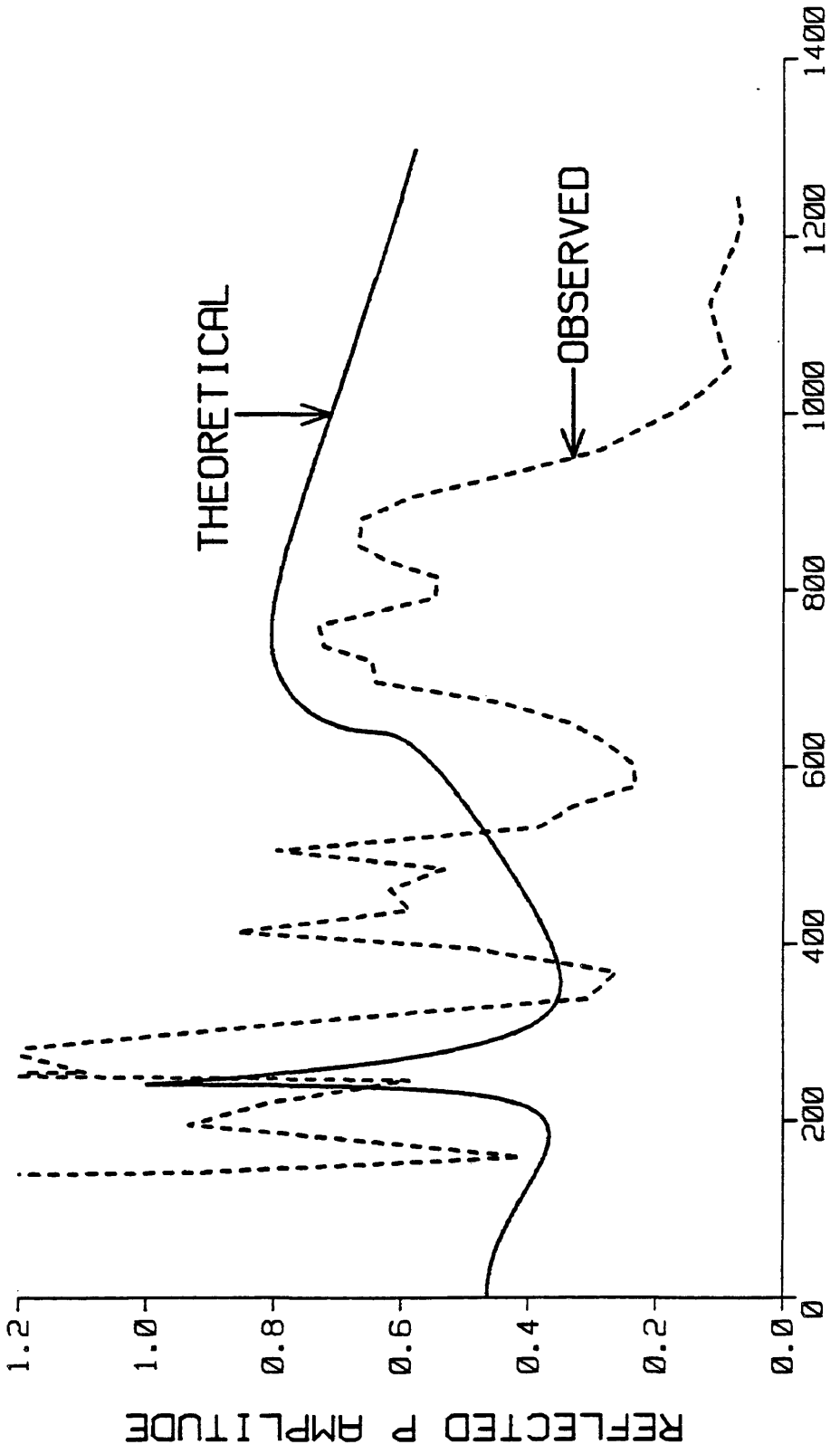

FIGURE 35. OBSERVED AND THEORETICAL AVO.
LINE 2 WELL 3 SHEAR VEL=2830

Table 4. Offsets of Maximum Amplitudes, Line 1.

Well	SP	X(data),m	P1,m/s	h1,m	X(model),m
1	1830	736	1997	122.7	735
2	2110	700	1891	119.9	701
3	2370	661	1722	112.6	657
4	2900	679	1807	116.3	674
5	3180	703	1820	116.6	710
6	3990	695	1925	115.0	695
7	4320	623	1898	118.1	625

Table 5. Offsets of Maximum Amplitudes, Line 2.

Well	SP	X(data),m	P1,m/s	h1,m	X(model),m
1	1260	626	2253	114.4	621
2	2560	688	2071	115.0	689
3	3340	751	1977	105.3	752

Figures 36 and 37 show the estimated shear velocities at each well for Lines 1 and 2, respectively. Along Line 1, the shear velocity varies only a few percent from well to well, as can be seen in Figure 36. The average shear velocity along Line 1 is 2960 m/s. Along Line 2, the shear velocity decreased almost linearly from a value of 3320 m/s at Well 1 to a value of 2830 m/s at Well 3 (about 10 m/s per km).

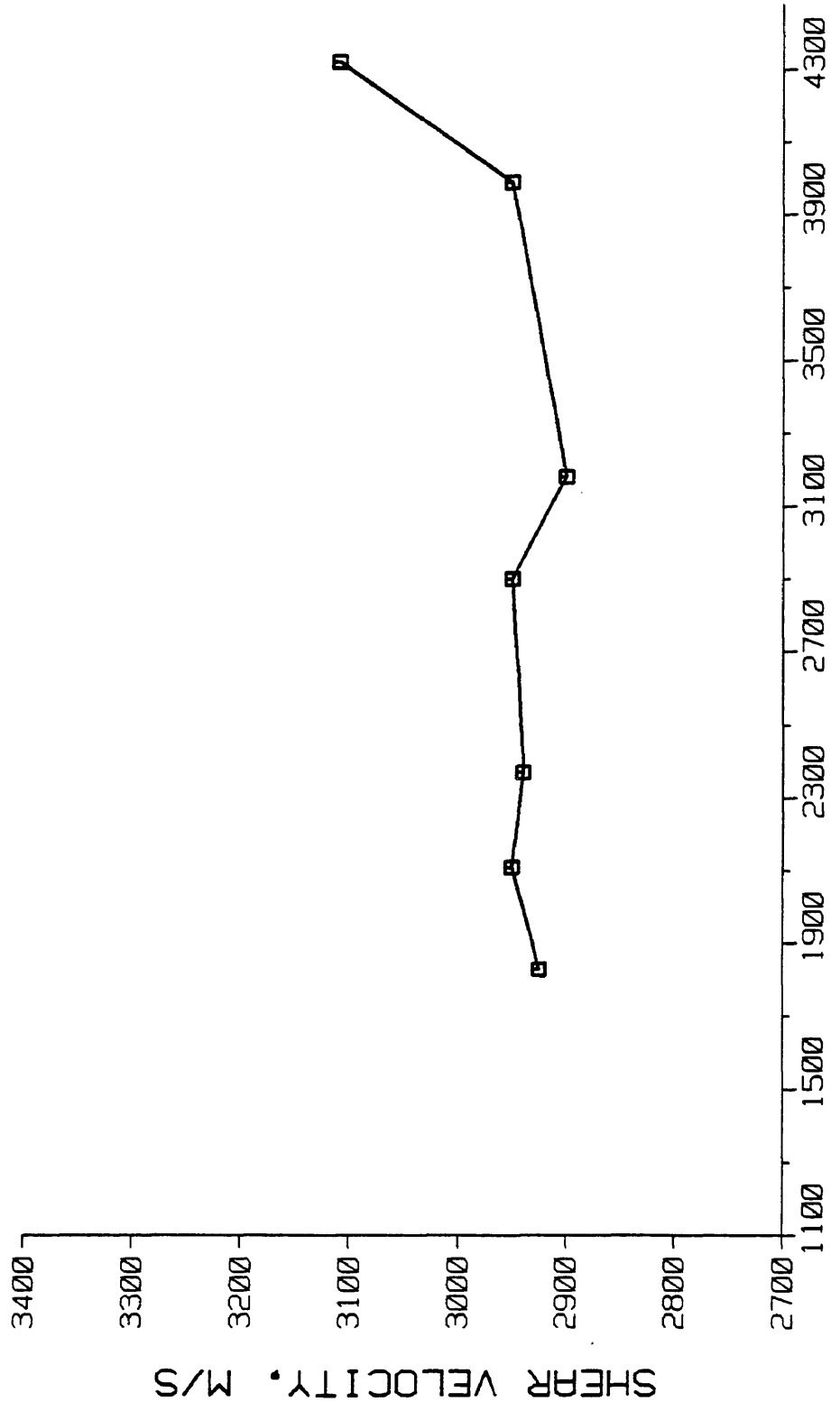

FIGURE 36. ESTIMATED SHEAR VELOCITY, LINE 1.
BASED ON 4-LAYER MODELS.

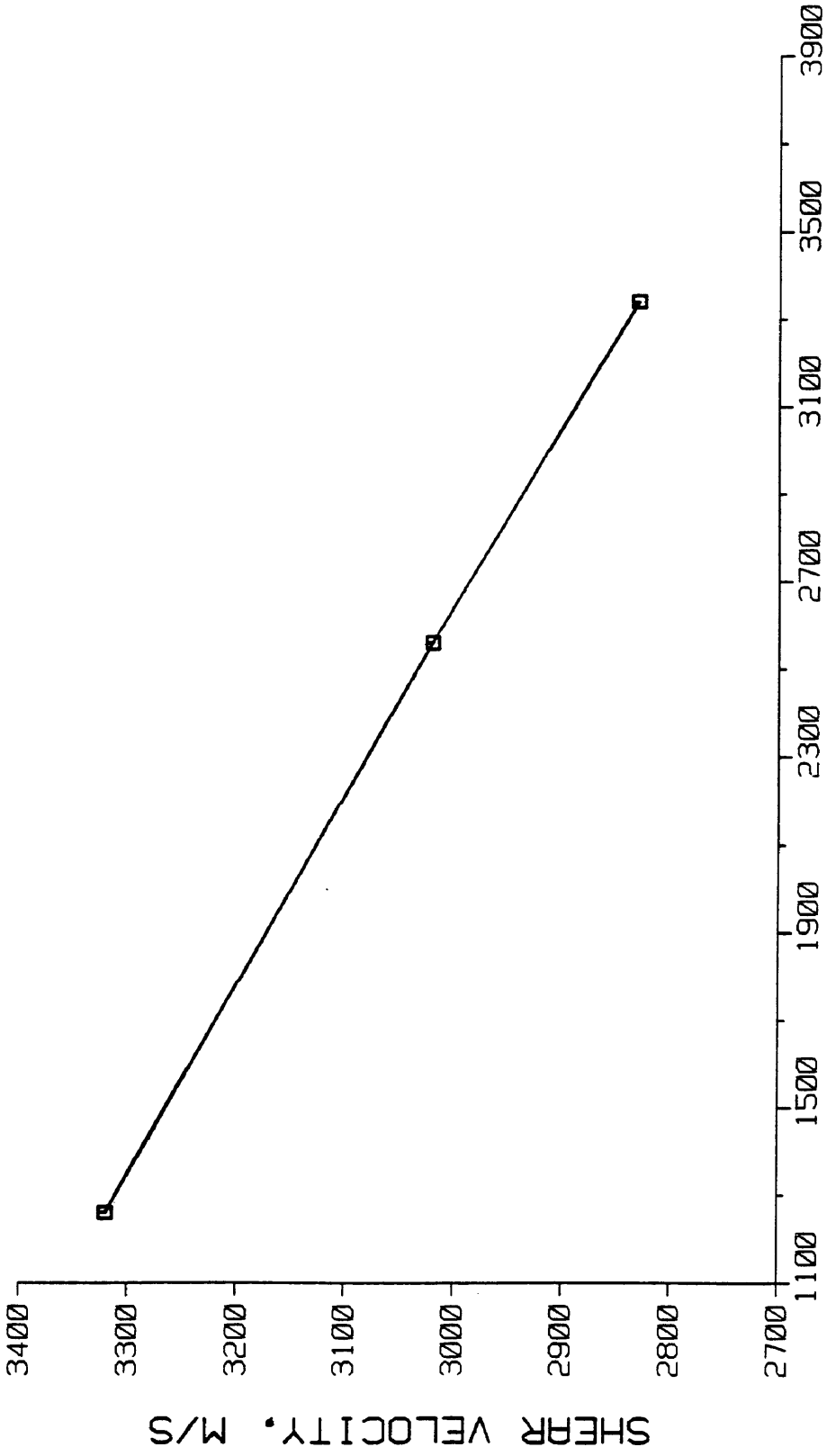

FIGURE 37. ESTIMATED SHEAR VELOCITY, LINE 2.
BASED ON 4-LAYER MODELS.

As described in previous sections, the multi-layer model can be approximated by a two-layer model with only small relative error. It follows that the shear velocities, if calculated at each well assuming a two-layer model, will not differ greatly from those obtained by modeling based on a four-layer model. Therefore, the shear velocities will be calculated assuming a two-layer model and the results will be compared to those from the four-layer model.

The shear velocity in the second layer, assuming a two-layer model, can be solved for directly from the final depth equation as follows:

$$S2 = P1/SIN\ (ARCTAN\ (X/2Z) - Gamma), \qquad (3)$$

With the stacking velocities taken as P1 and an angle of 6° for Gamma, the shear velocities are calculated and listed in Tables 6 and 7 for Lines 1 and 2, respectively. The previously obtained values from the four-layer model are listed for comparison.

As expected, the shear velocities calculated from the two layer model differ only slightly from those estimated with a four-layer model. The average difference is 1.5%.

Table 6. Shear Velocities, Line 1.

Well	SP	Vrms,m/s	X,m	Z,m	S2(2-layer),m/s	S2(4-layer)
1	1830	2182	736	263.7	2920	2925
2	2110	2130	700	260.9	2900	2950
3	2370	2050	661	253.6	2826	2940
4	2900	2090	679	257.3	2865	2950
5	3180	2096	703	257.6	2831	2900
6	3990	2152	695	256.0	2913	2950
7	4320	2135	623	259.1	3060	3110

Table 7. Shear Velocities, Line 2.

Well	SP	Vrms, m/s	X,m	Z,m	S2(2-layer),m/s	S2(4-layer)
1	1260	2310	626	255.4	3280	3320
2	2560	2224	688	256.0	3024	3020
3	3340	2186	751	246.3	2823	2830

From the above analysis, it can be concluded that the shear velocities along Line 1 are not changing much from well to well; they can be treated constant along the line (except at Well 7). This explains why the previously calculated depths along Line 1, by assuming a constant shear velocity of 3000 m/s, was very encouraging. On the other hand, the discrepancies between the calculated depths and the well depths along Line 2 can be explained by the

relatively large variations of shear velocity along the line.

Although not completely true, the differences between the calculated and the actual depths are assumed to be entirely due to lateral variations in the target shear velocity. Other factors, such as trace spacing and bad gathers, also contribute to the differences. These error factors will be further discussed in the section entitled Error Analysis.

CDP Data

Common depth point (CDP) gathers from Lines 1 and 2 were also analyzed. The depth was calculated (two-layer model) based on AVO brightening using equation (2).

The offsets of maximum amplitudes are plotted against shot point number in Figures 38 and 39 for the two lines. Figure 40 shows the offset vs shot point from both shot and CDP gathers for Line 1; Figure 41 shows similar data for Line 2.

It is clear from Figures 40 and 41 that the differences between shot and CDP gathers are generally small. Consequently, no detailed analysis will be made for the CDP data, except for the depth calculations.

The depths along Lines 1 and 2 were calculated assuming a constant shear velocity of 3000 m/s. The results are

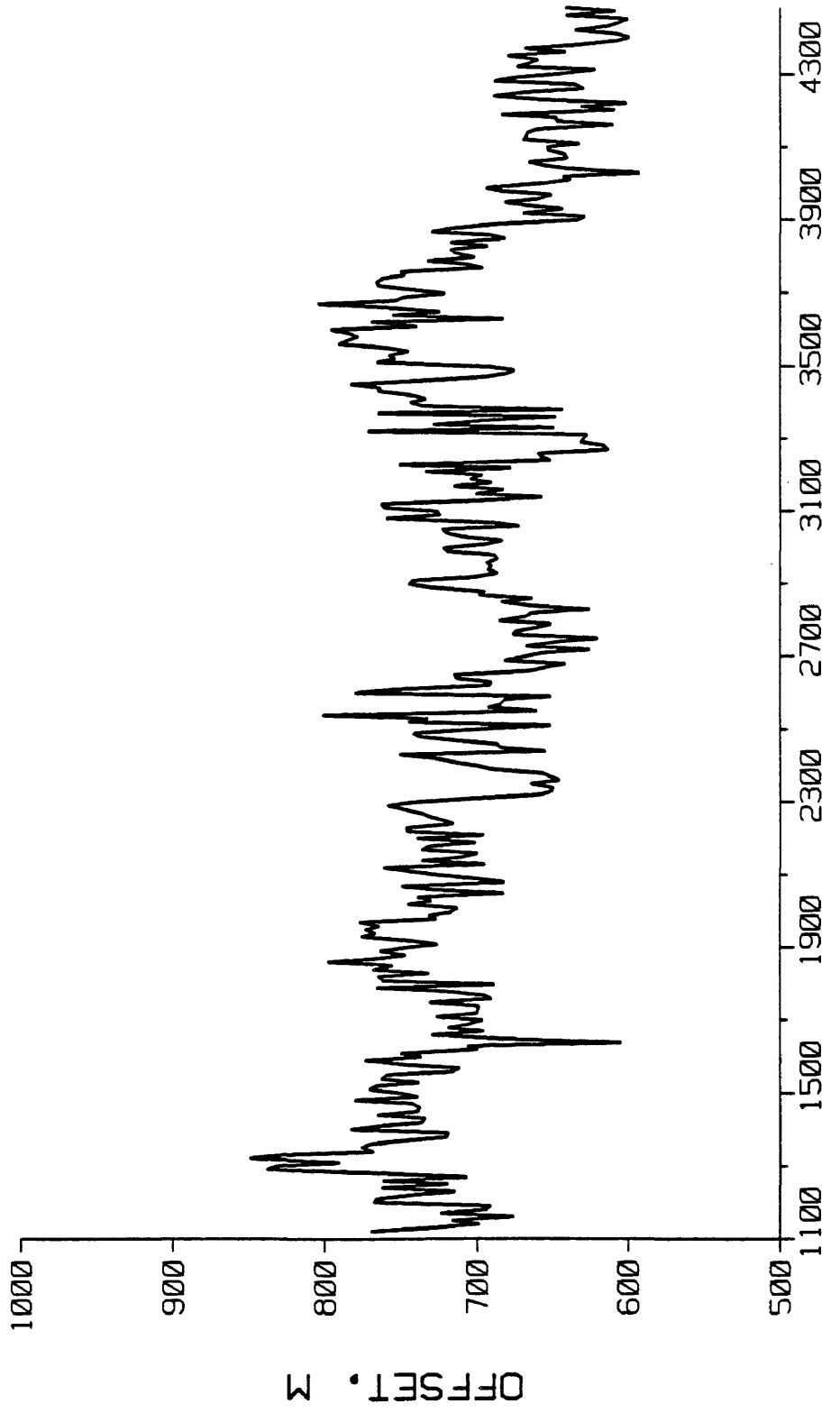

FIGURE 38. OFFSETS OF PEAK AMPLITUDES.
LINE 1. CDP GATHERS.

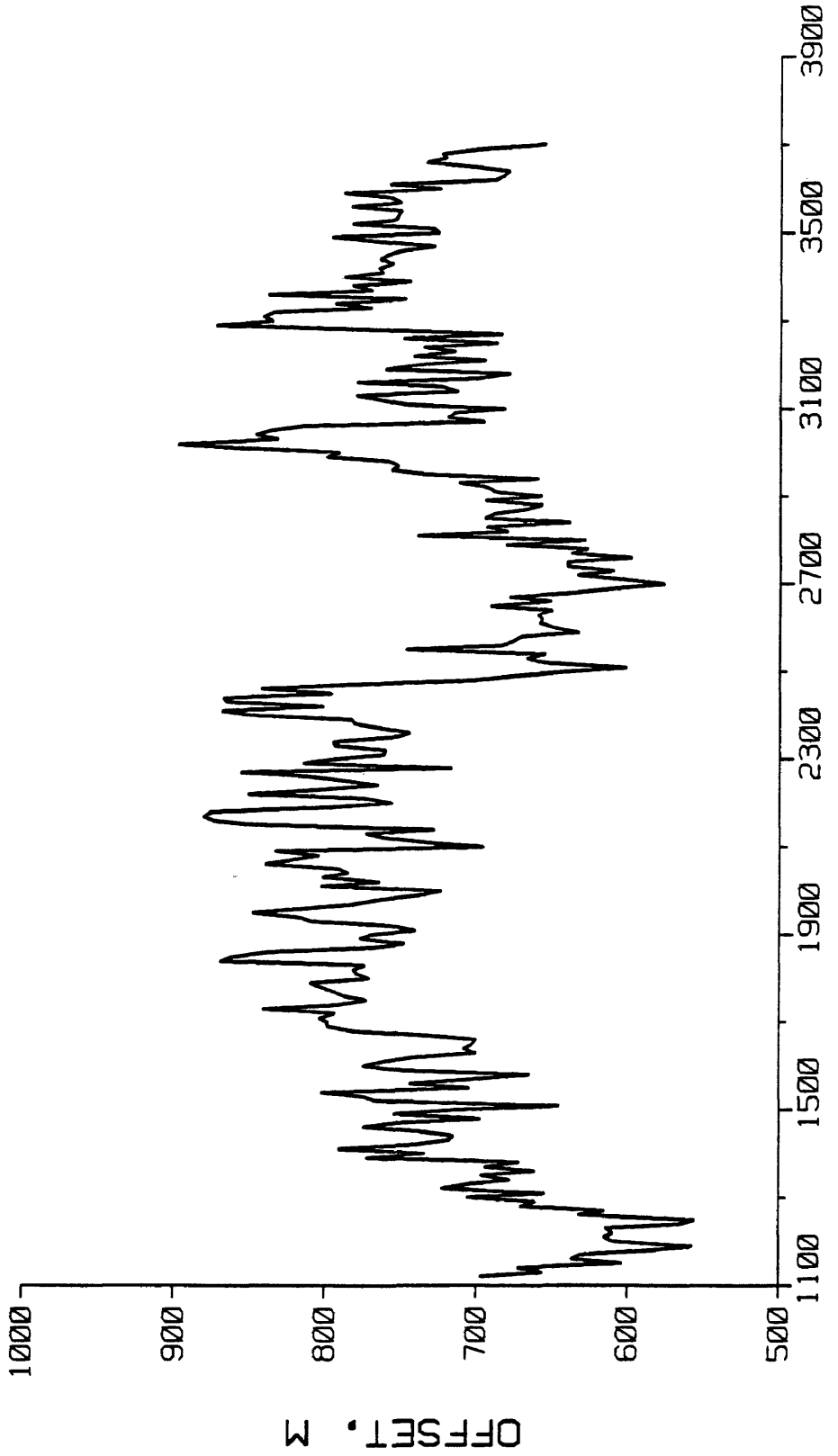

FIGURE 39. OFFSETS OF PEAK AMPLITUDES.
LINE 2, CDP GATHERS.

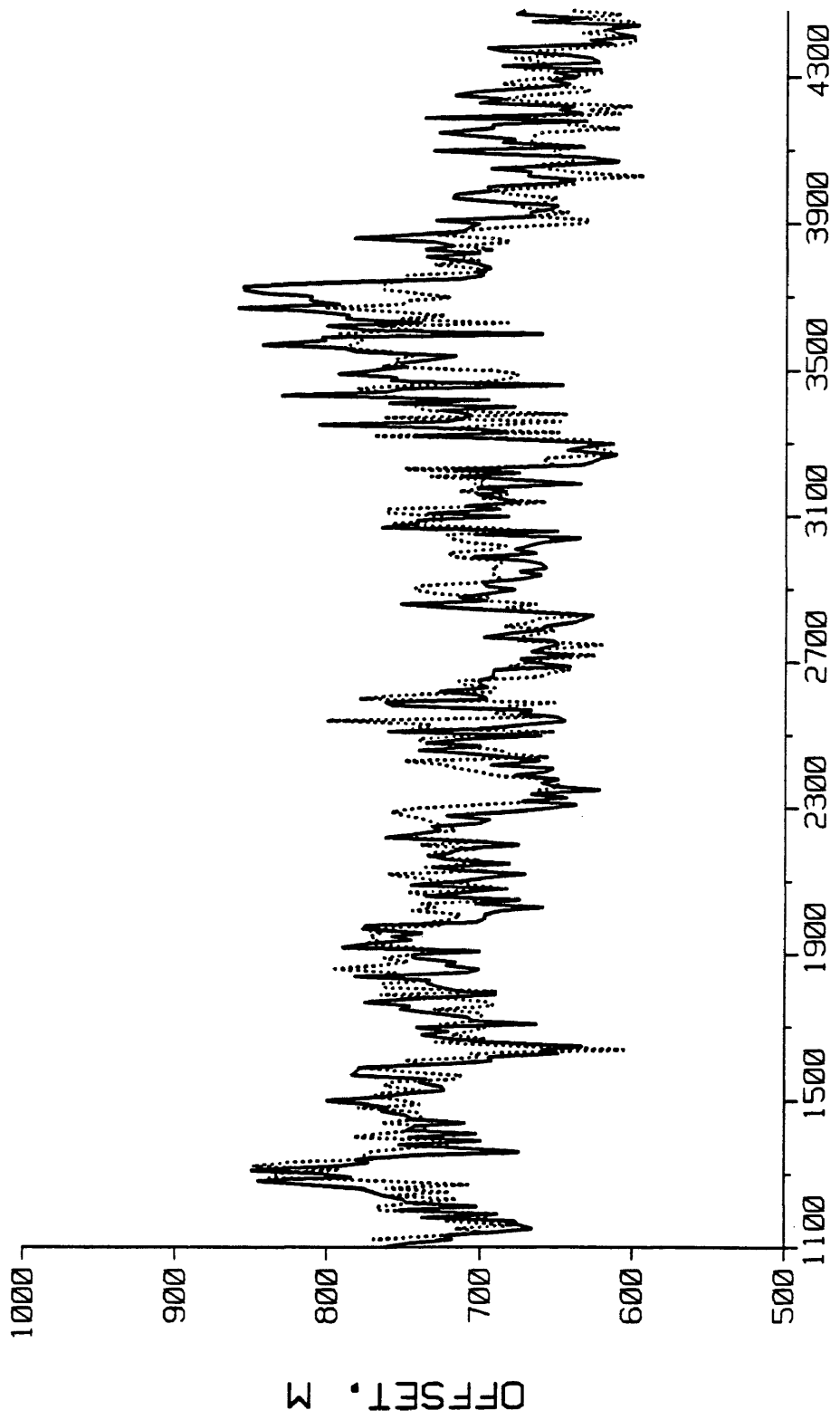

FIGURE 40. OFFSETS OF PEAK AMPLITUDES.
LINE 1, COP(DOTTED) AND SHOT GATHERS.

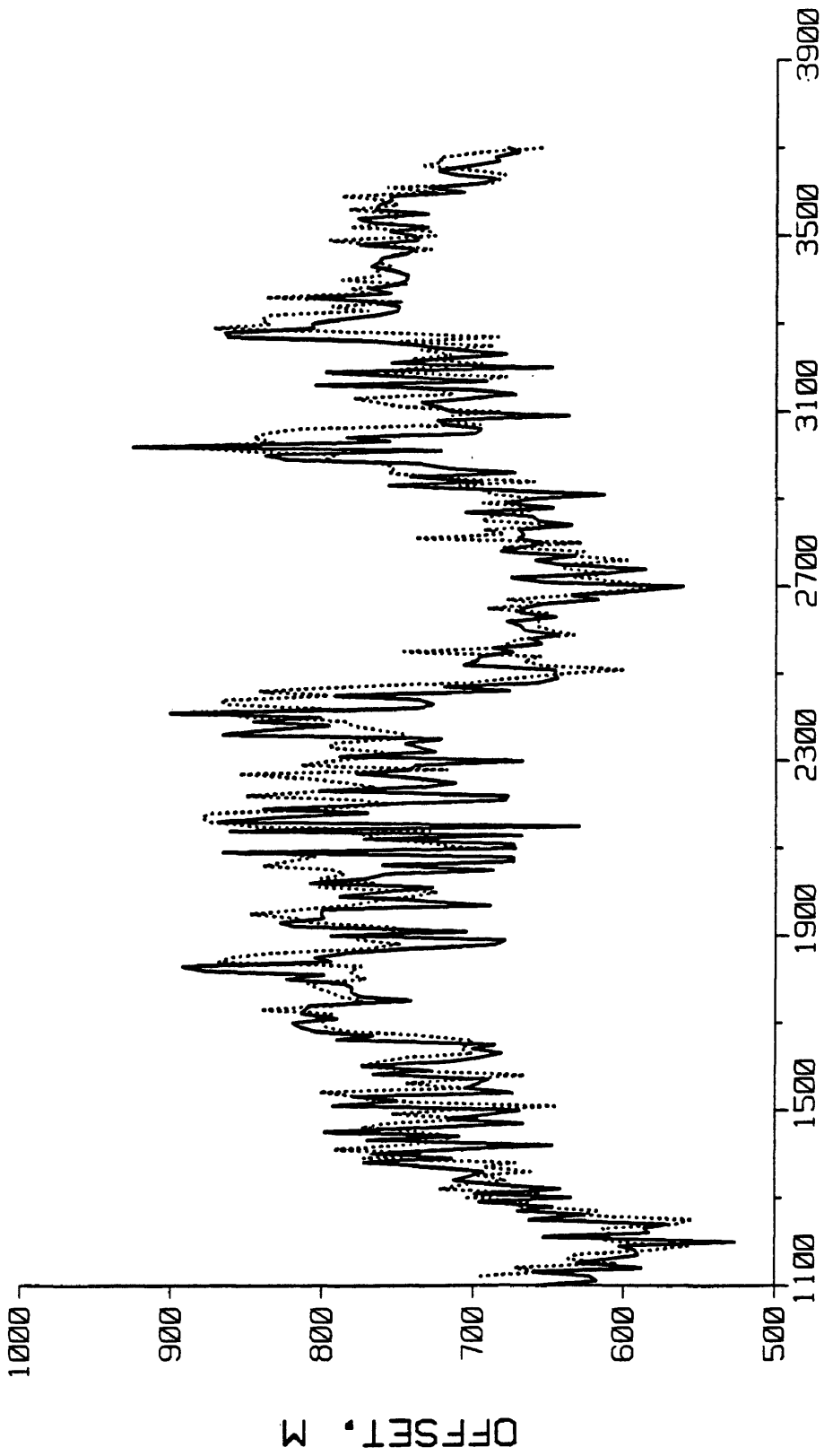

FIGURE 41. OFFSETS OF PEAK AMPLITUDES.
LINE 2. CDP(DOTTED) AND SHOT GATHERS.

shown in Figures 42 through 51 for the two lines. For comparison purposes, depths calculated from shot gathers and CDP gathers are shown in Figures 52 through 55 for the two lines. The discrepancies between the depths calculated from the two methods (CDP and shot gathers) are discussed in the next section.

Error Analysis

The following tables list the mean and the RMS errors for Lines 1 and 2 from the shot and CDP gathers. The error at each well is simply calculated by taking the difference between the calculated depth and the actual well depth.

Table 8. Errors, Line 1, Shot Gathers.

Description	Mean Error, m	RMS Error, m
Depth	19.1	9.7
Tied to 1	6.4	9.2
Smoothed	19.8	10.3
Smoothed, tied to 1	6.6	9.6
Smoothed, tied to 1,4 & 7	3.1	5.0

Table 9. Errors, Line 1, CDP Gathers

Description	Mean Error, m	RMS Error, m
Depth	26.6	16.5
Tied to 1	14.1	15.6
Smoothed	26.2	16.0
Smoothed, tied to 1	11.5	14.6
Smoothed, tied to 1,4 & 7	3.1	4.1

Table 10. Errors, Line 2, Shot Gathers.

Description	Mean Error, m	RMS Error, m
Depth	30.0	42.4
Tied to 1	48.5	50.1
Smoothed	31.7	43.1
Smoothed, tied to 1	45.6	50.4
Smoothed, tied to 1 & 3	5.2	9.1

Table 11. Errors, Line 2, CDP Gathers

Description	Mean Error, m	RMS Error, m
Depth	35.0	50.6
Tied to 1	62.0	62.5
Smoothed	35.8	31.2
Smoothed, tied to 1	69.4	67.6
Smoothed, tied to 1 & 3	0.2	0.3

When calculated depths are smoothed and tied to more than one well, the CDP data yield smaller errors.

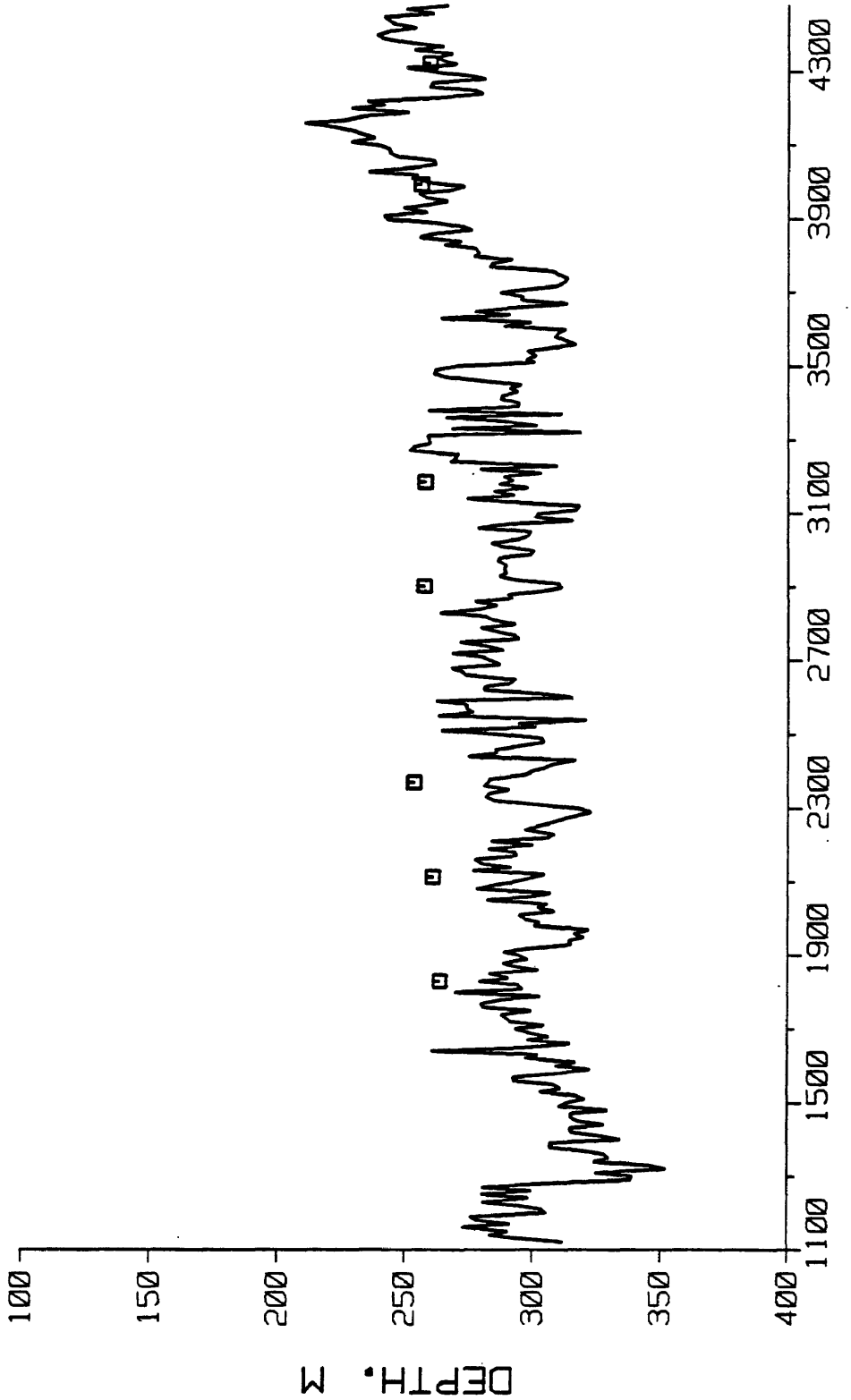

FIGURE 42. CALCULATED DEPTH. LINE 1. CDP GATHERS.

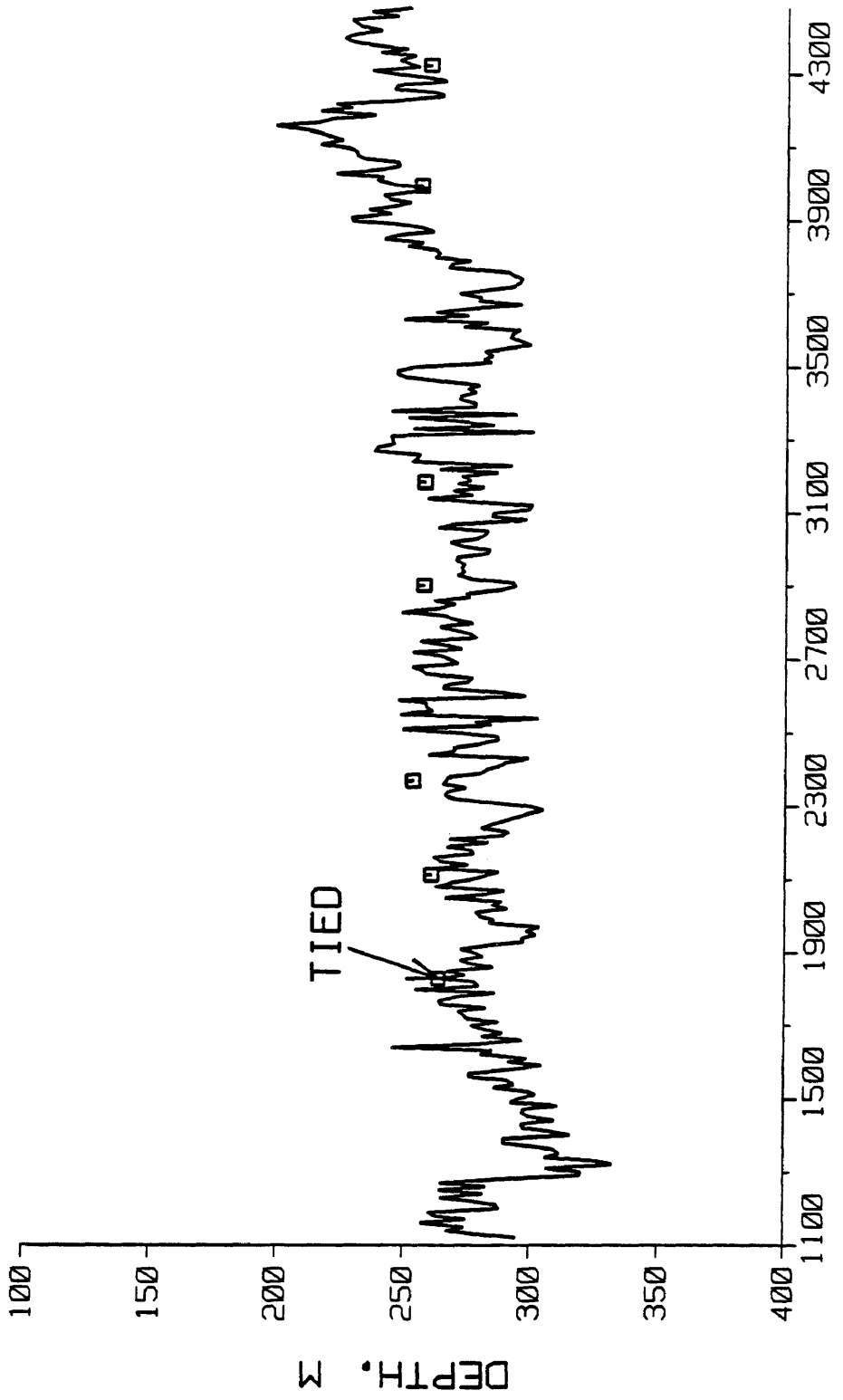

FIGURE 43. CALCULATED DEPTH. LINE 1. CDP GATHERS. TIED TO WELL 1.

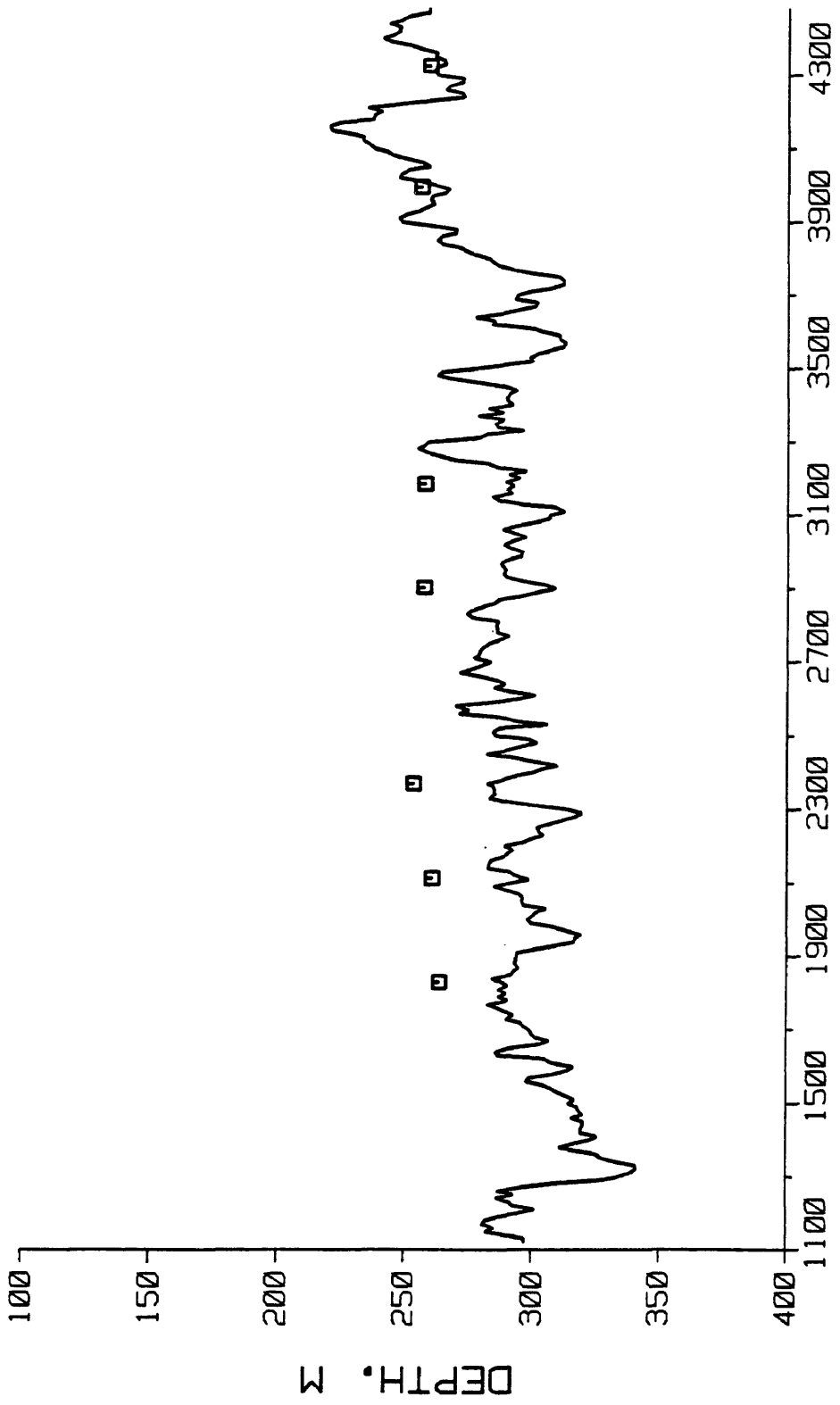

FIGURE 44. CALCULATED DEPTH, LINE 1, CDP GATHERS. SMOOTHED.

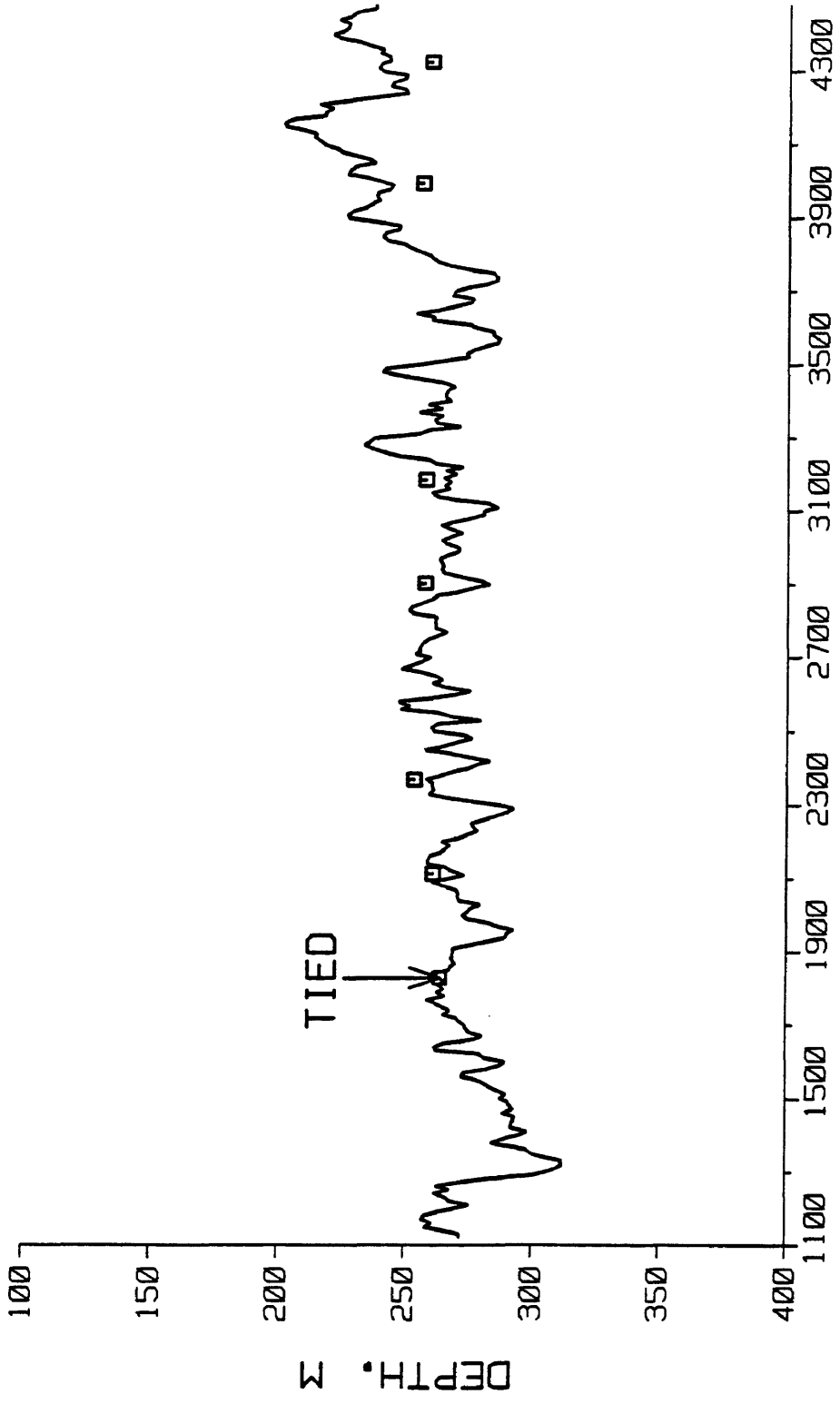

FIGURE 45. CALCULATED DEPTH, LINE 1, CDP GATHERS. SMOOTHED, TIED TO WELL 1.

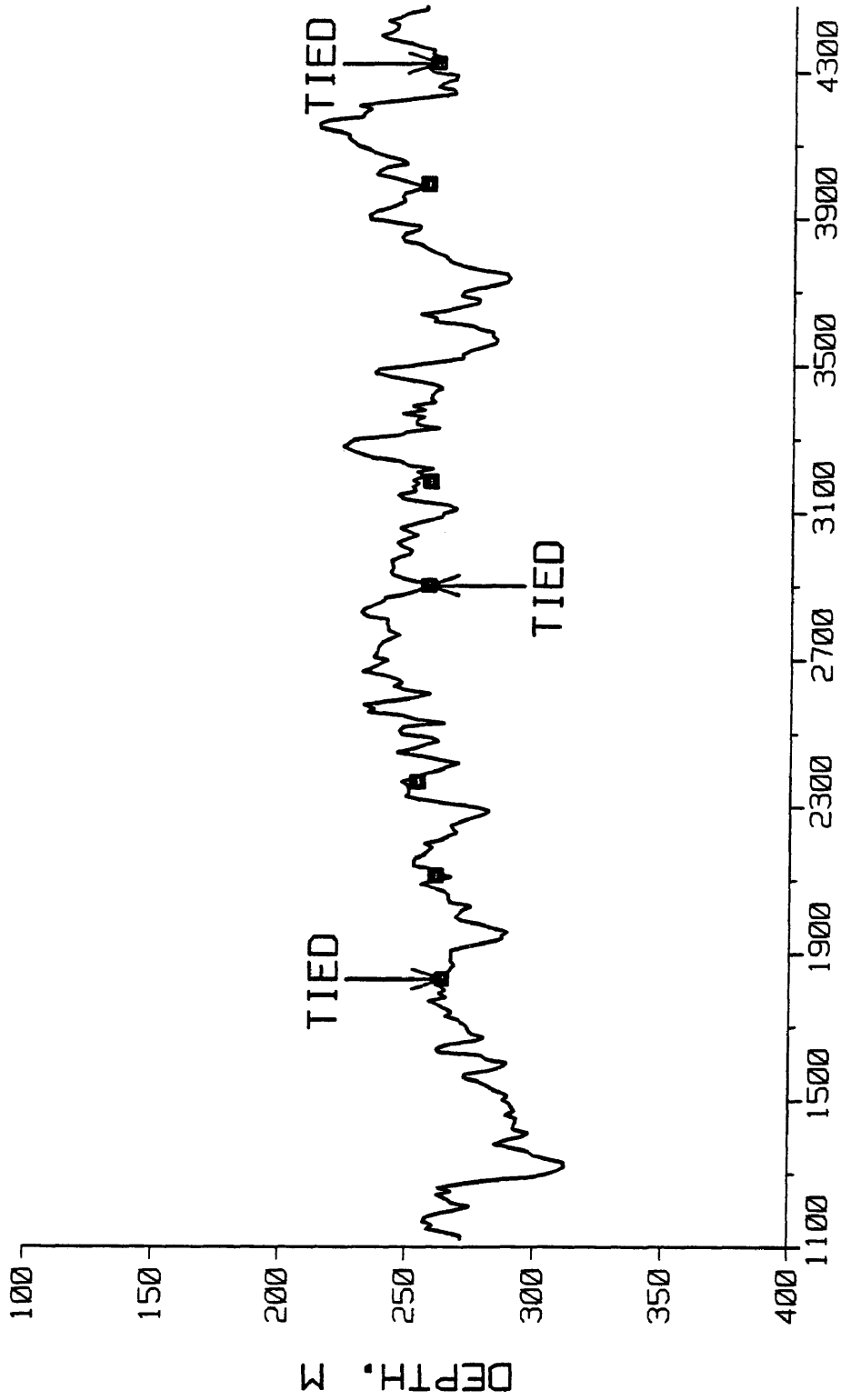

FIGURE 46. CALCULATED DEPTH, LINE 1, CDP GATHERS. SMOOTHED, TIED TO WELLS 1, 4, AND 7.

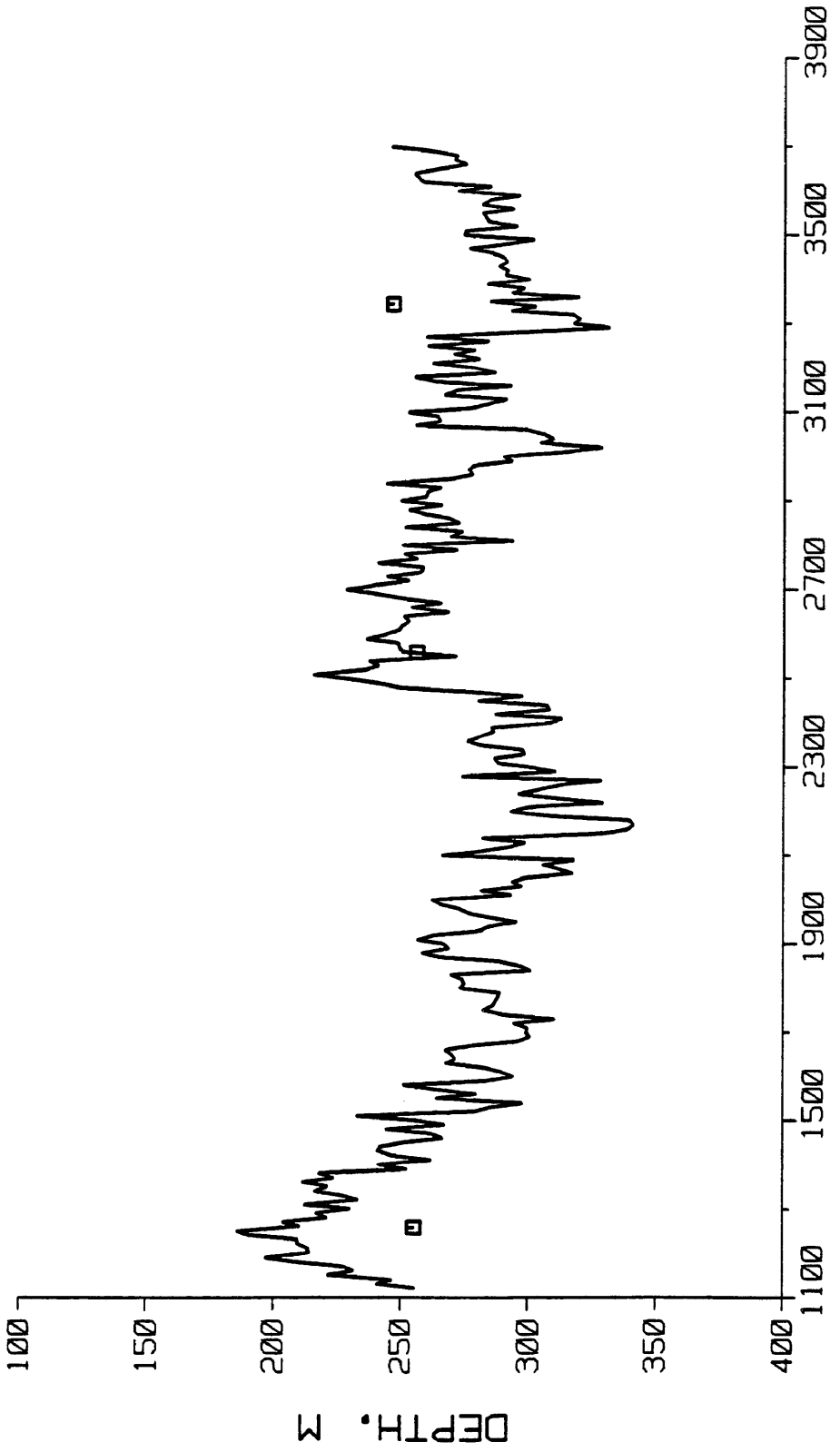

FIGURE 47. CALCULATED DEPTH, LINE 2, CDP GATHERS.

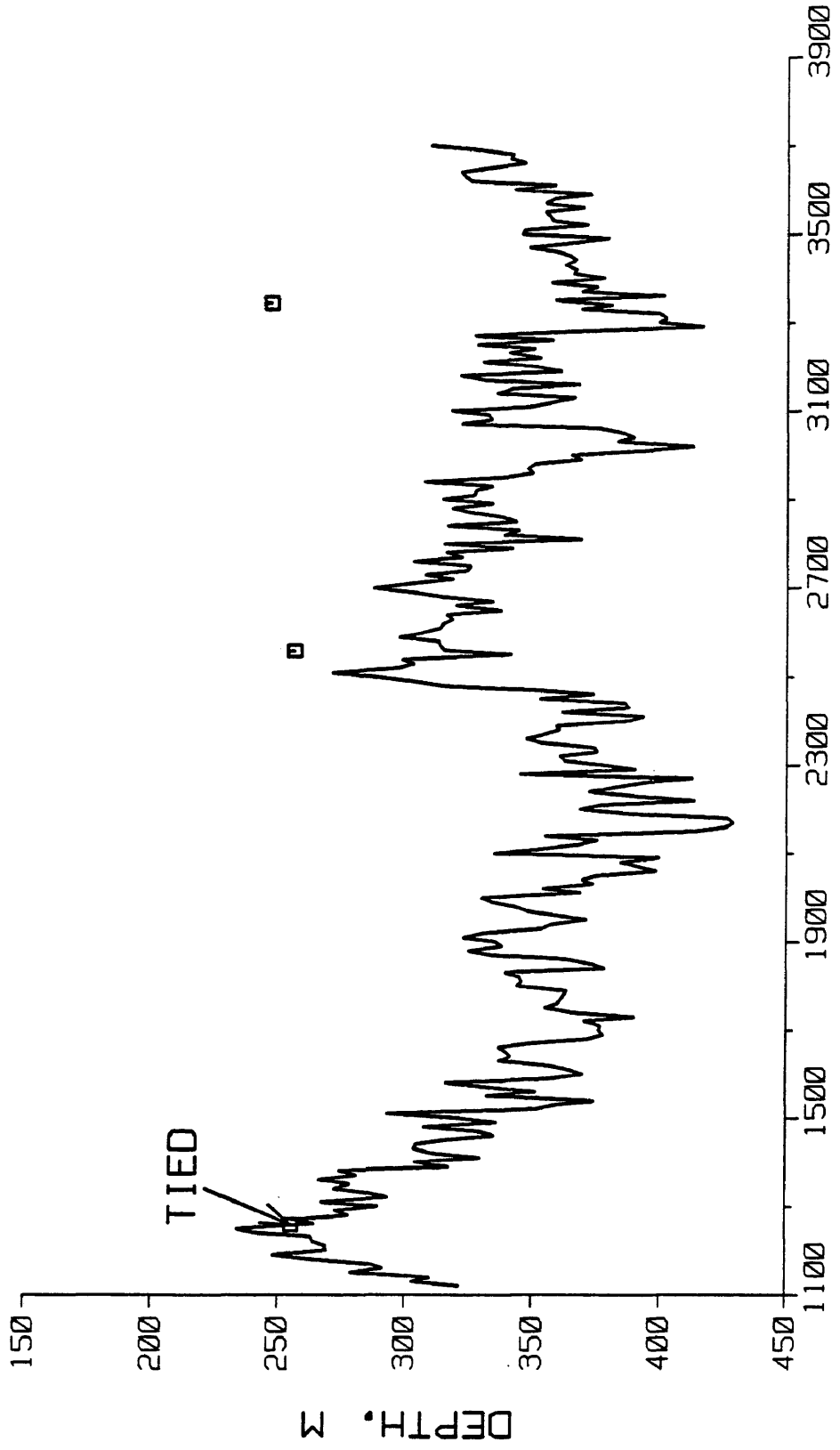

FIGURE 48. CALCULATED DEPTH, LINE 2, CDP GATHERS. TIED TO WELL 1.

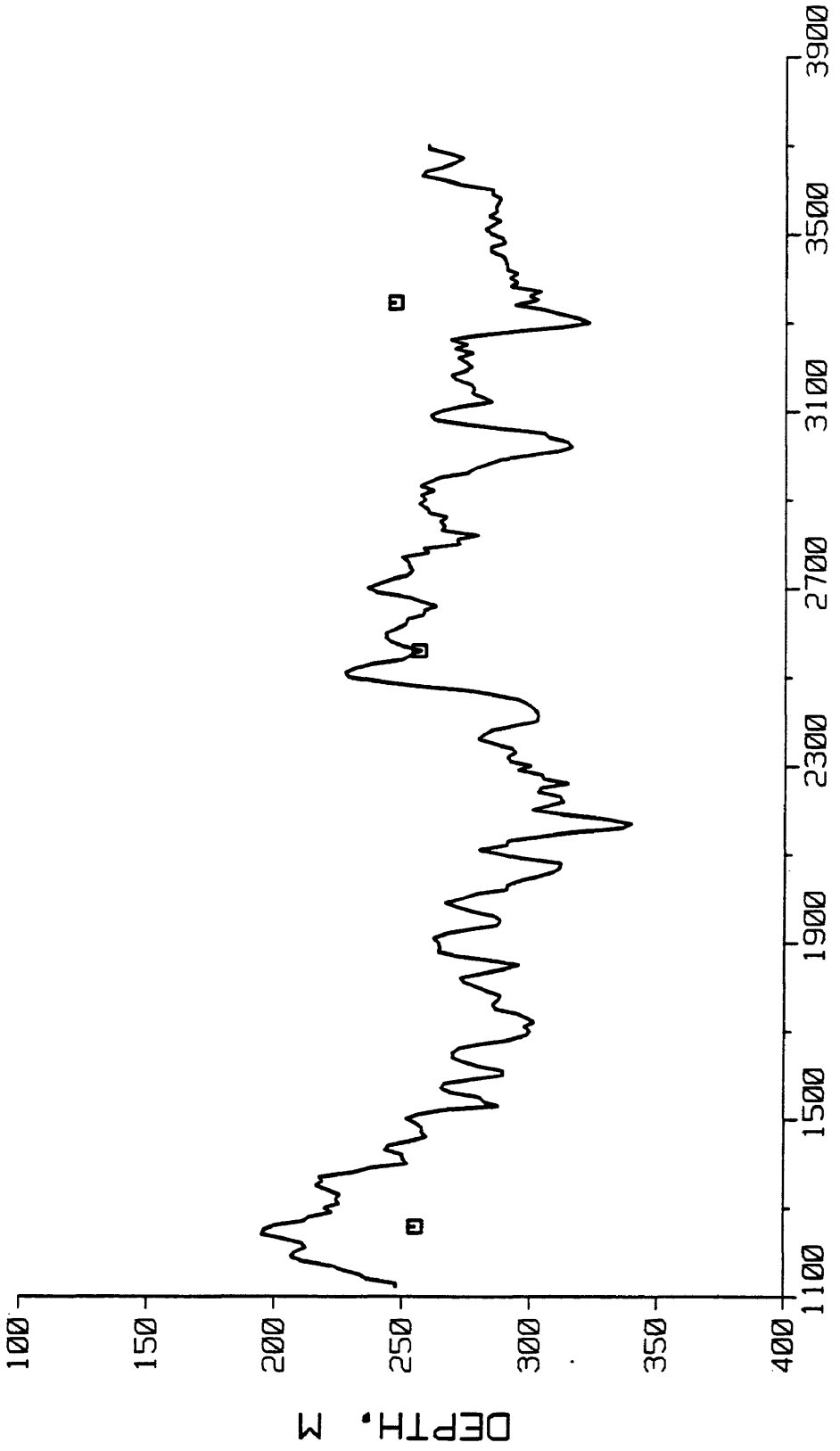

FIGURE 49. CALCULATED DEPTH, LINE 2, CDP GATHERS. SMOOTHED.

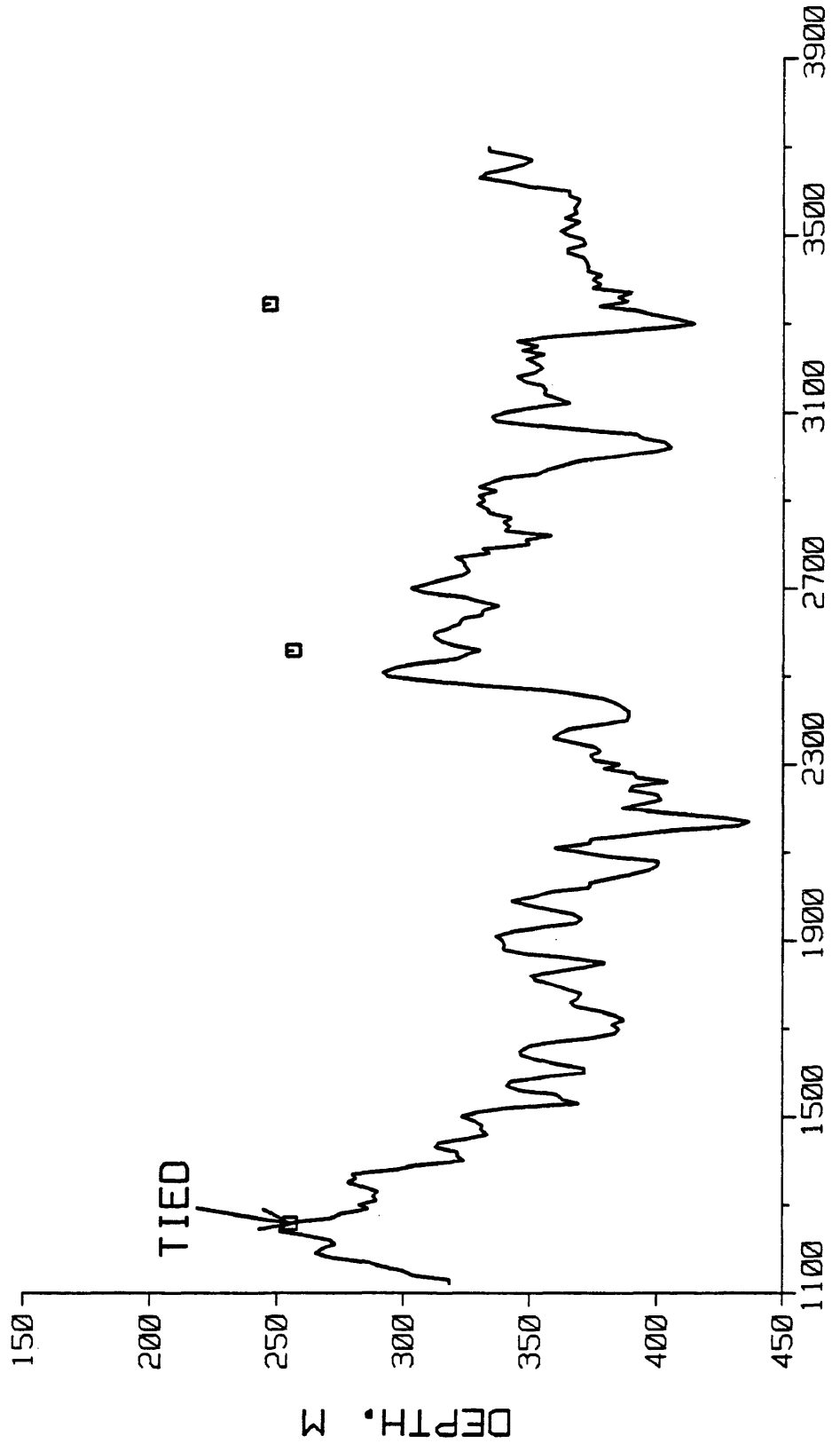

FIGURE 50. CALCULATED DEPTH, LINE 2, CDP GATHERS. SMOOTHED, TIED TO WELL 1.

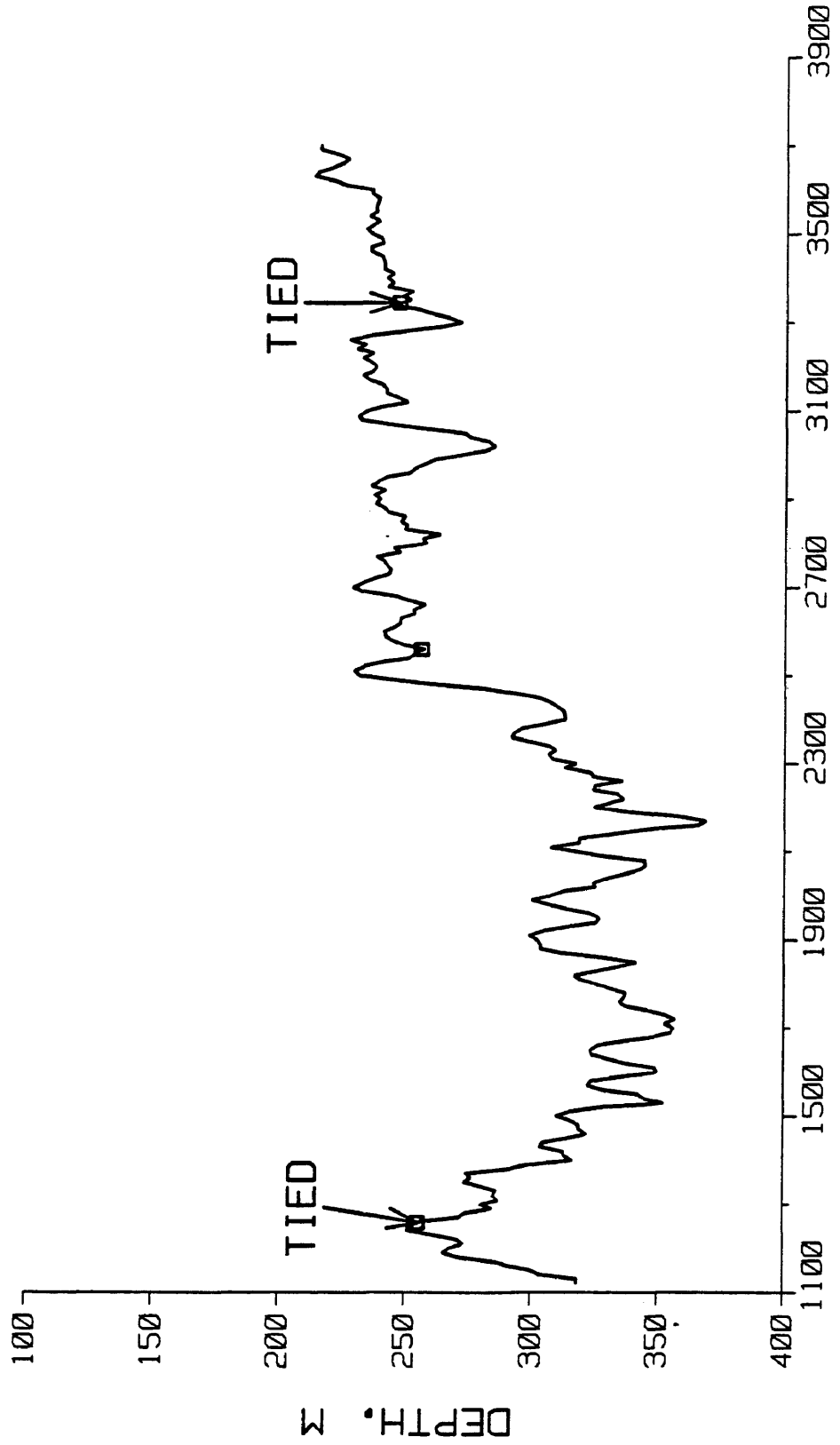

FIGURE 51. CALCULATED DEPTH. LINE 2. CDP GATHERS. SMOOTHED. TIED TO WELLS 1 AND 3.

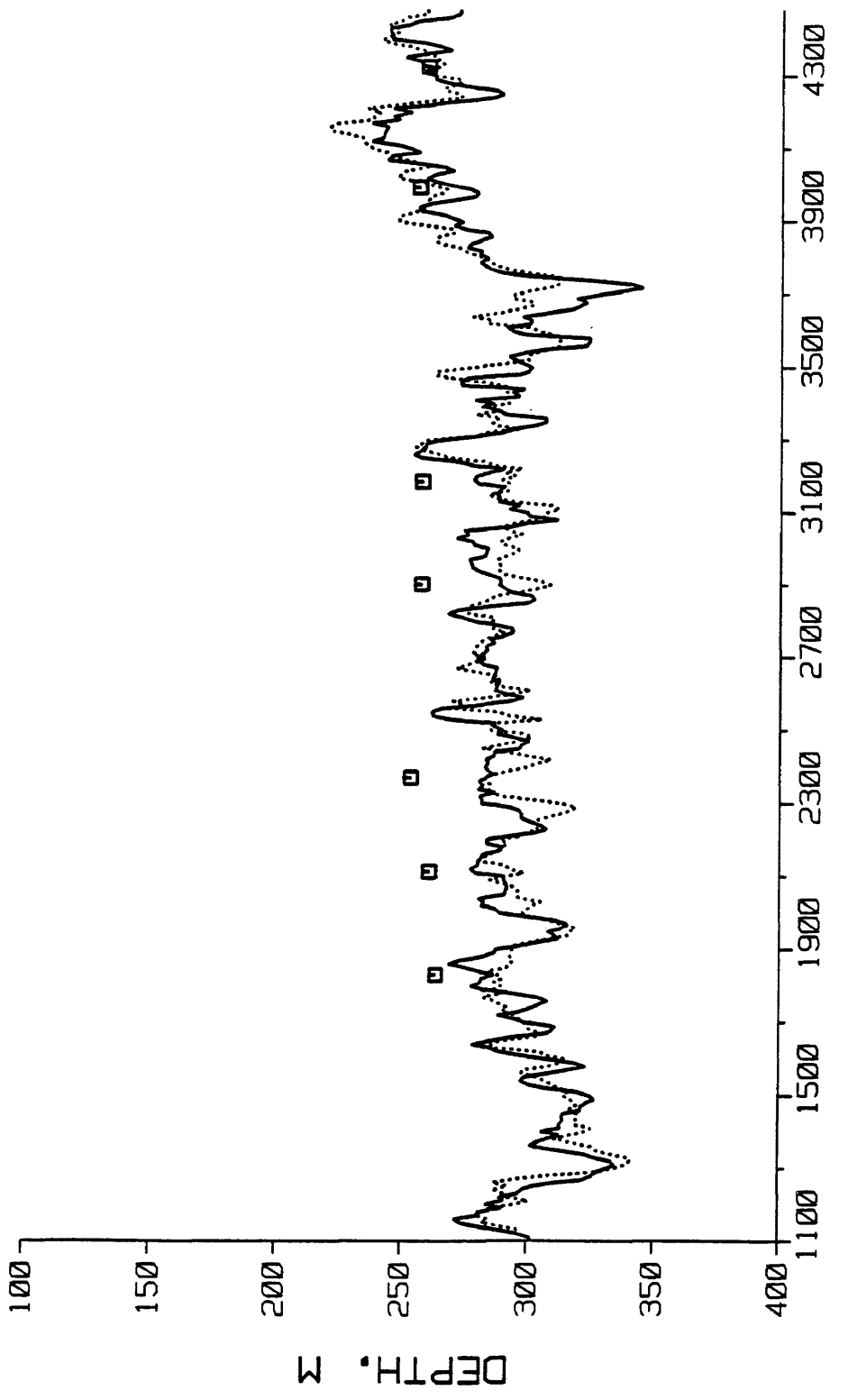

FIGURE 52. CALCULATED DEPTH, LINE 1.
SMOOTHED, COP(DOTTED) AND SHOT GATHERS.

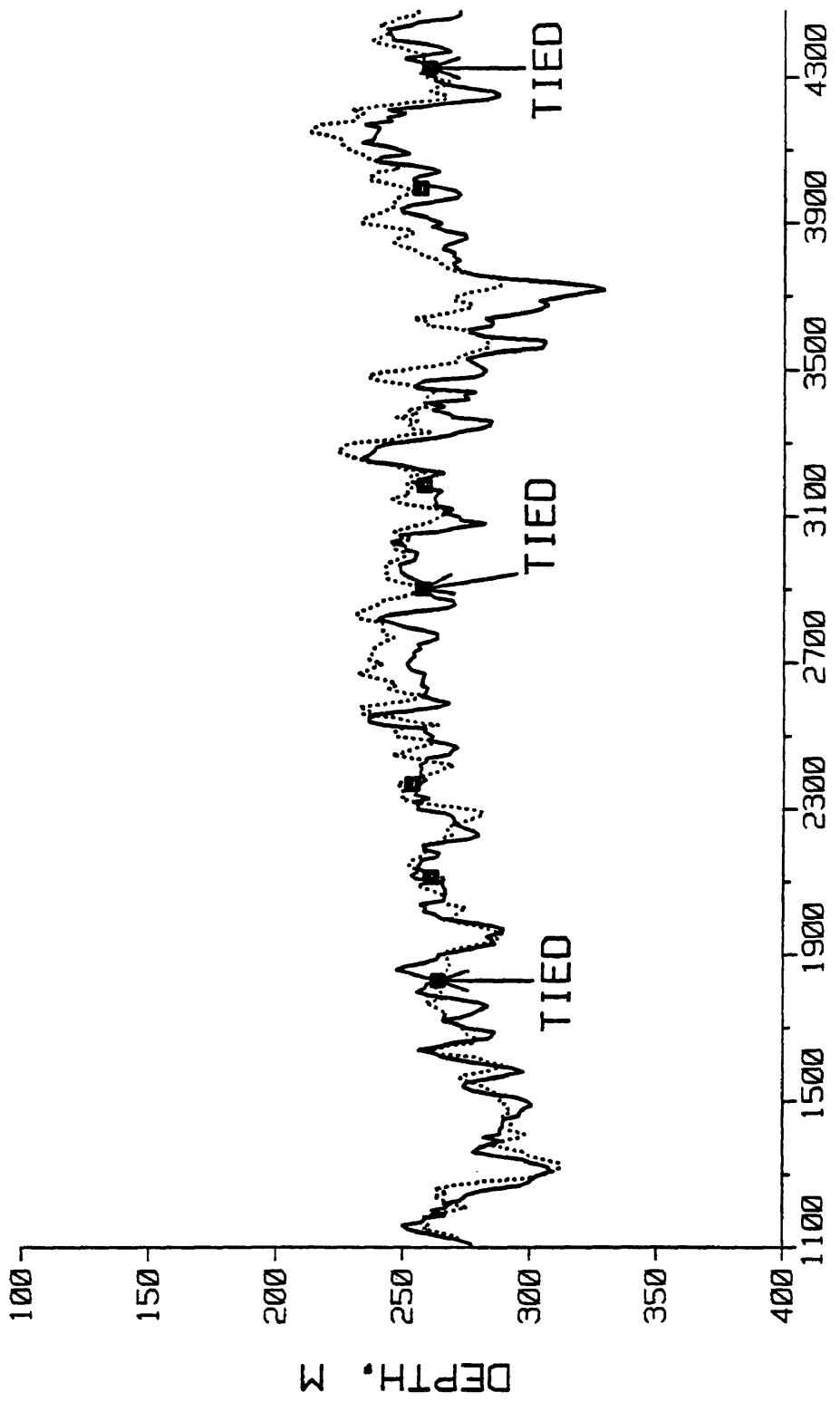

FIGURE 53. CALCULATED DEPTH, LINE 1. SMOOTHED. CDP(DOTTED) AND SHOT GATHERS. TIED TO 1, 4, AND 7.

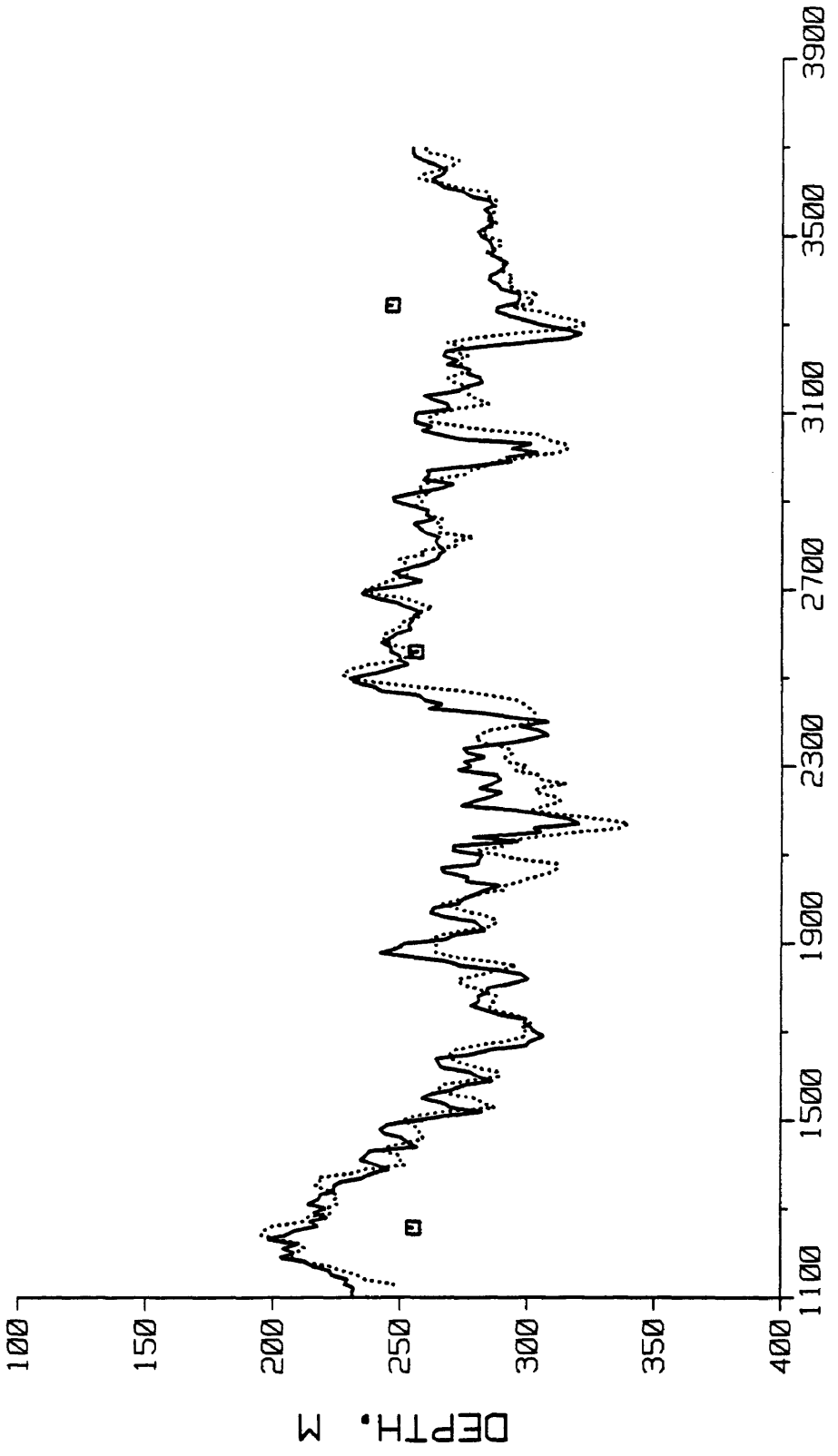

FIGURE 54. CALCULATED DEPTH, LINE 2. SMOOTHED. CDP (DOTTED) AND SHOT GATHERS.

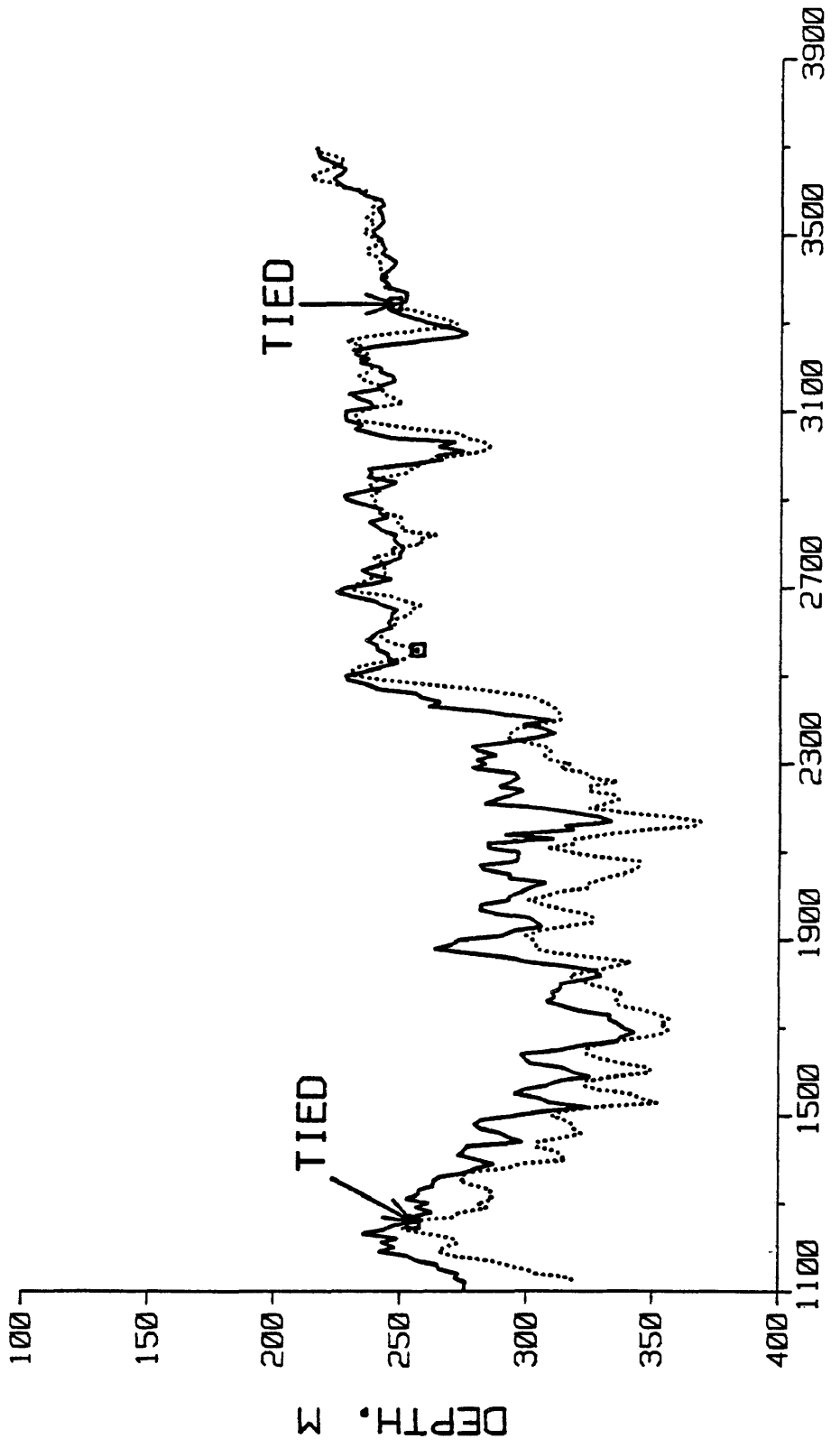

FIGURE 55. CALCULATED DEPTH. LINE 2. SMOOTHED. COP(DOTTED) AND SHOT GATHERS. TIED TO 1 AND 3.

There are many factors that can contribute to the error. A major factor is the quality of the gathers involved. In many of the noisy gathers, two or more peaks were present for a given AVO plot; in some, the peak was so broad that an offset could hardly be picked. To help overcome this difficulty, pattern recognition by comparing the bad gather to preceding and succeeding gathers was used.

Another source of error arises from the discreteness of the 24-meter trace spacing. the three-point curve-fitting technique is believed to be optimal for minimizing (and not completely eliminating) the error arising from such discreteness.

Surface elevations along the two lines of study can play a major role in the depth calculations. Unfortunately, surface elevation information was not available to be included in calculating depths.

The difference between the results from the shot and CDP gathers have been caused by the presence of bad gathers, and/or the way the curve-fitting was applied. Such a difference has nothing to do with surface elevations.

The calculated depths along Line 2 have larger errors than those calculated along Line 1. This big difference in error between the two lines might be related to the fact that Line 1 is along strike whereas Line 2 is along dip.

A lack of shear velocity control along the two lines constitutes another problem. A constant shear velocity of 3000 m/s was assumed. This assumption is probably acceptable for Line 1, as shown by modeling, but not for Line 2.

CHAPTER FIVE

Time Method and Further AVO Analysis

Time Method

The depths along the two lines were also calculated using a time-dependent method. Both shot and CDP gathers were analyzed. The results are then compared to those from the AVO method.

The time method was implemented by simply taking the data into the T - X domain. A straight line was fit through the first 20 points in a least-squares sense. From the slope and the T-intercept of the line, the zero-offset time and the stacking velocity were calculated for each gather. The depth was then calculated from the following equation:

$$Z = Vs.To \qquad (4)$$

where:

Vs is the calculated stacking velocity; and

To is the calculated zero offset time (one way).

No attempt was made to scale the calculated stacking velocities into average velocities. Rather, the calculated depths were scaled to known well depths.

Calculated Depths, Time Method

Line 1. Figure 56 shows the calculated depths from shot gathers for Line 1, using the AVO and time methods. A smoothed version of Figure 56, and tied to Well 1, is shown in Figure 57. The mean error (Figure 57) from the time method is 11.4 m as opposed to 6.6 m from the AVO method. The difference between the two methods is as large as 50 m (SP 1300 and SP 3700). When the results are tied to Wells 1, 4, and 7, the mean error from the time method dropped to 2.5 m as opposed to 3.1 m from the AVO method (Figure 58).

In Figure 59, a smoothed version of depths from CDP gathers tied to Wells 1, 4, and 7, is shown for the AVO and time methods. The mean errors are 5.0 m and 3.1 m for the time and AVO methods, respectively.

By comparing the calculated depths from the two methods along Line 1 (for example, Figures 57 and 58), it can be seen that the two methods generally agree although there are some large differences, notably around shot points 1300 and 3700. By taking the average error as a criterion, no conclusion can be drawn as to which method is favorable and more accurate. For instance, the average error from the calculated depths in Figure 57 (AVO method) is less than that when using the time method. Conversely, from Figure

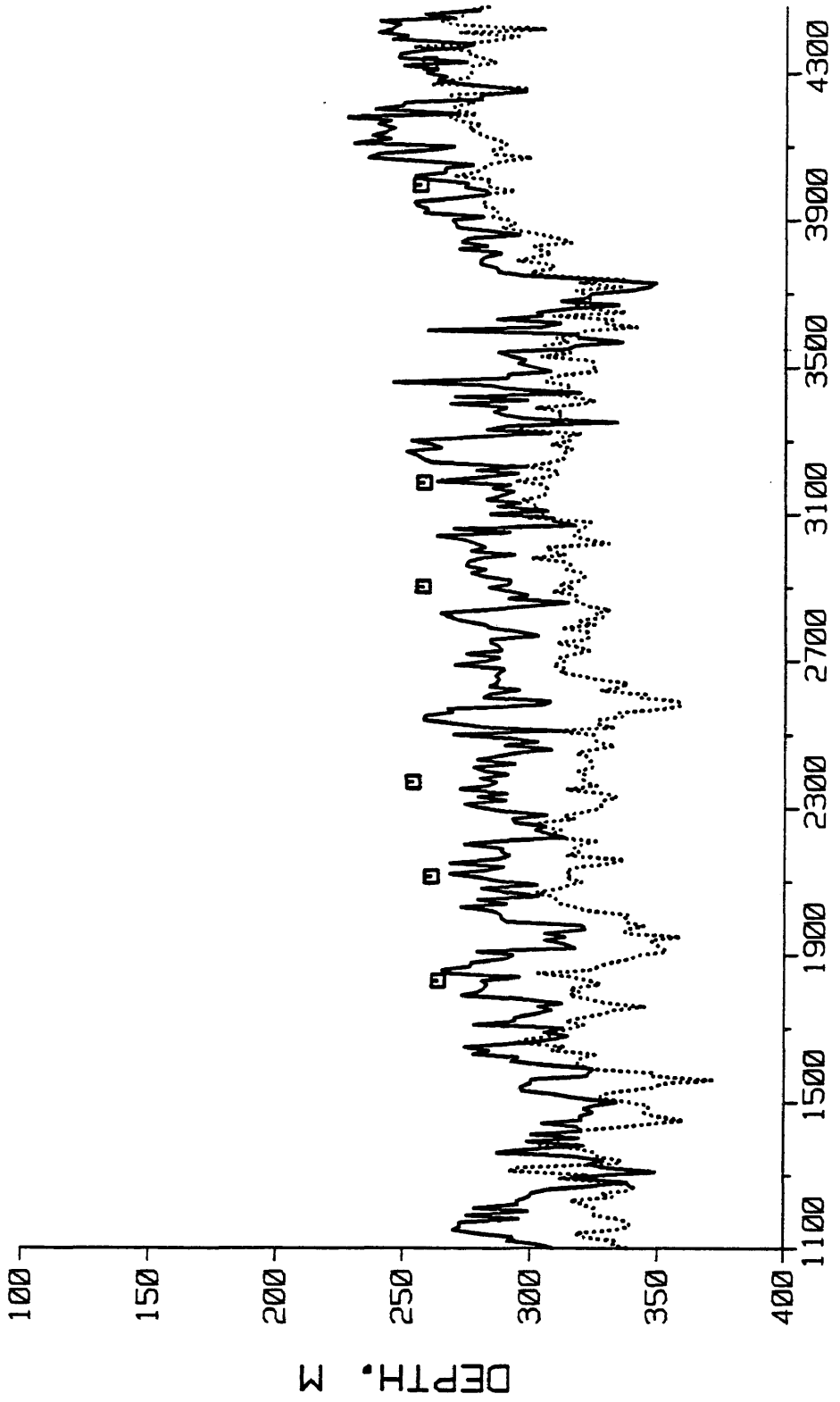

FIGURE 56. CALCULATED DEPTH. LINE 1. SHOT GATHERS.
TIME(DOTTED) AND AVO(SOLID) METHODS.

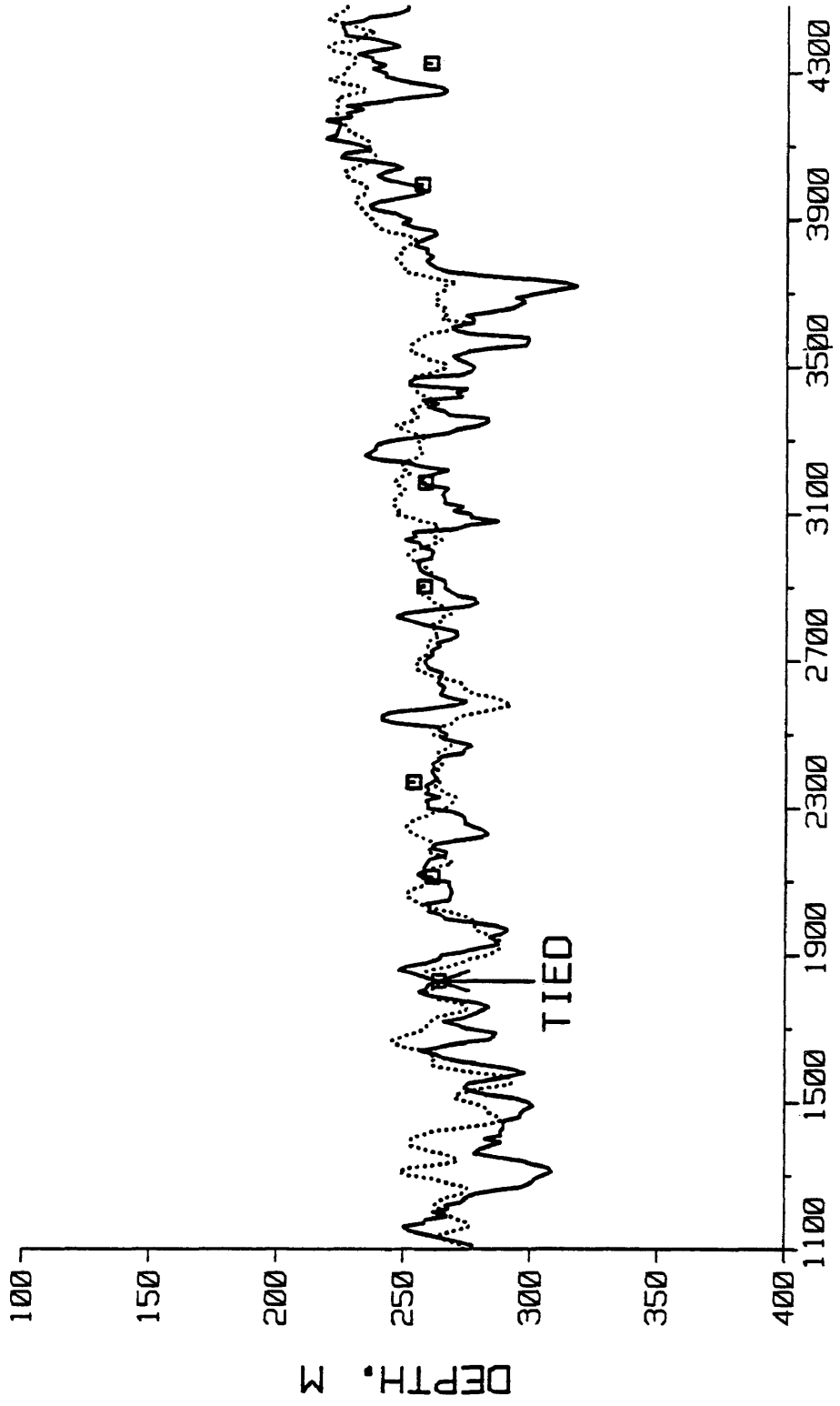

FIGURE 57. CALCULATED DEPTH, LINE 1. SHOT GATHERS. TIME(DOTTED) AND AVO(SOLID) METHODS. SMOOTHED, TIED TO WELL 1.

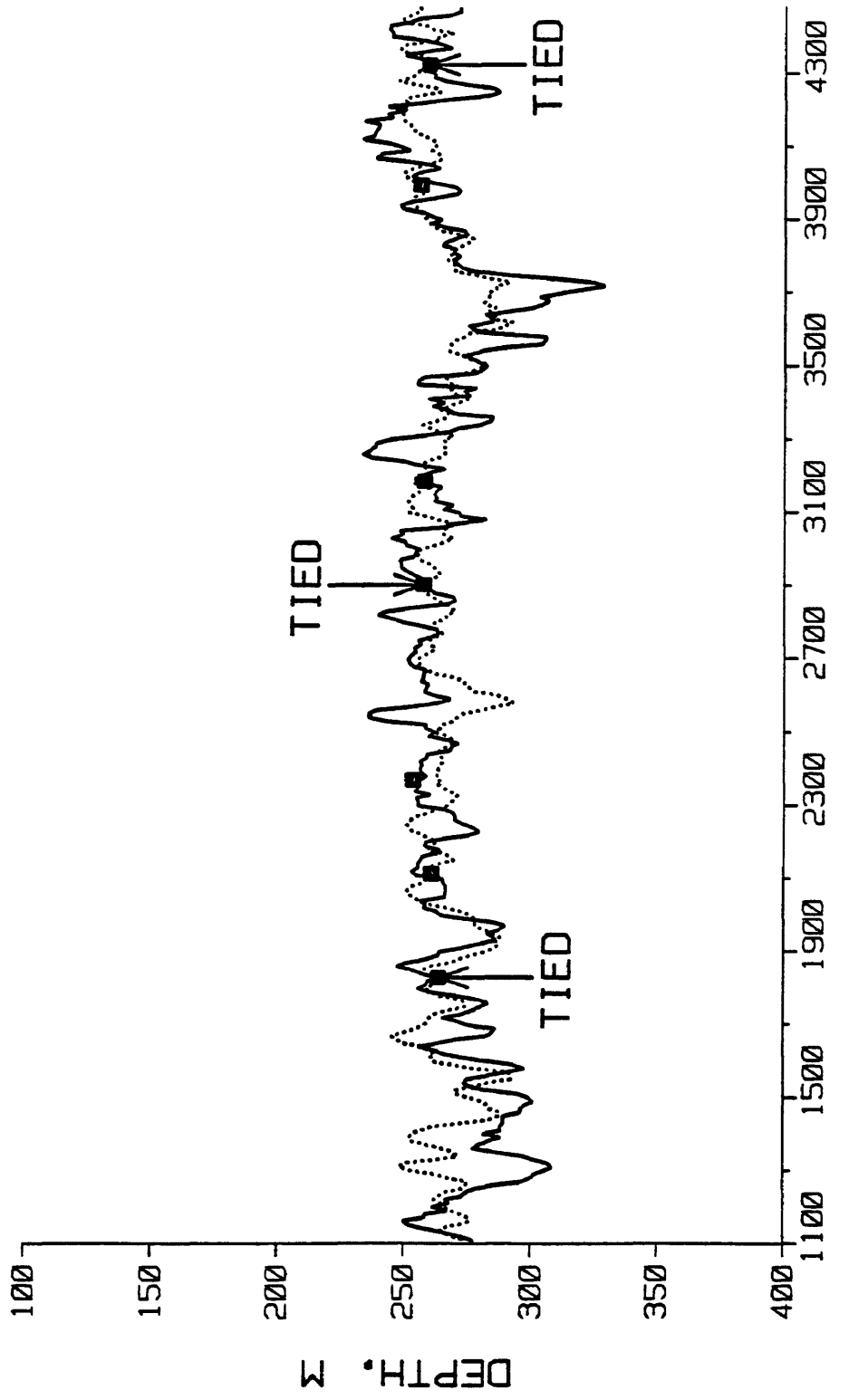

FIGURE 58. CALCULATED DEPTH, LINE 1. SHOT GATHERS. TIME(DOTTED) AND AVO(SOLID) METHODS. SMOOTHED. TIED TO WELLS 1, 4, AND 7.

58, the time method yields less average error than the AVO method.

Line 2. The calculated depths, from the time and AVO methods, are shown in Figure 60 for Line 2 using shot gathers. Figure 61 is a smoothed version of Figure 60 and tied to Well 1. The mean errors (Figure 61) are 8.6 m and 45.6 m for the time and AVO methods respectively. In Figure 62, the tie is made at Wells 1 and 3, yielding mean errors of 3.1 m (time) and 5.2 m (AVO). Figure 63 is the same as Figure 62 but with CDP gathers; the mean errors are 7.9 m (time) and 0.2 m (AVO).

The differences between the time method and the AVO method are pronounced along this dip line. The variations are greater than 50 m in many places. If the assumption that the shear velocity is varying laterally is true, then the time method is to be preferred over the AVO method.

Further AVO Analysis

The previous analysis dealt with shot and CDP gathers selected every tenth shot point. The distance between two consecutive gathers is therefore 10 X 24 = 240 m. An analysis was performed to some of the intervening gathers along Line 1. Every shot gather, for a total of 21 shot gathers, was analyzed in the vicinity of each well. This

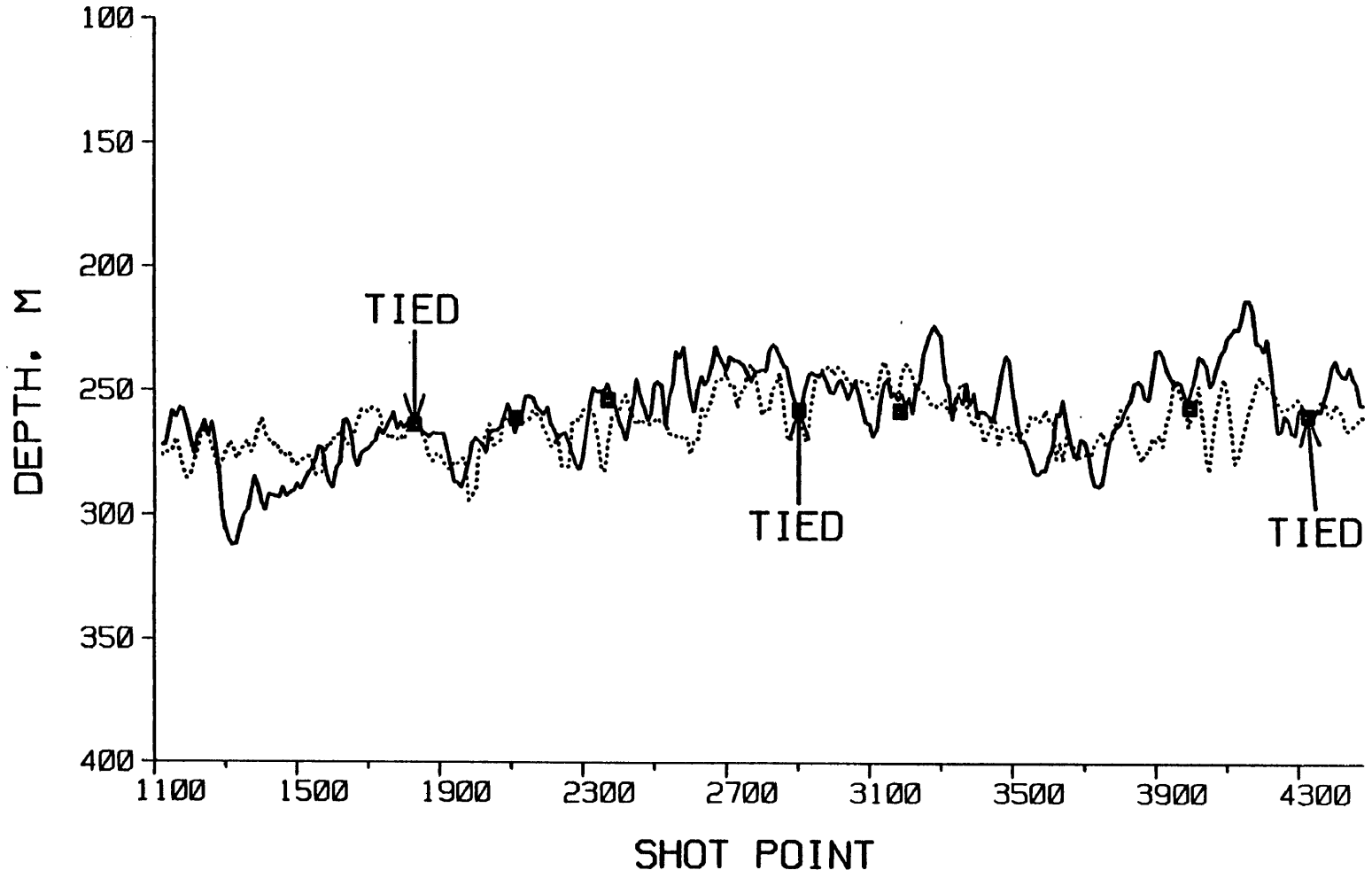

FIGURE 59. CALCULATED DEPTH, LINE 1. CDP GATHERS.
TIME(DOTTED) AND AVO(SOLID) METHODS.
SMOOTHED, TIED TO WELLS 1, 4, AND 7.

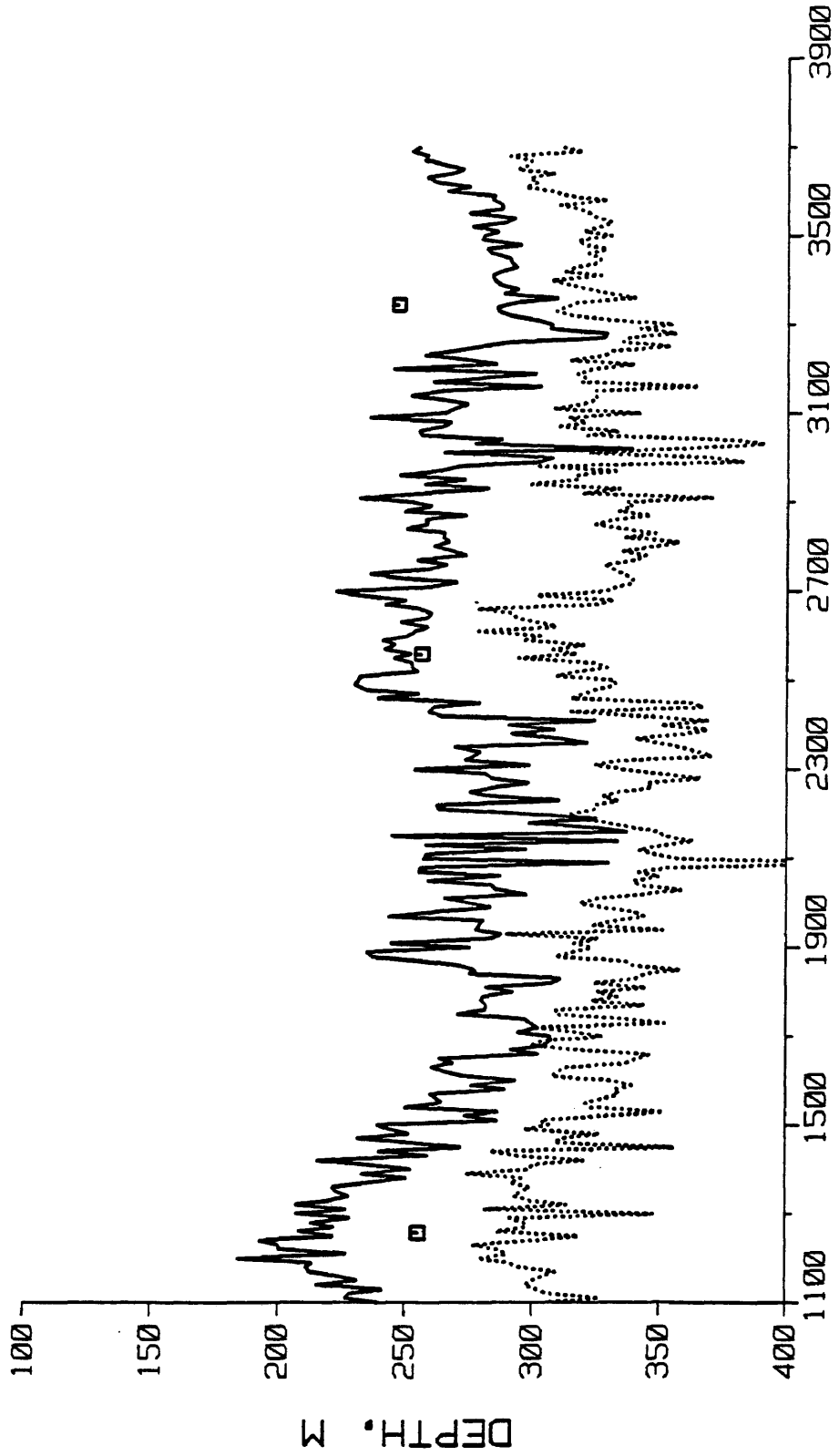

FIGURE 60. CALCULATED DEPTH, LINE 2. SHOT GATHERS.
TIME(DOTTED) AND AVO(SOLID) METHODS.

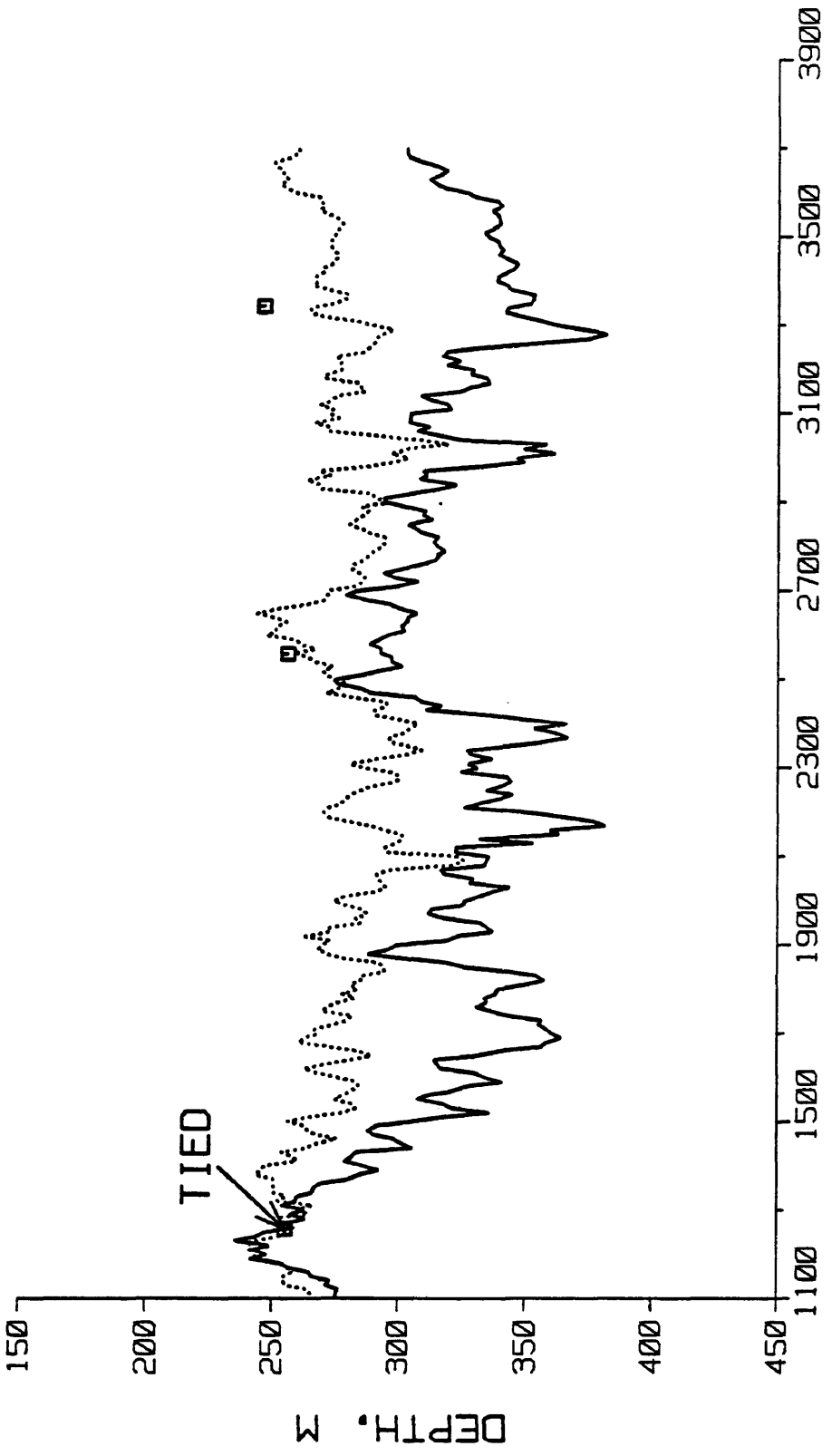

FIGURE 61. CALCULATED DEPTH, LINE 2. SHOT GATHERS. TIME(DOTTED) AND AVO(SOLID) METHODS. SMOOTHED, TIED TO WELL 1.

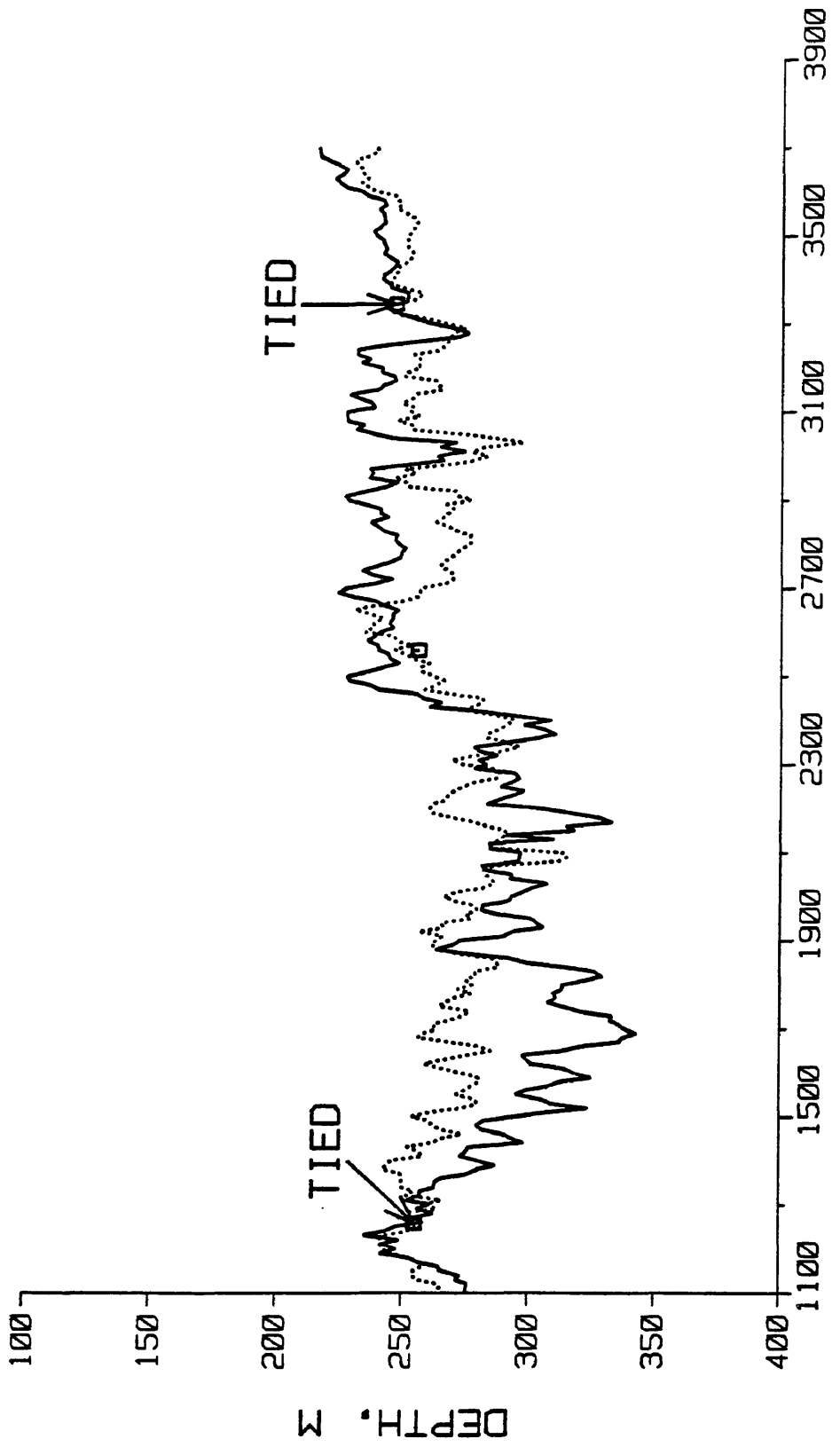

FIGURE 62. CALCULATED DEPTH, LINE 2. SHOT GATHERS.
TIME(DOTTED) AND AVO(SOLID) METHODS.
SMOOTHED, TIED TO WELLS 1 AND 3.

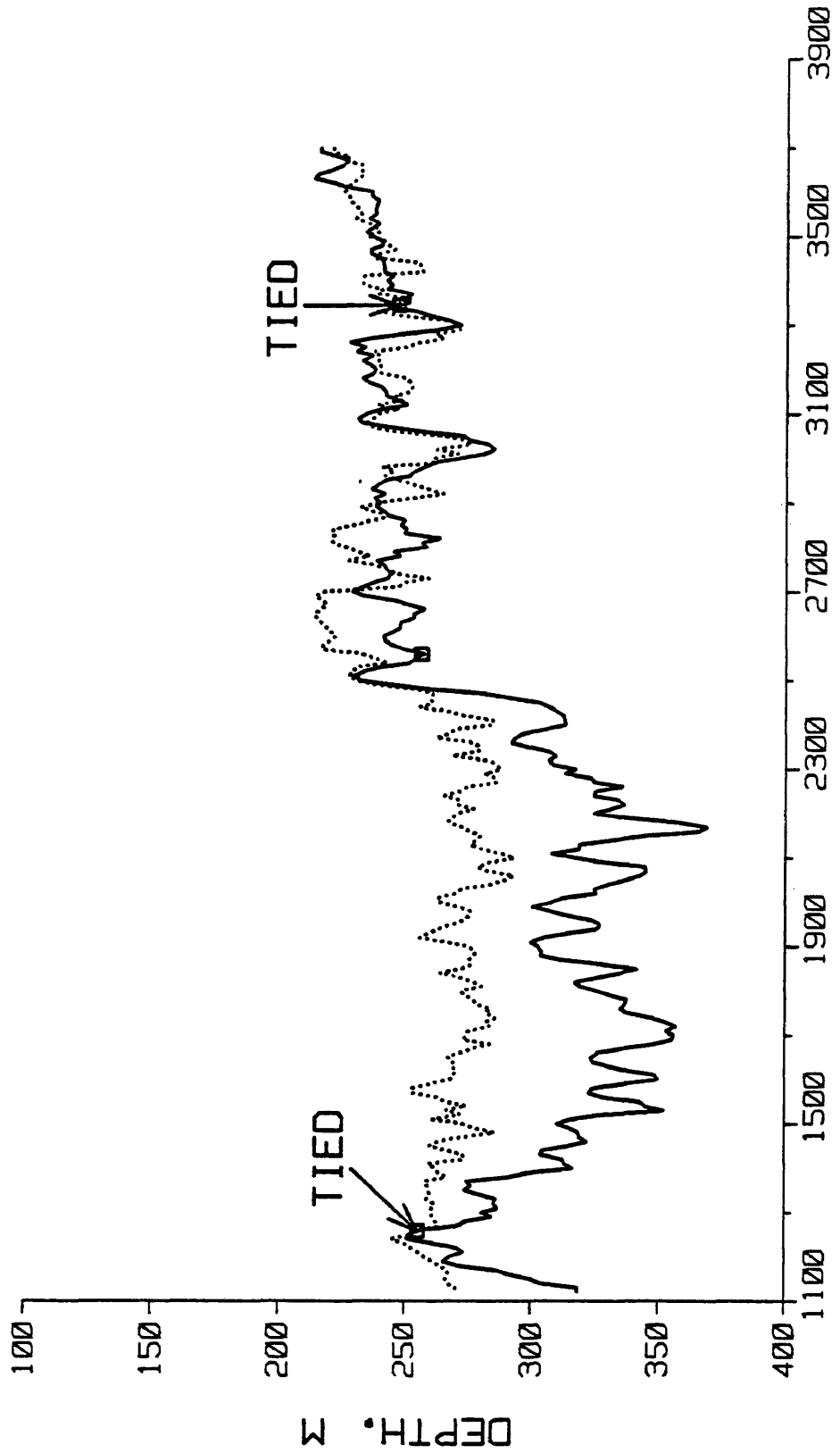

FIGURE 63. CALCULATED DEPTH, LINE 2. CDP GATHERS. TIME(DOTTED) AND AVO(SOLID) METHODS. SMOOTHED, TIED TO WELLS 1 AND 3.

analysis was made in order to see how consistent the picked offsets were.

Figure 64 shows the offsets of peak amplitudes for every shot point in the vicinity of Well 1 along with the previously-analyzed gathers. The same comparison is shown for Wells 2 through 7 in Figures 65 through 70.

The variations in peak amplitude offsets from one shot point to another are consistent and generally within an acceptable tolerance ($\pm$ 30 m, Figure 70). Occasionally however, the variations are not consistent and may reach over 100 m from one shot point to another (Figures 67 and 68).

Figure 71 shows a segment of Line 1 (SP 2900 - SP 4485) in which the offset of peak amplitude is plotted against shot point. Every tenth shot gather was analyzed. The solid line represents the segment previously used in depth calculations based on AVO. The dotted line represents the same line segment but displaced 5 shot points (SP 2905 - SP 4485). Again, consistency and divergence can be seen on this plot.

The above study suggests that a closer shot point interval be used in the analysis rather than every tenth shot point.

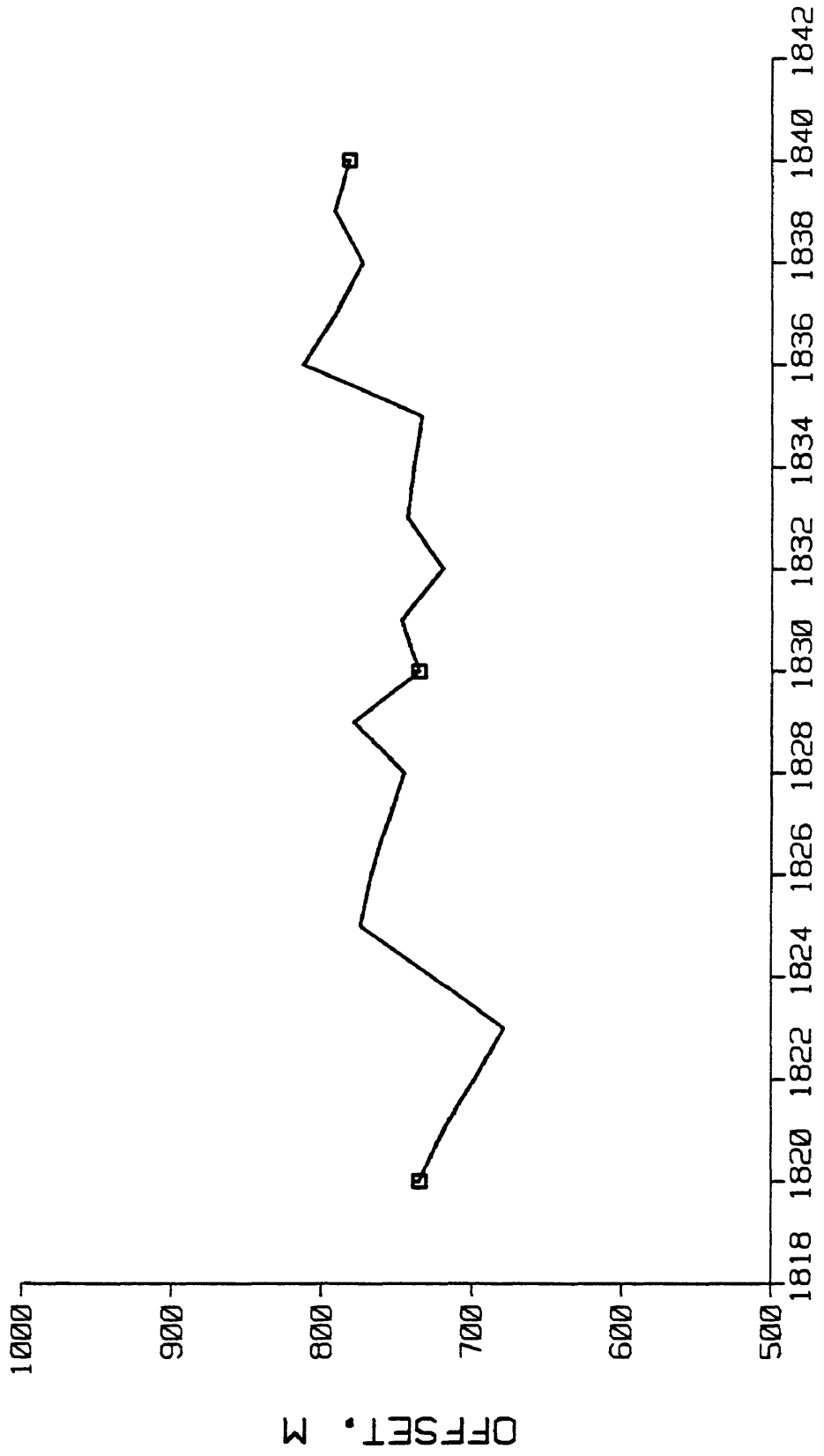

FIGURE 64. OFFSETS OF PEAK AMPLITUDES. EVERY SHOT POINT.
LINE 1, VICINITY OF WELL 1. 21 SHOT GATHERS.
SYMBOLS ARE GATHERS PREVIOUSLY ANALYZED.

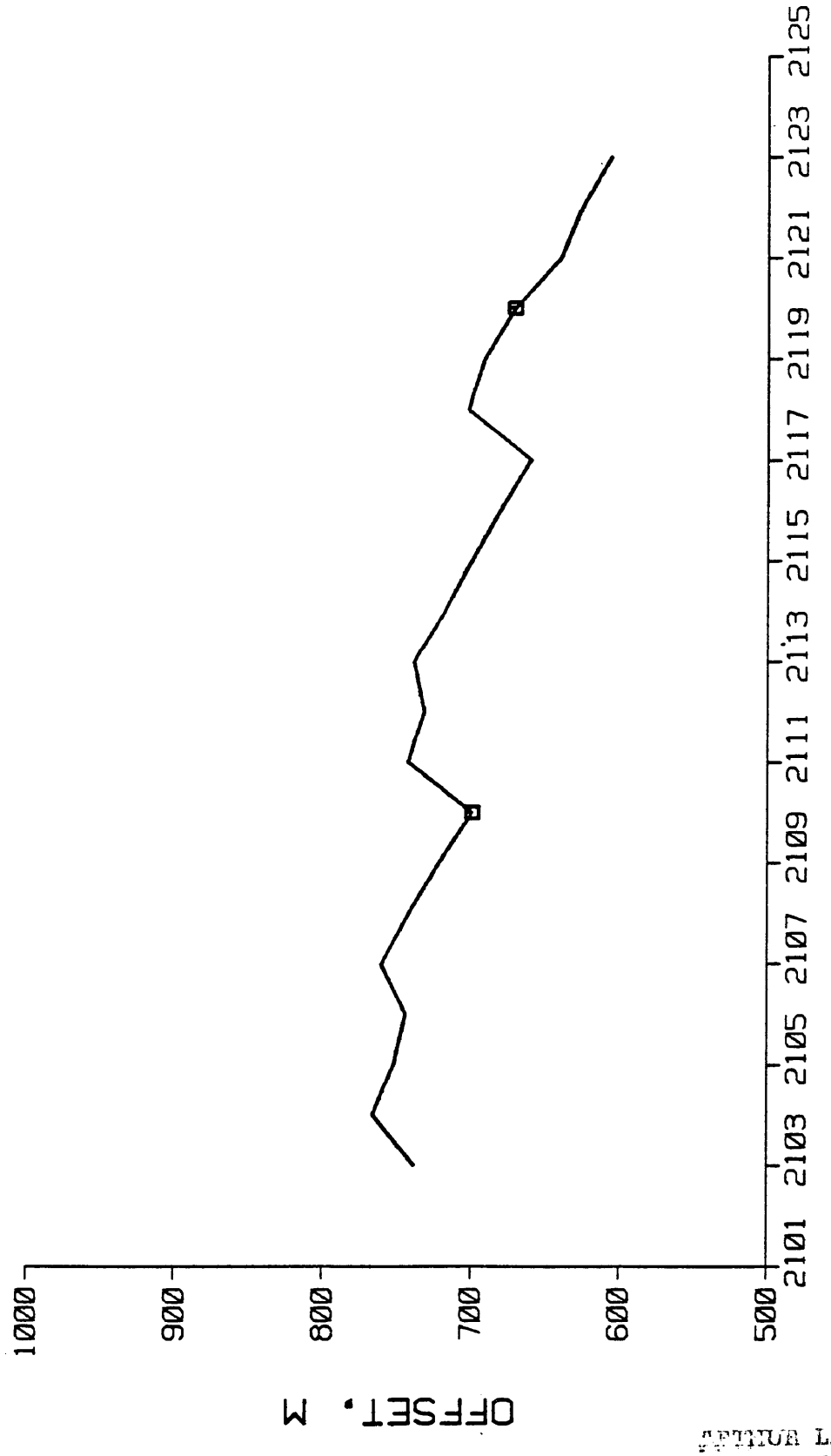

FIGURE 65. OFFSETS OF PEAK AMPLITUDES. EVERY SHOT POINT.
LINE 1, VICINITY OF WELL 2. 21 SHOT GATHERS.
SYMBOLS ARE GATHERS PREVIOUSLY ANALYZED.

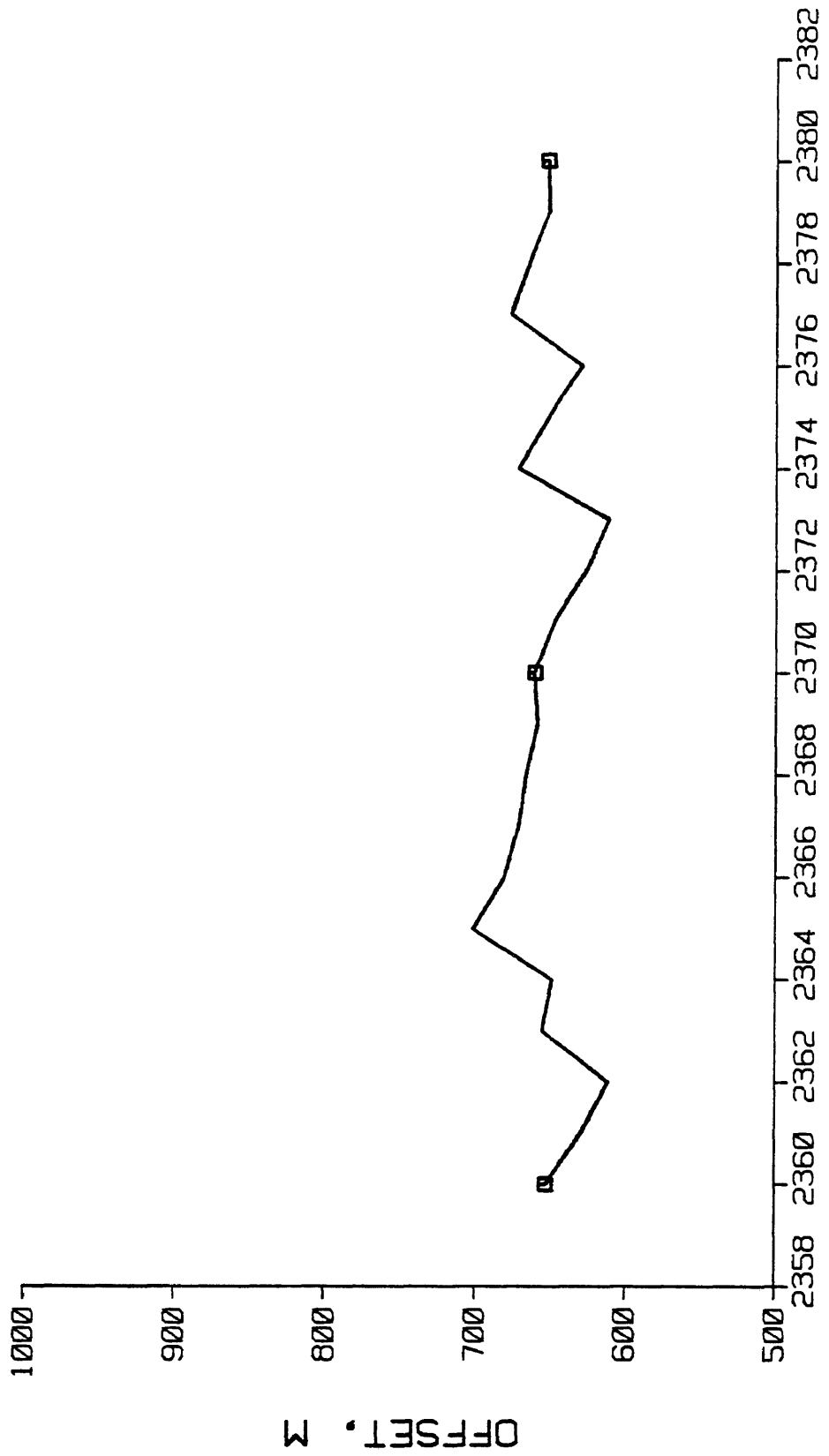

FIGURE 66. OFFSETS OF PEAK AMPLITUDES. EVERY SHOT POINT.
LINE 1, VICINITY OF WELL 3. 21 SHOT GATHERS.
SYMBOLS ARE GATHERS PREVIOUSLY ANALYZED.

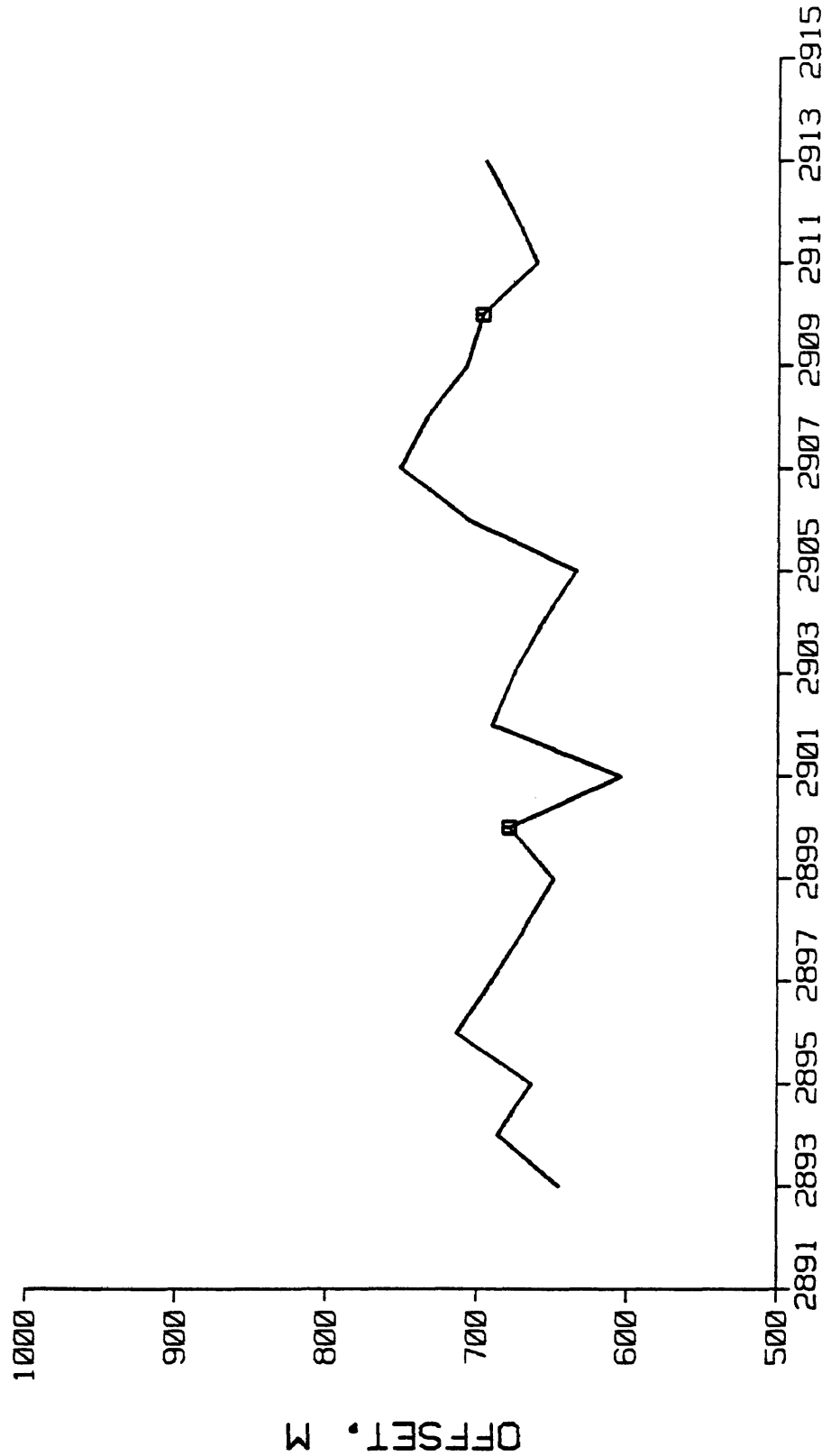

FIGURE 67. OFFSETS OF PEAK AMPLITUDES. EVERY SHOT POINT.
LINE 1, VICINITY OF WELL 4. 21 SHOT GATHERS.
SYMBOLS ARE GATHERS PREVIOUSLY ANALYZED.

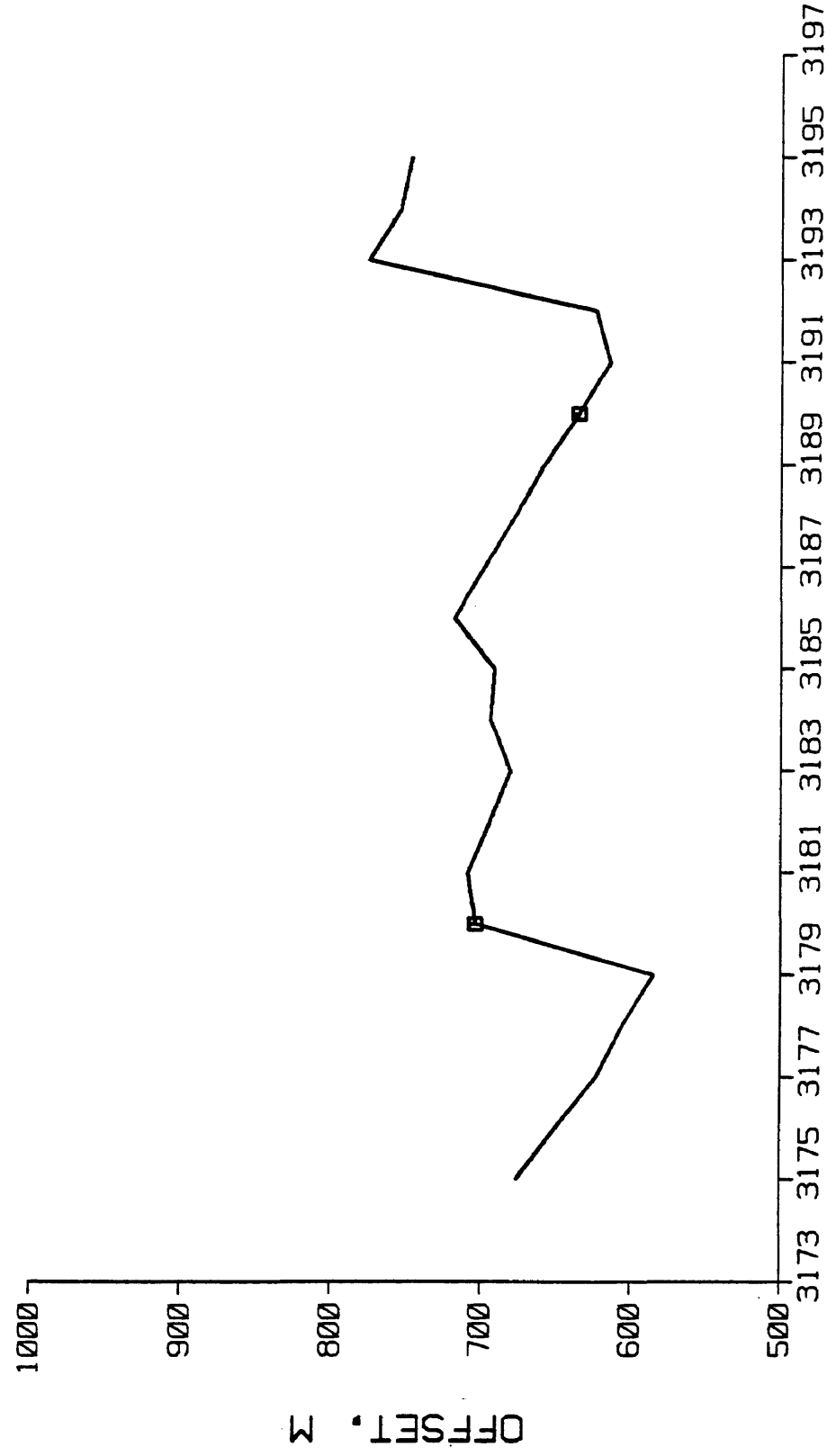

FIGURE 68. OFFSETS OF PEAK AMPLITUDES. EVERY SHOT POINT.
LINE 1, VICINITY OF WELL 5. 21 SHOT GATHERS.
SYMBOLS ARE GATHERS PREVIOUSLY ANALYZED.

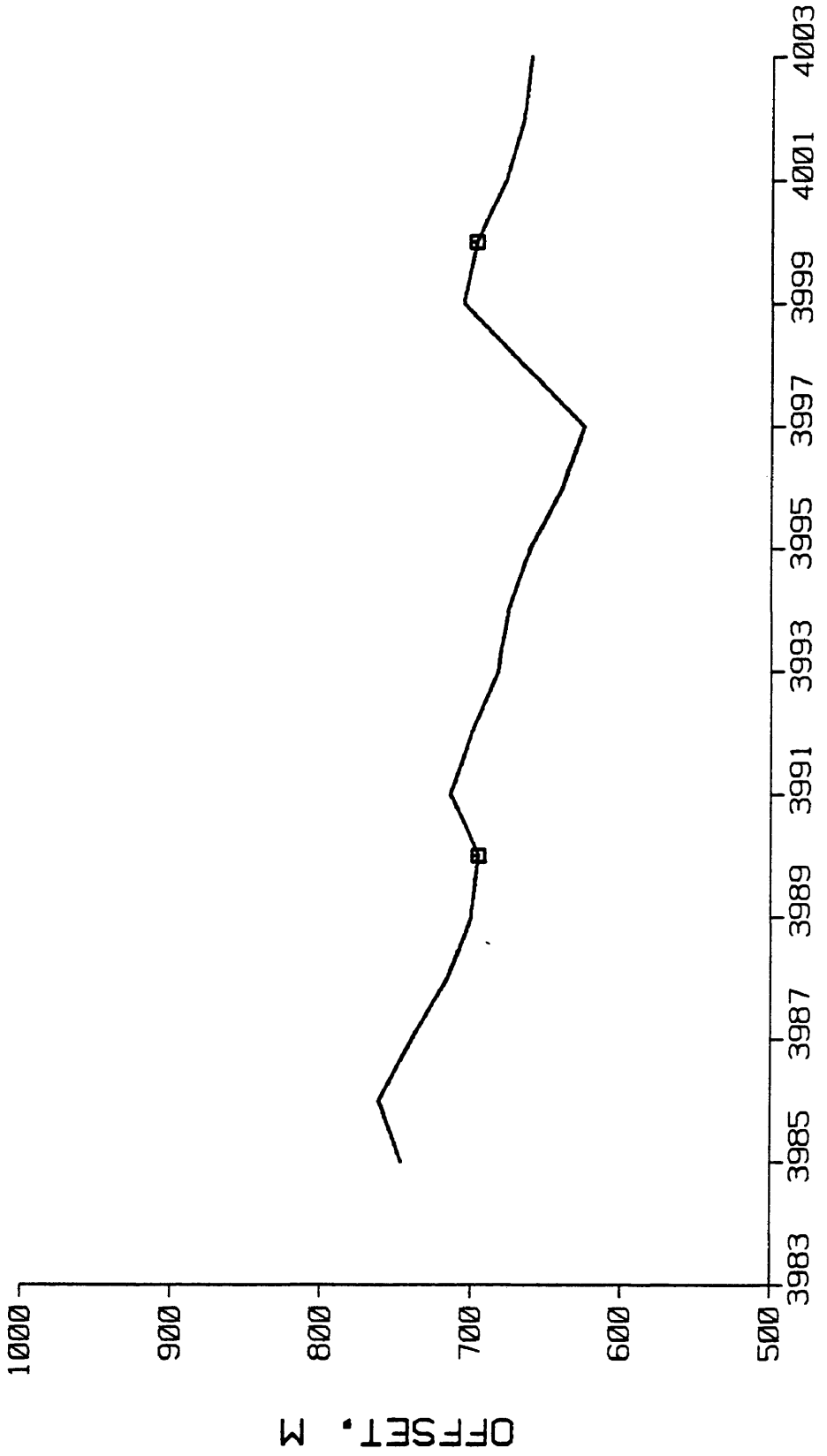

FIGURE 69. OFFSETS OF PEAK AMPLITUDES. EVERY SHOT POINT.
LINE 1, VICINITY OF WELL 6. 21 SHOT GATHERS.
SYMBOLS ARE GATHERS PREVIOUSLY ANALYZED.

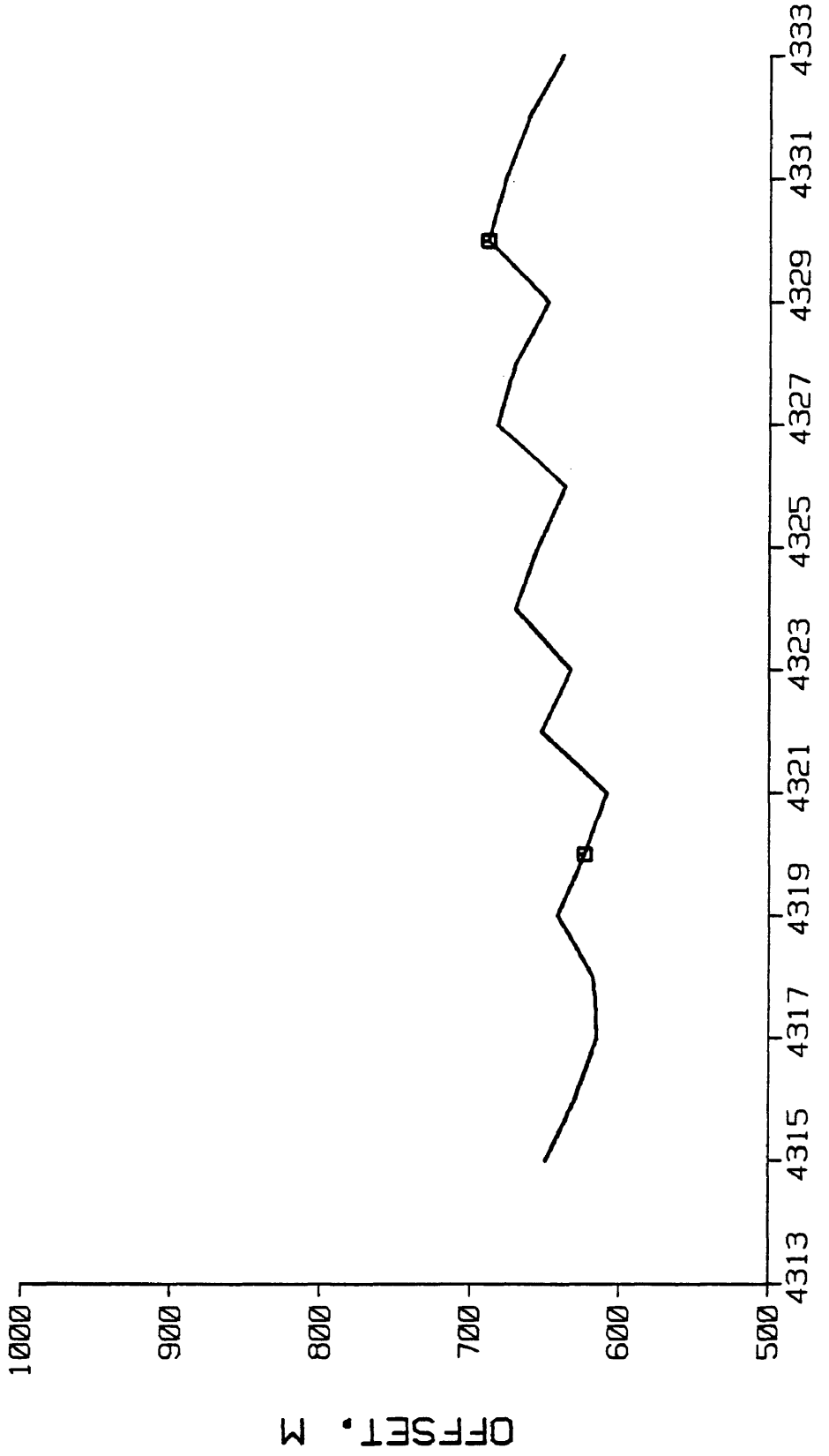

FIGURE 70. OFFSETS OF PEAK AMPLITUDES. EVERY SHOT POINT.
LINE 1, VICINITY OF WELL 7. 21 SHOT GATHERS.
SYMBOLS ARE GATHERS PREVIOUSLY ANALYZED.

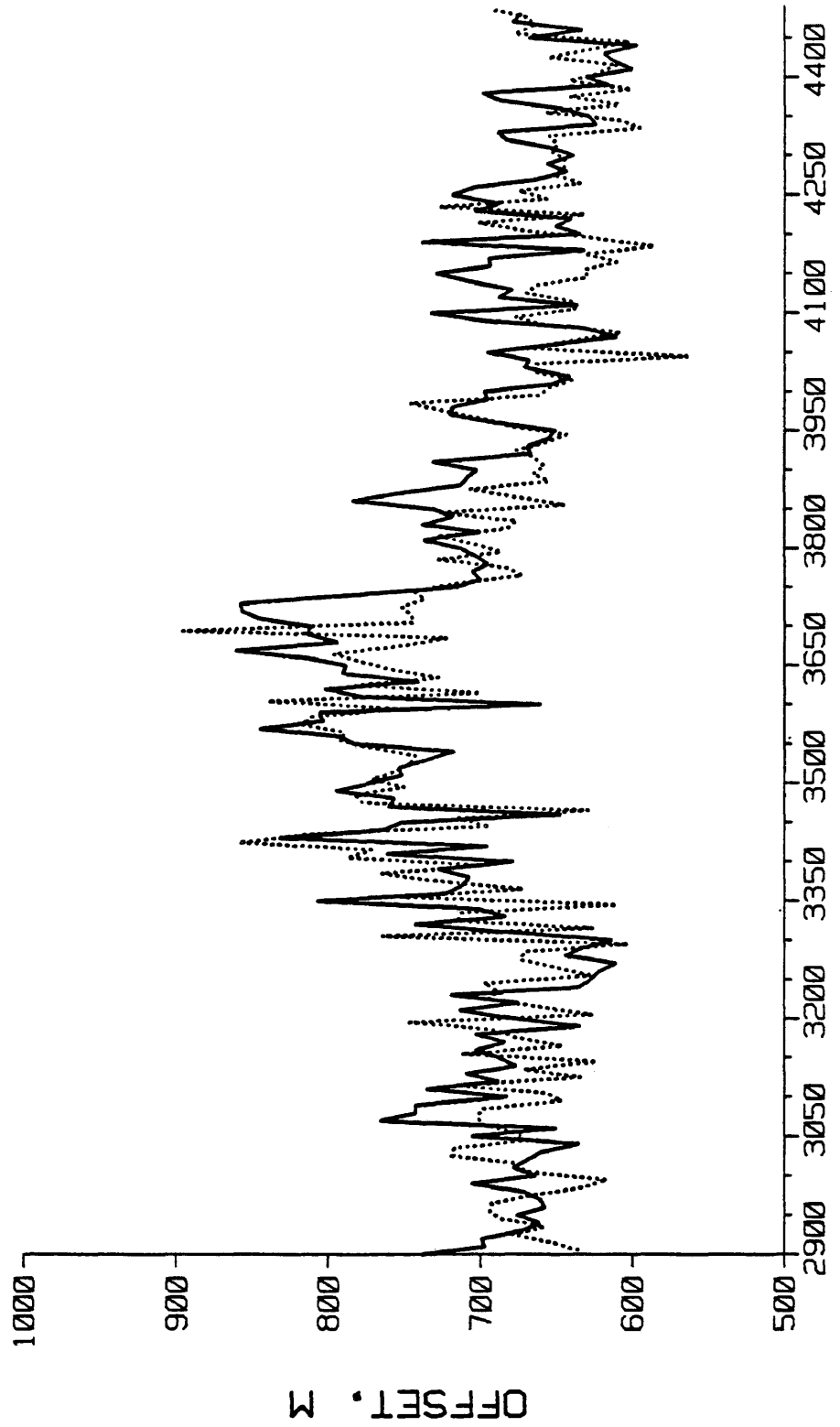

FIGURE 71. OFFSETS OF PEAK AMPLITUDES.
PART OF LINE 1. SHOT GATHERS. SP 2900 - SP 4480.
SOLID=EVERY TENTH SP; DOTTED=EVERY TENTH SP SHIFTED 5.

CHAPTER SIX

Conclusions and Recommendations

Since this AVO method of depth estimation is a new aspect in seismology, most of the conclusions drawn here are preliminary and subject to further investigation and evaluation. On the other hand, many recommendations can be suggested in order to avoid many of the pitfalls for future studies.

Conclusions

The conclusions from this study can be separated basically into two parts. The first part deals with the theoretical results obtained by modeling using Zoeppritz' equations. The other part deals with the output (calculated depths) resulting from the application of the theoretical results to real seismic data.

With geological knowledge and well control for a certain area, a two-layer or even a multi-layer model can be set up. When a two-layer model is assumed, the P velocity for the first layer can be taken as the stacking velocity for the corresponding reflector. The associated error is small, especially when the reflector is shallow. Zoeppritz' equations can then be used for amplitude modeling. By comparing theoretical AVO to actual AVO, one can determine

the origin of the amplitude brightening (P-critical or post-critical), if any. By the same token, the reflector producing the amplitude brightening can be identified.

If the amplitude brightening is due to post-critical reflections, then, by a proper study of the associated parameters, the angle corresponding to the peak amplitude can be studied relative to the shear-critical angle. In other words, the angle (Gamma) can be determined, and a time-independent depth equation can be developed. For the model of this study, Gamma was found to be 6°.

The calculated depths, based on the AVO method, are very encouraging for Line 1 (strike line); for Line 2 (dip line), the results are less so. Shear velocity modeling showed that the shear velocity could be assumed constant for Line 1, but not for Line 2. The depths from the time method exhibited some correlations with those from the AVO method for Line 1; the differences between the two methods were most pronounced along Line 2. Finally, the differences in the results between shot and CDP gathers can be neglected so far as the AVO depth estimation is concerned.

Recommendations

For future AVO depth estimation studies, it is recommended that surface elevation information be available in order to improve the quality of the results. Processing

of raw seismic data should be minimal so as to retain relative true amplitudes in the offset domain. The results could also be improved if the trace spacing is much smaller than 24 m as used in this study. Though it is exhaustively time consuming, every gather, instead of every 10th, should be analyzed. Either shot gathers or CDP gathers may be used, although CDP gathers are preferred if dip is suspected, or if the target has changing elastic constants.

This study can be extended to cover deeper events rather than restricting it to shallow reflectors. It would be interesting to conduct the same study over a reflector exhibiting P-critical amplitude brightenings with a high signal-to-noise ratio. A reliable depth estimation method, such as inversion, is needed beside the AVO method for a better comparison.

For post-critical reflection studies, two-component (vertical and horizontal) geophones are recommended for a better estimation of the angle that corresponds to the peak amplitude.

It should be noted that the necessary process of interactively picking amplitudes requires a great deal of concentration and patience.

And finally, it is worth mentioning that the vicinity of Trace 90 and about 1000 ms in Figure 1 is a potential

area for future research. It seems that refraction (and perhaps wide-angle reflection) events are present. This indeed assures the necessity for a wider-offset recording of seismic data.

REFERENCES

Aki, K., and Richards, P.G., 1980, Quantitative Seismology Theory and Methods, Volumes 1 and 2: W.H. Freeman and Company, San Francisco.

Chiburis, Edward F., 1987, Personal Communications: Arabian American Oil Company, Dhahran, Saudi Arabia.

Dobrin, M.B., 1960, Introduction to Geophysical Prospecting: McGraw-Hill Book Company, Inc., New York.

McQuillin R. et al, 1984, An Introduction to Seismic Interpretation: Gulf Publishing Company, Houston.

Meissner, R., 1967, Exploring Deep Interface by Seismic Wide Angle Measurements: Geophysical Prospecting, Volume 15, p. 598-617.

Richards, T.C., 1960, Wide Angle Reflections and their Application to Finding Limestone Structures in the Foothills of Western Canada: Geophysics, Volume XXV, p. 385-407.

Schultz, P.S. et al, 1983, A Case for Larger Offsets: Geophysics, Volume 48, p. 238-247.

Sengbush, R.L, 1983, Seismic Exploration Methods: IHRDC, Boston.

Winterstein, D.F., and Hanten, J.B., 1985, Supercritical Reflections Observed in P- and S-Wave Data: Geophysics, Volume 50, p. 185-195.

Yu, Gary, Offset-Amplitude Variation and Controlled-Amplitude Processing: Geophysics, Volume 50, No. 12, p. 2697-2708.